AD A044997

12

RADC-TR-77-100
Final Technical Report
March 1977

MEASUREMENT OF AMBIENT MAGNETIC FIELD GRADIENTS USING A SUPERCONDUCTING MAGNETIC GRADIOMETER

Physical Dynamics Inc

DDC
RECEIVED
OCT 7 1977
C

Sponsored by
Defense Advanced Research Projects Agency (DoD)
ARPA Order No. 1649

Approved for public release; distribution unlimited.

The views and conclusions contained in this document are those of the authors and should not be interpreted as necessarily representing the official policies, either expressed or implied, of the Defense Advanced Research Projects Agency or the U. S. Government.

AJ NO. _____
DDC FILE COPY

ROME AIR DEVELOPMENT CENTER
Air Force Systems Command
Griffiss Air Force Base, New York 13441

MEASUREMENT OF AMBIENT MAGNETIC FIELD GRADIENTS USING A SUPERCONDUCTING MAGNETIC GRADIOMETER

Walter N. Podney
George H. Gillespie

11 May 77 (12) 156 p.

(18) RADC (TR-77-104)

Contractor: Physical Dynamics Inc
Contract Number: F30602-72-C-0494
Effective Date of Contract: 1 May 1972
Contract Expiration Date: 31 December 1976
Short Title of Work: Ambient Magnetic Field Gradients Using a Superconducting Magnetic Gradiometer
Program Code Number: 6E20
Period of Work Covered: Jan 1976 - Dec 1976

(19) PD-76-197

Principal Investigator: Dr. Walter Podney
Phone: 703 525-2504
Project Engineer: Joseph J. Simons
Phone: 315 330-4157

(9) Final Technical rept. Jan — Dec 76,

Approved for public release;
distribution unlimited.

This research was supported by the Defense Advanced Research Projects Agency of the Department of Defense and was monitored by Joseph J. Simons (OCS), Griffiss AFB NY 13441 under Contract F30602-72-C-0494,

(15) ARPA Order — 1649

ACCESS for
NTIS White Section
DDC Buff Section
UNANNOUNCED
JUSTIFICATION
DISTRIBUTION/AVAILABILITY CODES
Dist. AVAIL. and/or SPECIAL
A

391 801

This report has been reviewed by the RADC Information Office (OI) and is releasable to the National Technical Information Service (NTIS). At NTIS it will be releasable to the general public, including foreign nations.

This report has been reviewed and is approved for publication.

APPROVED:

JOSEPH J. SIMONS
Project Engineer

Do not return this copy. Retain or destroy.

UNCLASSIFIED

SECURITY CLASSIFICATION OF THIS PAGE *(When Data Entered)*

REPORT DOCUMENTATION PAGE

READ INSTRUCTIONS BEFORE COMPLETING FORM

1 REPORT NUMBER RADC-TR-77-100	2 GOVT ACCESSION NO.
3 RECIPIENT'S CATALOG NUMBER	
4 TITLE *(and Subtitle)* MEASUREMENT OF AMBIENT MAGNETIC FIELD GRADIENTS USING A SUPERCONDUCTING MAGNETIC GRADIOMETER	5 TYPE OF REPORT & PERIOD COVERED Final Technical Report Jan 76 - ~~Nov~~ 76
	6 PERFORMING ORG. REPORT NUMBER PD-76-107
7 AUTHOR(s) Dr. Walter Podney Mr. George H. Gillespie	8 CONTRACT OR GRANT NUMBER(s) F30602-72-C-0494
9 PERFORMING ORGANIZATION NAME AND ADDRESS Physical Dynamics Inc P. O. Box 556 La Jolla CA 92037	10 PROGRAM ELEMENT, PROJECT, TASK AREA & WORK UNIT NUMBERS 62301E 16490402 (16) (17) 04
11 CONTROLLING OFFICE NAME AND ADDRESS Defense Advanced Research Projects Agency 1400 Wilson Blvd Arlington VA 22209	12 REPORT DATE March 1977 13 NUMBER OF PAGES 152
14 MONITORING AGENCY NAME & ADDRESS *(if different from Controlling Office)* Rome Air Development Center (OCS) Griffiss AFB NY 13441	15 SECURITY CLASS. *(of this report)* UNCLASSIFIED 15a DECLASSIFICATION DOWNGRADING SCHEDULE N/A

16 DISTRIBUTION STATEMENT *(of this Report)*

Approved for public release; distribution unlimited.

17 DISTRIBUTION STATEMENT *(of the abstract entered in Block 20, if different from Report)*

Same

18 SUPPLEMENTARY NOTES

RADC Project Engineer:
Joseph J. Simons (OCS)

19 KEY WORDS *(Continue on reverse side if necessary and identify by block number)*

Ocean Wave Spectra
Magnetic Fields
Superconducting Magnetic Gradiometer

20 ABSTRACT *(Continue on reverse side if necessary and identify by block number)*

This report presents the results of investigations involving the relationship of the motion of ocean waves to measurement of fluctuating magnetic fields that result from a wave progressing horizontally in a stratified ocean. This report (1) describes design features of a superconducting magnetic gradiometer that will be employed to measure gradients of magnetic fields generated at a fixed point above the ocean surface due to waves passing the oceanographic tower operated by the U. S. Naval Undersea Center near San Diego, CA.

(cont'd)

DD FORM 1 JAN 73 1473 EDITION OF 1 NOV 65 IS OBSOLETE

UNCLASSIFIED

SECURITY CLASSIFICATION OF THIS PAGE *(When Data Entered)*

In addition, the report gives a formulation describing instrument response to ambient magnetic gradients that are sensibly constant over the distance separating centers of the pickup loops in the gradiometer. This report also presents the first measurements of spectra that characterize noise in the frequency range 5 x 10 (-4) to 20 Hz of a superconducting magnetic gradiometer operating in a magnetically quiet environment. Two techniques that provide means of suppressing noise from nearby magnetic objects are examined. A procedure for operating at the Oceanographic tower that both uses the techniques to suppress noise from magnetization currents in the tower's steel structure, and gives a maximum response to gradients from internal waves is presented.

TABLE OF CONTENTS

SUMMARY

The extreme sensitivity of superconducting magnetic gradiometers affords means of measuring gradients of fluctuating magnetic fields generated by ocean waves. The fields fluctuate in concert with motions of ocean waves, so that reading fluctuations of magnetic fields above an ocean tells the motion of seawater below its surface. As a first step in developing requisite experimental and analytical techniques, we plan to use a superconducting magnetic gradiometer to measure fluctuating gradients of magnetic fields generated at a fixed point above the surface by waves passing the oceanographic tower operated by the Naval Undersea Center.*

The response of a superconducting magnetic gradiometer to ambient magnetic fields having gradients that are sensibly constant over the length of its axis (typically 25 cm or so) is a sum of two terms. One term is proportional to the magnetic field at the midpoint of the axis, and the other term, to a gradient of the magnetic field at the midpoint. The term proportional to the magnetic field results from slight differences in area and orientation of the loops forming the pickup circuit of the gradiometer and vanishes for a perfectly balanced gradiometer. The term proportional to a gradient of the magnetic field depends on five independent elements of a symmetric matrix having a vanishing trace that represents gradients of the ambient field at the midpoint.

The five elements define location, orientation, and moment of a dipole positioned on a sphere of unit radius about the midpoint that gives gradients at the midpoint equal to gradients of the ambient field there. The construct of an equivalent dipole concisely describes the gradient response. For example, fluctuations in location, orientation, and moment of an equivalent dipole describe gradients from fluctuating magnetization currents in magnetic objects as well as from fluctuations in position and orientation of a gradiometer.

*The tower is located about one mile off Mission Beach near San Diego, California, in 18 m of water.

Moreover, it provides a rationale for two techniques that afford means of suppressing gradient fluctuations from nearby magnetic objects; namely, (1) using a gradiometer axis having coplanar pickup loops (transverse configuration) and aligning it for a null response and (2) using a magnetic dipole to cancel steady gradients. Transverse gradients of the magnetic field of a dipole vanish in certain directions, so that aligning a gradiometer measuring transverse gradients for a null response suppresses fluctuating gradients from magnetic objects. Placing an opposing dipole at the location of an equivalent dipole nullifies gradients at the field point and so suppresses apparent gradient fluctuations owing to changes in gradiometer orientation.

Preliminary tests of suppression techniques conducted with our gradiometer, which has two coplanar pickup loops spaced 25 cm between centers, demonstrate that their effectiveness is limited only by precision of requisite alignments. Aligning the gradiometer within a few degrees ($\sim$ 0.1 radian) for a null response to gradient fluctuations from a spherical iron shell having a radius of 0.74 m and placed 4.5 m north of the gradiometer reduces RMS fluctuations in the frequency band 0.001 to 0.01 Hz by about a factor of ten. Crude positioning of a coil approximating an opposing magnetic dipole at the location of an equivalent dipole reduces steady gradients from the sphere by a factor of 100.

Design of the gradiometer, insofar as practical, eliminates sources of instrument noise driven by fluctuations of ambient temperature and pressure and of the earth's magnetic field by using materials within the helium bath that are free of paramagnetic impurities. A rectangular block of high-purity crystalline silicon, for example, supports the two niobium wire pickup loops on a lateral face. Spectra that characterize noise in the frequency range 5×10^{-4} to 20 Hz of the gradiometer operating in a magnetically quiet environment are effectively white at frequencies above about 0.1 Hz with a spectral

density* of 0.03 $(pT/m)^2/Hz$ and are of the form $S(f) = S(f_o)(f_o/f)^\gamma$ at frequencies below 0.1 Hz. A value of 1.3 for γ with $S(f_o) = 0.002\ (pT/m)^2/Hz$ at $f_o = 1$ Hz is representative. Intrinsic noise of the superconducting quantum interference device (SQUID) used in the instrument to sense magnetic flux dominates spectra observed in a quiet environment at freqencies below 0.1 Hz.

As shown in the following figure, spectral density of inherent noise of the instrument is well below the level of spectral densities of gradients expected from oceanic internal waves passing the oceanographic tower operated by the Naval Undersea Center. To measure gradients from waves passing the tower, we plan to jut the gradiometer over water on a rigid nonmagnetic cantilever extending horizontally 25 meters from the centerline of the tower off its south face. Measurements of steady gradients from magnetization currents in the steel structure of the tower show that gradients at positions in a vertical plane of symmetry of the structure are represented by gradients of equivalent dipoles located in the plane of symmetry. Aligning the gradiometer with a precision of 0.01 radians, or 0.6 degrees, for a null response from the equivalent dipole keeps noise from fluctuating magnetization currents in the tower below the level of instrument noise. Structural design of the cantilever limits translational and rotational RMS fluctuations of the instrument to 0.1 mm and a few seconds of arc (10^{-5} radians) in the bandwidth 0.002 to 0.005 Hz and, together with a coil positioned on the cantilever to reduce steady gradients from the tower, keeps noise from irregular motions of the instrument in the steady gradients below the level of instrument noise.

---

*We use MKS units throughout and conform to the international convention suggesting use of the unit Tesla, which is a Weber/m^2 and so 1 pT/m = 10^{-12}T/m = 10^{-10}G.cm = 10^{-3}gamma/m.

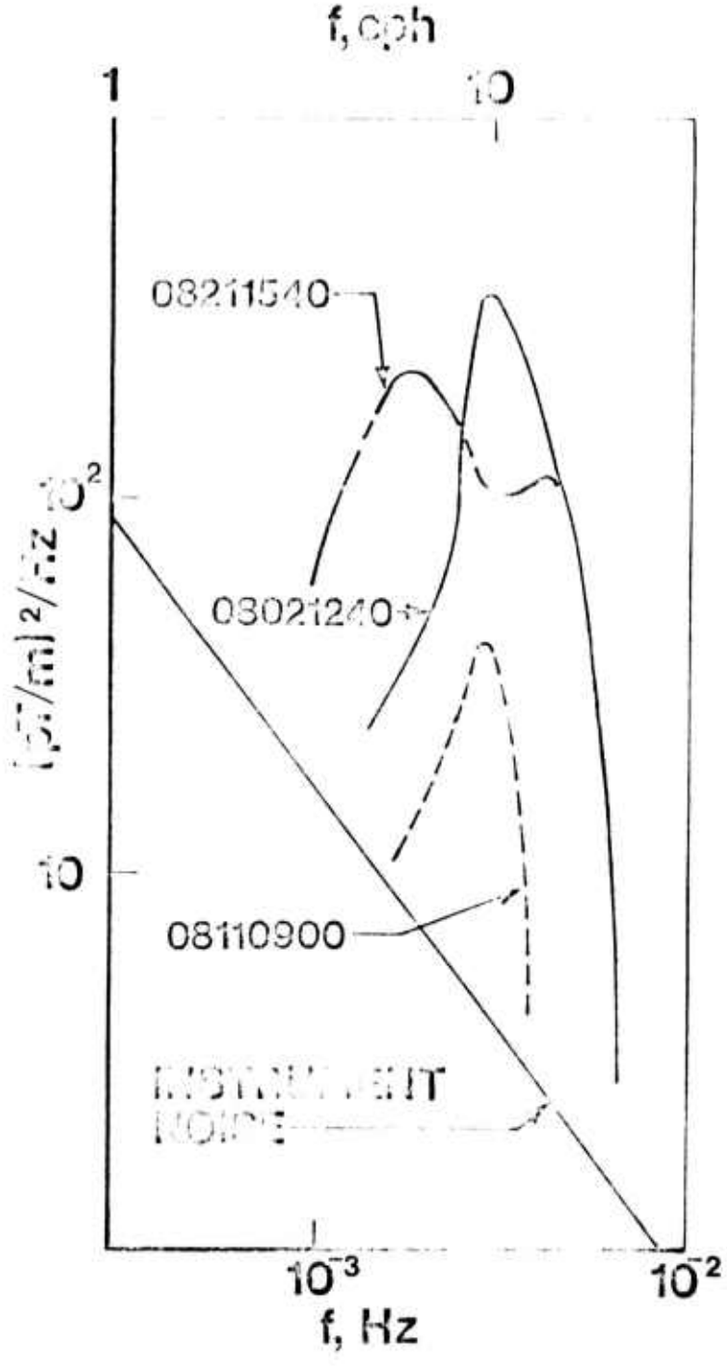

Three typical spectra of fluctuating gradients of magnetic fields expected 7 m above the surface from internal waves passing the oceanographic tower operated by the Naval Undersea Center as compared to the inherent noise spectrum of the instrument. Spectra are estimates based on spectral measurements of isotherm displacements made during August 1972. Serial numbers marking spectra tell the month, day, and local time at the beginning of corresponding time series; for example, 08211540 means August 21 at 15:40 hours (PST).

Section I
INTRODUCTION

The unprecedented sensitivity of superconducting magnetic gradiometers affords means of measuring fluctuating gradients of magnetic fields generated by ocean waves. Seawater moving across the earth's magnetic field drives electric currents that produce weak magnetic fields above the oceans. The fields fluctuate in concert with motions of ocean waves, so that reading fluctuations of magnetic fields above an ocean tells the motion of seawater below its surface. Podney (1975) among others describes the fluctuating magnetic field that results from a wave progressing horizontally in a stratified ocean.

Our aim is to tell motions of seawater from measurements of fluctuating magnetic fields over oceans. As a first step in developing requisite experimental and analytical techniques, we plan to use a superconducting magnetic gradiometer to measure fluctuating gradients of magnetic fields generated at a fixed point above the surface by waves passing the oceanographic tower operated by the Naval Undersea Center. The tower is located about one mile off Mission Beach near San Diego, California in 18 m of water. Successful completion of the first step provides the experience and information necessary for planning, carrying out, and interpreting measurements over the open ocean using an airborne gradiometer. Measurements at a fixed point above the surface, in effect, provide the code for reading motions of seawater in measurements made over an open ocean from aircraft.

The tower provides a stable platform for jutting the instrument over water on a cantilever support. Surface and internal waves passing the tower have simple spectra that are well

characterized by past measurements using thermistor chains and current meters (Cox, 1962; La Fond, 1962; Winant and Olson, 1976; and Ziemer, 1976) and provide a readily accessible source for first measurements. Nonetheless, magnetization currents in the steel structure of the tower make the task of measuring fluctuating gradients from the waves an exacting one. To prepare for carrying out measurements at the tower, we completed the following tasks:

- Specification, procurement, and acceptance tests of a suitable superconducting magnetic gradiometer*

- Land based trials of the gradiometer conducted to estimate spectra of inherent instrument noise in a quiet environment and to determine effectiveness of techniques designed to suppress noise from nearby magnetic objects

- Specification of fluctuating gradients of magnetic fields expected from waves passing the tower.

- Use of a fluxgate gradiometer to measure gradients of the steady magnetic field produced by magnetization currents in the steel structure of the tower (Gillespie and Podney, 1976)

- Design of a rigid nonmagnetic cantilever required to project the instrument over water**

Ziemer and Gillespie (1976) describe early planning for measurements at the tower and present a chronology of the design specification, procurement, and acceptance tests of the gradiometer. Here, we describe use of the instrument

* Superconducting Technology, Inc. constructed the instrument.

** Mechanics Research, Inc. developed a structural design to meet stability requirements set by Physical Dynamics, Inc. (Haire and Van Lerberg, 1976)

to measure gradients of ambient magnetic fields and develop a procedure for operating at the tower that suppresses noise from magnetization currents in the steel structure. The procedure unites results of the last three tasks.

We first describe design features of the instrument in Section II. Insofar as practical, the design eliminates sources of instrument noise driven by fluctuations of ambient temperature and pressure and of the earth's magnetic field by using materials within the helium bath that are free of paramagnetic impurities. Two loops of niobium wire mounted on a lateral face of a rectangular block (2 X 2 X 12 in.) of high-purity crystalline silicon, for example, form the pickup circuit of the gradiometer.

Section III gives a formulation describing instrument response to ambient magnetic gradients that are sensibly constant over the distance separating centers of the pickup loops. Because the loops are coplanar, the gradiometer responds to a transverse gradient of the magnetic field at the point midway between centers of the loops. Slight differences in area and orientation of the loops give an imbalance response proportional to the magnetic field at the midpoint as well. The gradient field of a magnetic dipole located on a sphere of unit radius about the midpoint describes the part of the response owing to ambient gradients.

Section IV describes procedures for making mechanical and electronic adjustments to nullify the part of the response owing to imbalance. Moving three small niobium disks mounted on slides near one loop adjusts its effective area and orientation and balances response of the loops to a uniform magnetic flux. Electronically substracting a fraction of the magnetic field components measured by a triaxial fluxgate magnetometer near

the midpoint from the gradiometer response provides easier balancing. Procedures for balancing a gradiometer in both uniform and nonuniform ambient magnetic fields are presented.

In Section V, we present the first measurements of spectra that characterize noise in the frequency range 5×10^{-4} to 20 Hz of a superconducting magnetic gradiometer operating in a magnetically quiet environment. Spectra are effectively white at frequencies above about 0.1 Hz with a spectral density* of $0.03\ (pT/m)^2/Hz$ and are of the form $S(f) = S(f_o)(f_o/f)^\gamma$ at frequencies below 0.1 Hz. A value of 1.3 for γ with $S(f_o) = 0.002\ (pT/m)^2/Hz$ at $f_o = 1$ Hz is representative of values observed during quiet periods. Intrinsic noise of the superconducting quantum interference device (SQUID) used in the instrument to sense magnetic flux then dominates observed spectra at frequencies below 0.1 Hz. Use of a dc-type SQUID (Clarke et. al., 1975) would improve instrument performance nearly tenfold.

In Section VI, we give a rationale for two techniques that provide means of suppressing noise from nearby magnetic objects; namely, (1) aligning the gradiometer to obtain a null response, and (2) using a magnetic dipole to cancel steady gradients. We describe noise from nearby magnetic objects in terms of gradient fluctuations corresponding to small changes in location, orientation, and moment of a magnetic dipole located on a sphere of unit radius about the midpoint of the gradiometer axis. Because transverse gradients of the magnetic field of a dipole vanish in certain directions, response of a gradiometer measuring transverse gradients vanishes at certain orientations. Aligning it for null response suppresses noise from magnetic objects. Placing an oppositely directed dipole at the location of an equivalent dipole nullifies steady gradients at the midpoint and so suppresses apparent gradient fluctuations owing to changes in gradiometer orientation.

* We use MKS units throughout and conform to the international convention suggesting use of the unit Tesla, which is a Weber/m^2 and so $1pT/m = 10^{-12}T/m = 10^{-10}G/cm = 10^{-3}$gamma/m.

Section VII presents results of preliminary tests of noise suppression techniques. Our field tests show that the construct of an equivalent dipole gives a useful description of the response to gradients that are sensibly constant over the length of a gradiometer axis. Preliminary tests using crude means of aligning the gradiometer reduce noise power by a factor of 100 and suggest that reduction of noise is limited by alignment precision alone.

Finally, Section VIII describes a procedure for operating at the tower that both uses the techniques to suppress noise from magnetization currents in the steel structure and gives a maximum response to gradients from internal waves. We plan to jut the gradiometer over water on a rigid nonmagnetic cantilever extending horizontally 25 meters from the centerline of the tower off its south face. Figure 1 shows that spectral densities of gradients expected from internal waves are well above the level of instrument noise. Aligning the gradiometer for a null response with a precision of 0.01 radians, or 0.6 degrees, keeps noise from fluctuating magnetization currents in the tower below the level of instrument noise. Limiting translational and rotational RMS fluctuations of the instrument to 0.1 mm and a few seconds of arc (10^{-5} radians) in the bandwidth 0.002 to 0.005 Hz keeps noise from irregular motions of the instrument in the steady gradient field of the tower below the level of instrument noise.

Section II
INSTRUMENT DESCRIPTION

As shown in Figure 2a, the instrument comprises a gradiometer probe immersed in a bath of liquid helium contained in the interior vessel of a Dewar made of a fiber glass laminate. A wrapping of about 50 alternating layers of fiber glass cloth and aluminized Mylar covering the interior vessel reduces radiative heat flow across the vacuum separating the inner vessel and outer jacket of the Dewar. The outer jacket is 26" in diameter and 48" in length, and the Dewar weighs about 250 lbs. Liquid helium in the reservoir, which has a capacity of 160 liters, boils off to the atmosphere at a rate somewhat less than 3 liters per day.

The probe supports a rectangular block (2" X 2" X 12") of high-purity, crystalline silicon. Two loops of niobium wire mounted on a lateral face of the block form the pickup circuit of the gradiometer. Three small niobium disks mounted on slides near the top loop provide means of adjusting the effective area and orientation of the loop in order to balance response of the loops to a uniform magnetic flux. A niobium capsule fixed midway between loop centers contains a torodial, point-contact type SQUID that senses differential magnetic flux threading the pickup loops.

The silicon block is housed at the foot of the probe in a tube 3" in diameter and 15" long, which fits into a matching socket fixed to the bottom of the helium reservoir. Both the housing and its socket are made of a laminate reinforced with Kevlar* cloth. Four fiber glass rods with reinforcing spacers attach the foot of the probe to its top plate, which bolts to the top of the Dewar. The top

* Kevlar is a trade name for an organic fiber manufactured by the Du Pont Co.

plate of the probe holds an rf electronics box used to drive the SQUID, three removable brass micrometers used to adjust slides during balancing, and a three-axis fluxgate magnetometer used both to orient the gradiometer axis and to provide vernier balancing, as described subsequently.

A. DESIGN FEATURES

Because susceptibility of paramagnetic substances is inversely proportional to temperature at temperatures of a few degrees Kelvin, we use, where practical, materials within the helium bath that are free of paramagnetic impurities in order to eliminate noise from magnetization currents driven by fluctuations of ambient temperature and pressure and of the earth's magnetic field. In addition to its high purity, crystalline silicon has a high thermal conductivity that smooths thermal gradients in the neighborhood of the gradiometer pickup loops.

Although the laminate reinforced with Kevlar cloth is effectively free of paramagnetic impurities, the fiber glass laminate is contaminated. Susceptibility of the fiber glass laminate, resulting from paramagnetic impurities, is about 2×10^{-4} at $4.2^{\circ}K$. Nonetheless, alternatives to a fiber glass interior vessel, such as quartz, are as yet impractical for the large capacity Dewars required for operating at remote field sites.

Fluctuations of the earth's magnetic field also drive eddy currents in the aluminized Mylar layers wrapped around the interior vessel to reduce radiative heat flow. Because dielectric materials are poor reflectors, conducting layers are required to reflect radiant heat. Noise resulting from fluctuating eddy currents, however, does not markedly in-

crease with decreasing frequency because amplitude of eddy current fluctuations is proportional to excitation frequency.

B. SUPERCONDUCTING CIRCUIT

Figure 2b is a diagram of the superconducting circuit. Two coplanar pickup loops, each 1.45 cm in diameter and spaced 25 cm between centers, are oppositely wound in series, so that fluctuations of the super current, I_1, in the pickup circuit are driven by fluctuations in the net ambient flux threading the pickup loops. Fluctuations in the net flux are coupled to the SQUID sensor through an rfi transformer containing a normal metal shield between its superconducting windings that attenuates interference at radio frequencies (above 19 KHz). The flux coupled to the sensor is the product of the super current, I_2, in the coupling circuit and the mutual inductance between the sensor and the field coil. The SQUID sensor itself is effectively an open circuit for low frequency fluctuations (Zimmerman, 1971).

Because the net voltage around each superconducting circuit vanishes, the flux coupled to the sensor, Φ_s, is proportional to the net flux threading the pickup loops, Φ_p; namely,

$$\frac{\Phi_s}{\Phi_p} = \frac{K_t K_s \left[(L_s/L_p)\ \ell_1 \ell_2\right]^{1/2}}{(1+\ell_1)(1+\ell_2)-K_t^2 \ell_1 \ell_2} \qquad (1a)$$

where $\ell_1 = L_1/L_p$; $\ell_2 = L_2/L_f$; L_p, L_s, L_f, L_1, and L_2 are self inductances of the circuit components labeled in Figure 2b; and the coefficients K_t and K_s are a measure of coupling between windings of the rfi transformer and between the field coil and the SQUID sensor, respectively. Equation 1a shows

that the flux coupled to the sensor is greatest for $\ell_1 = \ell_2 = (1-K_t^2)^{-1/2}$, at fixed values of L_p and L_s, and that its greatest value is given by

$$\left(\frac{\Phi_s}{\Phi_p}\right)_m = \frac{K_s}{2}\,(L_s/L_p)^{1/2}\left[\frac{K_t}{1+(1-K_t^2)^{1/2}}\right] \qquad (1b)$$

In our instrument, L_p = 300 nH, L_s = 0.05 nH, K_s = 0.7, and windings in the rfi transformer are adjusted to give a maximum flux ratio of

$$\left(\frac{\Phi_s}{\Phi_p}\right)_m = 2.26 \times 10^{-3} \qquad (2)$$

with K_t = 0.8.

From the diameter and spacing of the pickup loops, we find that an ambient gradient* of 5.32 pT/m produces a net ambient flux of one quantum, Φ_o, at the pickup loops. Equation 2 then tells us that a gradient of 1 pT/m at most applies a flux of $4.25 \times 10^{-4}\ \Phi_o/(\text{pT/m})$ at the SQUID sensor. A change in flux of one quantum applied to the SQUID gives an output of 12.7 volts. At best, then, we expect a calibration constant of 5.4 mV/(pT/m). Our measured value is 4.5 mV/(pT/m) $\pm$ 15%, which indicates that the instrument is operating with nearly the maximum flux ratio.

* We use MKS units throughout and conform to the international convention suggesting use of the unit Tesla, which is a Weber/m^2 and so 1pT/m = 10^{-12}T/m = 10^{-10}G/cm = 10^{-3}gamma/m and $\Phi_o = 2.07 \times 10^{-3}\,\text{pTm}^2$.

Section III
INSTRUMENT RESPONSE TO AMBIENT MAGNETIC GRADIENTS

We describe the response of an axis of a superconducting magnetic gradiometer to ambient magnetic gradients in terms of the differential magnetic flux threading the two pickup loops whose centers are separated by a distance 2s. Areas of the loops are A_1 and A_2, and respective normals to the plane of each loop are directed along unit vectors $\hat{n}_1$ and $\hat{n}_2$, as shown in Figure 3. Pickup loops are connected in opposition, so that the instrument responds to the differential magnetic flux threading the loops; namely, $\Phi = \Phi_1 - \Phi_2$.

The relations

$$\Phi_1 = \int_{A_1} d\vec{\rho}_1 \hat{n}_1 \cdot \vec{b}(\vec{R}+\vec{s}+\vec{\rho}_1, t) \tag{3a}$$

and

$$\Phi_2 = \int_{A_2} d\vec{\rho}_2 \hat{n}_2 \cdot \vec{b}(\vec{R}-\vec{s}+\vec{\rho}_2, t) \quad , \tag{3b}$$

express magnetic flux threading each loop in terms of integrals of the density of magnetic flux, $\vec{b}(\vec{R}+\vec{s}+\vec{\rho}_1, t)$ and $\vec{b}(\vec{R}-\vec{s}+\vec{\rho}_2, t)$, at points within each loop. Here, $\vec{R}$ is a position vector locating the point midway between loop centers; vectors $\vec{s}$ and $-\vec{s}$ locate loop centers with respect to the midpoint; $\vec{\rho}_1$ and $\vec{\rho}_2$ are radius vectors locating points within a loop contour; and integrals extend over the area of each loop. By expanding flux densities in Taylor's series about the midpoint, we express the flux threading each loop as

$$\Phi_1 = A_1 \left[1 + \sum_{m=1}^{\infty} \frac{(\vec{s}\cdot\vec{\nabla})^m}{m!} \right] \hat{n}_1 \cdot \vec{b}(\vec{R},t)$$

$$+ \sum_{m=1}^{\infty} \sum_{k=1}^{m} \frac{(\vec{s}\cdot\vec{\nabla})^{m-k}}{(m-k)!\ k!} \int_{A_1} d\vec{\rho}_1 (\vec{\rho}_1 \cdot \vec{\nabla})^k \hat{n}_1 \cdot \vec{b}(\vec{R},t) \qquad (3c)$$

and

$$\Phi_2 = A_2 \left[1 + \sum_{m=1}^{\infty} \frac{(-1)^m (\vec{s}\cdot\vec{\nabla})^m}{m!} \right] \hat{n}_2 \cdot \vec{b}(\vec{R},t)$$

$$+ \sum_{m=1}^{\infty} \sum_{k=1}^{m} \frac{(-1)^{m-k} (s\cdot\nabla)^{m-k}}{(m-k)!\ k!} \int_{A_1} d\vec{\rho}_2 (\vec{\rho}_2 \cdot \vec{\nabla})^k \hat{n}_2 \cdot \vec{b}(\vec{R},t) \qquad (3d)$$

where $\vec{b}(\vec{R},t)$ is the magnetic flux density at the point midway between loor centers. For symmetrical pickup loops, integral terms of odd order in Equations 3c and 3d vanish because integrands are periodic.

If area and orientation of the loops are identical so that $A_1 = A_2 = A$ and $n_1 = n_2 = \hat{n}$, then the relation

$$\frac{\Phi}{2sA} = \frac{1}{s} \sum_{m=1}^{\infty} \frac{(\vec{s}\cdot\vec{\nabla})^{2m-1}}{(2m-1)!} \hat{n}\cdot\vec{b}(\vec{R},t)$$

$$+ \frac{1}{sA} \sum_{m=1}^{\infty} \sum_{k=1}^{m} \frac{(\vec{s}\cdot\vec{\nabla})^{2(m-k)+1}}{[2(m-k)+1]!\,(2k)!} \int_{A} d\vec{\rho} (\vec{\rho}\cdot\vec{\nabla})^{2k} \hat{n}\cdot\vec{b}(\vec{R},t) \qquad (3e)$$

gives the response, and so to first order

$$\Phi/2sA \cong (\vec{s}\cdot\vec{\nabla})\hat{n}\cdot\vec{b}(\vec{R},t). \qquad (3f)$$

Higher order terms are negligible provided gradients of the ambient field are sensibly constant over the distance between pickup loops. Specifically, we require that $(s/R)^2 \ll 1$, where R is a characteristic scale of the ambient field. In the field of a dipole, for example, R is distance from the dipole.

Because of slight differences in area and orientation of the pickup loops, however, the response includes an imbalance or error term. Using loop number two as a reference and defining $A = A_2$ and $\hat{n} = \hat{n}_2$, we then express the response of a gradiometer axis, $\Sigma(\hat{s},\hat{n};\vec{R},t) = \Phi/2sA$, to first order as

$$\Sigma(\hat{s},\hat{n};\vec{R},t) \cong \Gamma(\hat{s},\hat{n};\vec{R},t) + \vec{\delta}\cdot\vec{b}(\vec{R},t) \tag{4a}$$

where

$$\Gamma(\hat{s},\hat{n};\vec{R},t) = (\hat{s}\cdot\vec{\nabla})\hat{n}\cdot\vec{b}(\vec{R},t) \tag{4b}$$

and

$$\vec{\delta} = \frac{1}{2s}\left(\frac{A_1}{A}\ \hat{n}_1 - \hat{n}\right) \tag{4c}$$

To a first order approximation, then, the gradient term $\Gamma(\hat{s},\hat{n};\vec{R},t)$ of the response depends on gradients at the point midway between loop centers, and the imbalance or error term, $\vec{\delta}\cdot\vec{b}$, is proportional to the magnetic field at the midpoint.

We represent gradients of magnetic fields in free space by a matrix G having elements $g_{ij}(\vec{R},t)$, where

$$g_{ij} = \hat{x}_i \cdot \vec{\nabla}(\hat{x}_j \cdot \vec{b}) \quad , \qquad (i,j = 1,2,3) \tag{5a}$$

in an orthogonal basis $\{\hat{x}_i\}$. An element g_{ij} represents the gradient in a direction $\hat{x}_i$ of the component of magnetic field in a direction $\hat{x}_j$. Consequently, the relation

$$\Gamma(\hat{s},\hat{n}) = \sum_{i,j} g_{ij} s_i n_j, \tag{5b}$$

expresses the gradient in a direction $\hat{s}$ of the component of magnetic field in a direction $\hat{n}$ in terms of matrix elements in a basis $\{\hat{x}_i\}$, where s_i and n_i are components of the unit vectors $\hat{s}$ and $\hat{n}$ in the same basis.

By choosing a basis fixed at the point midway between loop centers with its $\hat{x}_3$ axis aligned along the gradiometer axis s and its x_1 axis aligned along n X s, then, we obtain the expansion

$$\Gamma(\hat{s},\hat{n},\vec{R},t) = n_2\, g_{23}(\vec{R},t) + n_3\, g_{33}(\vec{R},t) \tag{6}$$

for the gradient term of the response. For coplanar pickup loops (transverse configuration), n_3 vanishes and $n_2 = 1$; for coaxial pickup loops (longitudinal configuration), n_2 vanishes and $n_3 = 1$. A perfectly balanced gradiometer axis having a transverse configuration, then, measures skew elements of a gradient matrix, and one having a longitudinal configuration measures diagonal elements.

The axis of our gradiometer has a transverse configuration, so that its response to ambient gradients that are sensibly

constant over the distance between centers of the pickup loops (25 cm) is the sum of a transverse gradient at the point midway between pickup loops and an imbalance term that is proportional to the magnetic field at the midpoint, as expressed by the relation

$$\Sigma(\hat{s},\hat{n};\vec{R},t) = g_{23}(\vec{R},t) + \vec{\delta}\cdot\vec{b}(\vec{R},t) \qquad (7)$$

The imbalance part of the response resulting from small differences in orientation and area of the pickup loops, in effect, is the response of a magnetometer that measures the component of magnetic field in a direction $\hat{\delta}$ at the midpoint. The gradient part of the response is equivalent to a gradient of the field of a magnetic dipole located on a sphere of unit radius about the midpoint.

A. EQUIVALENT DIPOLE OF A GRADIENT FIELD

Because a magnetic field in free space is both nondivergent and irrotational, its gradients are elements of a symmetric matrix that has a vanishing trace. A matrix that is both real and symmetric is diagonal in an orthogonal basis comprised of principal axes with diagonal elements or eigenvalues λ_1, λ_2, and λ_3. Since its trace vanishes, $\lambda_1 + \lambda_2 + \lambda_3 = 0$.

We express gradients at a point of a magnetic field, then, in terms of their eigenvalues, λ_i, and eigenvectors $\hat{e}_i$, which define directions of principal axes, by using the matrix product

$$G = R\Lambda\tilde{R}, \qquad (8)$$

where the matrix G represents gradients in a fiducial basis $\{\hat{x}_i\}$. The matrix R represents a rotation from the fiducial basis to a basis comprised of eigenvectors $\hat{e}_i$, in which gradients are represented by the diagonal matrix Λ having elements λ_1, λ_2, and λ_3. Components of eigenvectors in the fiducial basis form the columns of the matrix R; namely, $r_{ik} = \hat{x}_i \cdot \hat{e}_k$. A real matrix representing a rotation is orthogonal, so that $R\tilde{R} = \tilde{R}R = I$, where tilde marks a transposed matrix and I is the unit matrix.

By adding a magnetic dipole to a gradient field, we find that the relation

$$\Gamma = R(\Lambda - R_a \Lambda_d \tilde{R}_a)\tilde{R} \qquad (9)$$

gives gradients at a field point. Here, Λ_d is a diagonal matrix whose elements are eigenvalues of the gradients of the dipole field at the point, and the matrix R_a specifies a rotation from principal axes of the ambient gradient field to principal axes of the dipole gradient field at the point. Equation 9 tells us that gradients of an ambient field are equal to gradients of a dipole field at a point whenever $R_a=I$ and $\Lambda_d=\Lambda$. At each point of an ambient field, then, we use the conditions $R_a=I$ and $\Lambda_d=\Lambda$ to define location, orientation, and moment of a dipole positioned on a sphere of unit radius about the point so that gradients of the dipole field at the point are equal to ambient gradients.*

Gradients at each point of an ambient field, then, are equivalent to the gradient field of a magnetic dipole located on a sphere of unit radius surrounding the point. Because the sense of an eigenvector is indeterminate, the dipole has three images, so that gradients at a point of an ambient field are equivalent to the gradient field of a dipole located at

* Equality of eigenvalues at a point is always possible because eigenvalues are ordered, $\lambda_1 \geq \lambda_2 \geq \lambda_3$, and their sum vanishes. The Appendix describes means of determining location, orientation, and moment of an equivalent dipole from gradients of the ambient field.

any one of four positions on the sphere. Radius of the sphere is arbitrary provided the ratio m/r^4 is constant, where m is the moment of the dipole and r, its distance from the field point. Location, orientation, and moment of equivalent dipoles change continuously from point to point.

B. GRADIENT FIELD OF A MAGNETIC DIPOLE

As illustrated in Figure 4, we specify location of a magnetic dipole, $\vec{m}$, with respect to the gradiometer basis $\left\{\hat{x}_i\right\}$ in terms of polar angles ϕ and θ defining direction of the position vector $\vec{r}$ and specify its orientation with respect to the position vector in terms of the polar angle χ and azimuthial angle Ω. The basis $\left\{\hat{y}_i\right\}$ is defined so that the $\hat{y}_3$ axis points along the position vector; the $\hat{y}_2$ axis, along $\hat{r} \times \hat{m}$; and the $\hat{y}_1$ axis, along $(\hat{r} \times \hat{m}) \times \hat{r}$.

As shown in the Appendix, the matrix

$$G_y(g,\chi) = g \begin{bmatrix} \cos\chi & 0 & \sin\chi \\ 0 & \cos\chi & 0 \\ \sin\chi & 0 & -2\cos\chi \end{bmatrix} \tag{10a}$$

represents gradients at position $\vec{r}$ of a dipole field in the basis $\left\{\hat{y}_i\right\}$, where

$$g = \frac{3\mu_o m}{4\pi r^4} \quad \text{and} \quad \mu_o = 4\pi \times 10^{-7} \text{ H/m.} \tag{10b}$$

Equation 10a tells us that longitudinal gradients result from the component of the dipole along $\vec{r}$ and that transverse gradients result from the component perpendicular to $\vec{r}$. Nonetheless, each component produces both longitudinal and transverse gradients in the gradiometer basis.

Three consecutive rotations represented by the matrix

$$R(\phi,\ \theta,\ \Omega) = Z(\phi + \pi/2)X(\theta)Z(\Omega) \tag{11a}$$

bring the gradiometer basis into coincidence with the basis $\left\{\hat{y}_i\right\}$, where

$$Z(\psi) = \begin{bmatrix} \cos\psi & -\sin\psi & 0 \\ \sin\psi & \cos\psi & 0 \\ 0 & 0 & 0 \end{bmatrix} \tag{11b}$$

and represents a rotation through an angle ψ about the $\hat{x}_3$ axis of the gradiometer basis and

$$X(\psi) = \begin{bmatrix} 1 & 0 & 0 \\ 0 & \cos\psi & -\sin\psi \\ 0 & \sin\psi & \cos\psi \end{bmatrix} \tag{11c}$$

and represents a rotation about the $\hat{x}_1$ axis.

Consequently, the matrix

$$G_x(\phi,\ \theta,\ \Omega;\ g,\chi) = R(\phi,\ \theta,\ \Omega)G_y(g,\chi)\tilde{R}(\phi,\ \theta,\ \Omega) \tag{12a}$$

represents gradients of the dipole field in the gradiometer basis. We then find that

$$\begin{aligned} G_x = {} & g\cos\chi\left[I - 3/2\ A_1\ (\phi,\ \theta)\right] \\ & +g\ \sin\chi\left[\cos\Omega\ A_2(\phi,\ \theta) - \sin\Omega\ A_3(\phi,\ \theta)\right] , \end{aligned} \tag{12b}$$

where I denotes the unit matrix,

$$A_1(\phi, \theta) = \begin{bmatrix} 2\cos^2\phi\sin^2\theta & \sin2\phi\sin^2\theta & \cos\phi\sin2\theta \\ \sin2\phi\sin^2\theta & 2\sin^2\phi\sin^2\theta & \sin\phi\sin2\theta \\ \cos\phi\sin2\theta & \sin\phi\sin2\theta & 2\cos^2\theta \end{bmatrix} \quad (12c)$$

$$A_2(\phi, \theta) = \begin{bmatrix} -\sin2\phi\sin\theta & \cos2\phi\sin\theta & -\sin\phi\cos\theta \\ \cos2\phi\sin\theta & \sin2\phi\sin\theta & \cos\phi\cos\theta \\ -\sin\phi\cos\theta & \cos\phi\cos\theta & 0 \end{bmatrix} \quad (12d)$$

and

$$A_3(\phi, \theta) = \begin{bmatrix} \cos^2\phi\sin2\theta & (1/2)\sin2\phi\sin2\theta & \cos\phi\cos2\theta \\ (1/2)\sin2\phi\sin2\theta & \sin^2\phi\sin2\theta & \sin\phi\cos2\theta \\ \cos\phi\cos2\theta & \sin\phi\cos2\theta & -\sin2\theta \end{bmatrix} \quad (12e)$$

The first term of Equation 12b results from the component of the dipole along $\vec{r}$, and the second term, from the component perpendicular to $\vec{r}$. We see that each component produces both longitudinal and transverse gradients in the gradiometer basis.

C. GRADIENT RESPONSE

From Equation 12b, then, we find that the relation

$$g_{23} = \frac{-3}{2} g \cos\chi \sin\phi \sin2\theta + g \sin\chi(\cos\Omega\cos\phi \cos\theta - \sin\Omega \sin\phi \cos2\theta) \quad (13)$$

expresses the gradient term of the instrument response in terms of the five parameters ϕ, θ, Ω, χ, and g that specify location, orientation, and moment of a dipole. Because gradients at a point are equivalent to the gradient field of a dipole located on a sphere of unit radius about the point, Equation 13 completely specifies the gradient response.

The construct of an equivalent dipole furnishes a convenient transformation of the five independent elements of a matrix representing gradients of a magnetic field in free space to five parameters (ϕ, θ, Ω, χ, and g) that provide ready means of describing the gradient response. For example, Equation 13 tells us that a dipole located along the $\hat{x}_1$ axis of the gradiometer basis ($\phi = 0$ and $\theta = \pi/2$) gives a null response whatever its orientation. Moreover, oppositely located and oppositely directed dipoles ($\phi \rightarrow \phi + \pi$, $\theta \rightarrow \pi - \theta$, and $\Omega \rightarrow -\Omega$) give the same gradient response.

The gradient field of a dipole represents gradients of a magnetic field at a point in free space even though the actual source of the field is not a dipole. Because of the principal of superposition, separate equivalent dipoles represent gradients from distinct sources. The gradient field of a dipole describing gradients resulting from a sum of distinct sources is simply the sum of fields of equivalent dipoles representing gradients from each source, but the dipoles themselves are not simply additive unless they are located colinearly. Nonetheless, fields of a sum of equivalent dipoles conveniently describe contributions of distinct sources.

D. INSTRUMENT CALIBRATION

To calibrate the gradiometer, we use a current oscillating in a coil placed equidistant from the center of each pickup loop with its dipole moment parallel to the line joining centers of the pickup loops. We face the plane containing pickup loops toward the coil to obtain a maximum response and keep the distance from the midpoint of the gradiometer axis to the center of the coil much larger than both the spacing between centers of the pickup loops (25 cm) and the radius of the coil (21 cm).

The coil, in effect, is a dipole located along the $\hat{x}_2$ axis of the gradiometer basis and directed parallel to the $\hat{x}_3$ axis, so that $\phi = 3\pi/2$, $\theta = \pi/2$, $\Omega = 3\pi/2$, and $\chi = \pi/2$. The expression

$$g_{23} = \frac{3\mu_o m(t)}{4\pi r^4} \tag{14}$$

obtained from Equation 13 then gives the gradient produced at the gradiometer, where m(t) is the dipole moment of the coil and r is its distance from the gradiometer. Equation 13 also shows that misalignment of the coil and gradiometer adds terms of second order in angular deviations and so produces negligible error for reasonably precise alignment. Errors result largely from uncertainties in the distance of the coil from the gradiometer.

By measuring current in the coil and output voltage of the gradiometer at several values of r, we find that a gradient of 1 nT/m gives an output voltage of 4.5 V $\pm$ 15%. Calibration is independent of frequency and of the quantum state of the SQUID sensor.

We also use the dipole used for calibration to align the triaxial fluxgate magnetometer with respect to the gradiometer basis. Turning the gradiometer about its axis until a null response is obtained aligns the plane containing pickup loops with the plane defined by the dipole moment of the calibration coil and the gradiometer axis. Oscillating magnetic field components along the $\hat{x}_1$ and $\hat{x}_2$ axes of the gradiometer basis then vanish, so we align corresponding axes of the fluxgate magnetometer to obtain null responses as well.

Section IV

GRADIOMETER BALANCING

Both mechanical and electronic means of balancing the gradiometer are available. We balance mechanically by using micrometers on the top plate of the probe to move three small niobium disks mounted on slides near the top pickup loop. Because a superconducting disk distorts the magnetic field in its vicinity, movement of the disks adjusts the effective orientation and area of the loop. Axes of the disks are mutually orthogonal, so that movement of each disk, in effect, adjusts the corresponding component of the imbalance vector $\vec{\delta}$.

Because precision of disk movements is limited, however, we use the triaxial fluxgate magnetometer mounted on the top plate of the probe to provide vernier balancing electronically. We balance electronically by subtracting an adjustable fraction of the magnetic field components measured by the fluxgate magnetometer from the gradiometer response.

To make mechanical and electronic balance adjustments, we rotate the gradiometer axis in the earth's steady magnetic field. Because gradients of the earth's steady magnetic field are small ($\sim$10 pT/m), rotation in the earth's field furnishes a time varying field that is nearly uniform, so that the gradiometer response effectively results from imbalance alone.

A. BALANCING IN A UNIFORM MAGNETIC FIELD

Rotating a gradiometer about an axis in a direction $\hat{\Omega}$ in a uniform magnetic field, $\vec{B}$, produces a response owing to imbalance of its pickup loops that is expressed in terms of

the angle of rotation Ω by the relation

$$\vec{\delta}\cdot\vec{B} = (\vec{B}\cdot\hat{\Omega})(\hat{\Omega}\cdot\vec{\delta}_o) + \left[\hat{\Omega}x(\vec{B}x\hat{\Omega})\right]\cdot\vec{\delta}_o\cos\Omega + (\vec{B}x\hat{\Omega})\cdot\vec{\delta}_o\sin\Omega \quad , \tag{15}$$

where $\vec{\delta}_o$ is the initial position of the imbalance vector $\vec{\delta}$. The imbalance vector is fixed to the gradiometer, so that $\vec{\delta}_o$ depends on initial orientation of the gradiometer. As is evident from Equation 15, we define a fiducial basis using the vectors $\vec{B}$ and $\hat{\Omega}$.

As before, we choose a right-handed basis fixed to the point midway between centers of the pickup loops with its $\hat{x}_3$ axis along their line of centers and its $\hat{x}_2$ axis normal to the plane containing pickup loops. We denote components of the imbalance vector in the gradiometer basis by δ_1, δ_2, and δ_3.

In our balancing procedure, the axis of rotation is vertical, and the earth's magnetic field provides an effectively uniform field. We use two initial orientations of the gradiometer basis in order to make sequential and independent adjustments of components of the imbalance vector.

First, we initially orient the gradiometer with the $\hat{x}_3$ axis directed vertically upwards; the $\hat{x}_2$ axis, northward; and the $\hat{x}_1$ axis, eastward. Rotating the gradiometer about its $\hat{x}_3$ axis through an angle Ω then gives the response

$$\vec{\delta}\cdot\vec{B} = -\delta_3 B\sin\beta + (\delta_1\sin\Omega + \delta_2\cos\Omega)B\cos\beta \quad , \tag{16}$$

where β is the local dip angle of the earth's magnetic field and B is its magnitude. Equation 16 tells us that a cosine response corresponds to the δ_2 component of the imbalance

vector and that a sine response corresponds to the δ_1 component. The δ_3 component determines a reference level of the sinusoidal response. To nullify components δ_1 and δ_2 of the imbalance vector, we first adjust the niobium disk having its axis parallel to $\hat{x}_1$ until rotation produces a cosine response and then adjust the disk having its axis parallel to $\hat{x}_2$ until rotation produces a flat response.

Next, we initially align the gradiometer with the $\hat{x}_3$ axis parallel to the earth's magnetic field and the $\hat{x}_2$ axis directed westward. Rotating the gradiometer about a vertical axis through an angle Ω then gives the response

$$\vec{-\delta}.\vec{B} = (\delta_1\cos\beta + \delta_3\sin\beta)\, B\sin\beta + \left[\delta_2\sin\Omega - (\delta_1\sin\beta - \delta_3\cos\beta)\cos\Omega\right] B\cos\beta \qquad (17)$$

Equation 17 tells us that a cosine response corresponds to components δ_1 and δ_3 of the imbalance vector and that a sine response corresponds to the δ_2 component. To complete balancing the gradiometer, then, we only adjust the disk having its axis parallel to $\hat{x}_3$ until rotation produces a flat response, because the first procedure nullifies components δ_1 and δ_2.

B. LIMITS ON GRADIOMETER BALANCE

Both limited precision of disk movements and mutual inductances between disks limit the balance attainable mechanically, and so prevent attainment of precisely flat responses during rotations. Mechanical adjustments reduce components of the imbalance vector to values of the order of 10^{-5} m^{-1}*. To reduce imbalance further, we electronically subtract a fraction of magnetic field components measured by the flux-

* Balance of a gradiometer is also commonly expressed in terms of a common mode rejection ratio (CMRR) that is the magnitude of the imbalance vector multiplied by the distance between centers of its pickup loops. For our gradiometer, an imbalance of 10^{-5} m^{-1} gives a CMRR of 2.5 ppm.

gate magnetometer from the gradiometer response during rotations, after reaching the limit of mechanical adjustments. Combined mechanical and electronic adjustments reduce components of the imbalance vector to values of about 4×10^{-6} m^{-1}.

Further refinement of gradiometer balance presently is limited by hysteresis observed during rotation when the imbalance is somewhat less than 10^{-5} m^{-1}. The record in Figure 5 illustrates the effect. The trace records gradiometer response during a clockwise rotation followed by a counter clockwise rotation with the gradiometer axis vertical. Rotations are made stepwise in sixteen increments of 22.5^{o}, as shown in Figure 6, starting with the $\hat{x}_2$ axis pointing northward. Spikes in Figure 5 mark movements between incremental positions and result from eddy currents excited in aluminized Mylar layers used to insulate the helium reservoir. Plateaus mark values recorded while dwelling at incremental positions. As is evident, values recorded at incremental positions are not unique and depend on the sense of rotation; namely; the value recorded at a position during a clockwise rotation differs from the value recorded at the same position during a counter clockwise rotation.

Figure 7 shows the hysteretic signature of the effect. The trace records response during a stepwise oscillation of the $\hat{x}_2$ axis about position 5 marked in Figure 6. Oscillation begins with a clockwise movement of two increments from position 5 to position 7, then reverses with a counter clockwise movement to position 5, continues with a counter clockwise movement of two increments to position 3, returns to position 5 with a clockwise movement, and repeats the cycle thereafter. As is evident in Figure 7, the value recorded at position 5 depends on the direction of approach; namely, the value recorded during a

clockwise crossing differs from the value recorded during a counter clockwise crossing. The difference depends on amplitude of the oscillation.

We observe a similar hysteretic signature when oscillations are made with a crescent wrench taped to the top of the Dewar and so suspect that the hysteretic effect results from ferromagnetic contaminants in the vicinity of the pickup loops. Although hysteresis precludes further reduction of gradiometer imbalance, the residual imbalance is insignificant for our immediate purposes.

Eddy currents excited in the aluminized Mylar insulation during rotations do not limit refinement of gradiometer balance but do require that rotations be made stepwise. Continuous rotation, in effect, averages values at spikes and plateaus and so is misleading for purposes of refining balance. The response resulting from eddy currents, Σ_e, is consistent with the description given by the relation

$$\Sigma_e = C \frac{d}{dt}(\vec{B}.\vec{A}) = CB\cos\beta\ A\left(\frac{d\Omega}{dt}\right)\sin\Omega \quad , \tag{18}$$

where $\vec{B}$ is the earth's magnetic field; $\vec{A}$, the effective area of eddy current loops; C, a coupling constant; and Ω is the angle of rotation, reckoned positive for a clockwise rotation. The vector representing effective area of eddy current loops is normal to the plane containing pickup loops. Allowing for a difference in rates of movement between increment positions, Figure 5 shows that spikes resulting from eddy currents are greatest at $\pi/2$ and $3\pi/2$, least at 0 and π, and of opposite sense for clockwise and counter clockwise rotations, as described by Equation 18.

Gradients of the earth's magnetic field are a more fundamental limit on refinement of gradiometer balance. Gradients of the earth's magnetic field are of the order of 10 pT/m and so give a response comparable to the response owing to imbalance when magnitude of the imbalance vector is about 5×10^{-7} m^{-1} or less. In the absence of the limit imposed by hysteresis, reduction of gradiometer imbalance below about 10^{-6} m^{-1} is limited by gradients of the earth's magnetic field.

C. BALANCING IN A NONUNIFORM MAGNETIC FIELD

Because a matrix representing gradients of a magnetic field in free space is symmetric, it is diagonal in a basis comprised of principal axes. Transverse gradients vanish along principal axes, so that a perfectly balanced gradiometer having a transverse configuration gives a null response when its axis is aligned along a principal axis of an ambient gradient field. The Appendix describes both a means of determining directions of principal axes of a gradient field from values of its matrix elements measured in a fiducial basis and response of a perfectly balanced gradiometer during rotation about an arbitrary axis.

To refine balance of our gradiometer in the presence of a nonuniform magnetic field, then, we align its axis along a principal axis of the ambient gradient field and rotate it about its axis. Because transverse gradients vanish along a principal axis, the response during rotation results from imbalance alone. We then adjust components of the imbalance vector to obtain a flat response during rotation. Precise determination of directions of principal axes, however, requires a finely balanced gradiometer, so we devise an iterative procedure.

We suppose that directions of principal axes of the ambient gradient field are known approximately. For example, two principal axes of the earth's dipolar magnetic field lie in a vertical plane containing the magnetic field vector, and the third principal axis is normal to the plane.* If ambient gradients exceed about 10 nT/m, then we use the gradiometer itself to estimate approximate directions of principal axes, because magnitude of its imbalance vector without refinement is at most about 10^{-4} m^{-1}. Rotating the gradiometer about its axis when it is aligned with the local magnetic field vector gives an estimate of the magnitude of ambient gradients, since the response owing to imbalance then vanishes.

The relation

$$g_{23}(\Omega) = (\gamma_{13}^2 + \gamma_{23}^2)^{1/2} \cos(\Omega + \Omega_o) \tag{19a}$$

with

$$\tan\Omega_o = \gamma_{13}/\gamma_{23} \tag{19b}$$

gives the response owing to ambient gradients when the gradiometer is rotated through an angle Ω about its axis. Coefficients γ_{13} and γ_{23} are elements of the matrix representing the ambient gradient field in the basis defined by initial orientation of the gradiometer. If the gradiometer axis is aligned along a principal axis of the ambient gradient field, then γ_{13} and γ_{23} vanish, so that the response owing to ambient gradients during rotation is flat. If polar angles defining direction of the axis of rotation in a fiducial basis deviate by amounts $\Delta\phi$ and $\Delta\theta$, respectively, from polar angles defining

*The Appendix describes the gradient field of a magnetic dipole in terms of its eigenvalues and directions of its principal axes.

direction of the principal axis corresponding to eigenvalue λ_3 say, then

$$\gamma_{13} \cong 1/2 \left[3\lambda_3 - (2\lambda_1 + \lambda_3)\cos 2\Psi_p\right] \sin\theta_p(\Delta\phi) \qquad (19c)$$

$$-1/2(2\lambda_1 + \lambda_3)\sin 2\Psi_p(\Delta\theta)$$

and

$$\gamma_{23} \cong -1/2(2\lambda_1 + \lambda_3)\sin 2\Psi_p \sin\theta_p(\Delta\phi) \qquad (19d)$$

$$+1/2 \left[3\lambda_3 + (2\lambda_1 + \lambda_3)\cos 2\Psi_p\right] (\Delta\theta)$$

where Φ_p, Θ_p and Ψ_p are Euler angles(defined in Figure A1) specifying a rotation from the fiducial basis to the basis comprised of principal axes and λ_1, λ_2, and λ_3 are corresponding eigenvalues.

We choose a fiducial basis $\left\{\hat{X}_i\right\}$ with its $\hat{X}_3$ axis directed vertically downwards, its $\hat{X}_1$ axis, northward, and its $\hat{X}_2$ axis, eastward. To align the gradiometer axis with a principal axis, we start with the gradiometer basis coincident with the fiducial basis and first rotate the gradiometer through an angle θ about the $\hat{X}_1$ axis and then through an angle ϕ about the $\hat{X}_3$ axis, where the polar angles ϕ and θ approximately define direction of the principal axis in the fiducial basis. We then rotate the gradiometer about its axis and mark the amplitude of its response. We next make an incremental rotation $\delta\phi$ about the $\hat{X}_3$ axis and again rotate the gradiometer about its axis and mark the amplitude of its response. We continue making incremental rotations about the $\hat{X}_3$ axis followed by rotations about the gradiometer axis until we determine the polar angle $\phi + \delta\phi$ at which amplitude of the response is least.

With the gradiometer axis fixed at the polar angle $\phi + \delta\phi$, we carry out a similar procedure to determine the polar angle $\theta + \delta\theta$ at which amplitude of the response is least and so locate the polar angles $\phi + \delta\phi$ and $\theta + \delta\theta$ defining direction of the principal axis more precisely.

The response resulting from imbalance is sensibly constant for incremental changes $\delta\phi$ and $\delta\theta$ in the polar angles, but the response resulting from ambient gradients changes markedly for small deviations of the axis of rotation from the principal axis. Nonetheless, imbalance eventually masks changes in amplitude of the response to rotation as the axis of rotation approaches the principal axis. When incremental changes in polar angles defining direction of the axis of rotation produce imperceptible changes in amplitude of the response, we then adjust components δ_1 and δ_2 of the imbalance vector to reduce the response owing to imbalance, following a procedure similar to that used in a uniform field.

After refining the balance, we refine alignment of the gradiometer axis with the principal axis by again making incremental changes in polar angles until we determine the direction of the axis of rotation for which amplitude of the response is least. We then again refine the balance and repeat the procedure until further refinements are imperceptible.

The iterative procedure affords means of reducing components δ_1 and δ_2 of the imbalance vector. To reduce the δ_3 component, we rotate the gradiometer about its $\hat{x}_1$ axis through an angle χ after aligning its axis with the principal axis. The relation

$$g_{23}(\chi) = 1/2 \left[3\lambda_3 + (2\lambda_1 + \lambda_3)\cos 2\Psi_p \right] \sin 2\chi \qquad (20)$$

gives the response resulting from ambient gradients. The response resulting from imbalance, however, is sinusoidal with respect to χ rather than 2χ. Consequently, we adjust the δ_3 component of the imbalance vector during rotation until the response is proportional to sin 2χ.

Because our present means of rotating the gradiometer only provides for rotation about a horizontal and a vertical axis, the suggested procedure for balancing in a nonuniform ambient magnetic field is as yet untried.

Section V

INSTRUMENT PERFORMANCE

Past reports (Clarke, 1974; Wynn et al., 1975; Zimmerman and Frederick, 1971) have specified performance of superconducting magnetic gradiometers in terms of a noise level without regard to spectral shape. Recent measurements (Clarke et al., 1975) of noise spectra of a superconducting quantum interference device (SQUID), however, show that their noise power density increases approximately in inverse proportion to frequency as frequency falls below about 1 Hz. Moreover, fluctuations of ambient temperature and pressure and of the earth's magnetic field drive fluctuating magnetization currents and eddy currents in materials within the Dewar that generate noise whose power density characteristically increases with decreasing frequency as well. Characterizing instrument performance in terms of a noise level, then, is inadequate in the frequency range of interest (f<1 Hz).

In what follows, we first present spectral data in the frequency range 5×10^{-4} Hz to 20 Hz that characterize performance of the instrument, which is designed insofar as practical to eliminate sources of noise driven by fluctuations of ambient temperature and pressure and of the earth's magnetic field, and demonstrate that its performance in a magnetically quiet environment is limited by noise of its SQUID sensor at frequencies below about 0.1 Hz. We then compare performance demonstrated using a torodial point-contact type SQUID sensor with performance expected using a thin-film dc type SQUID, in order to mark limits on enhancing instrument performance. Finally, we delineate improvements in instrument design.

A. GRADIOMETER NOISE SPECTRA IN A MAGNETICALLY QUIET ENVIRONMENT

To characterize performance of the gradiometer in the frequency range 5 X 10^{-4} Hz to 20 Hz, we made a number of records* of its output, ranging from 12 to 24 hours in duration, for a variety of ambient conditions during an observational period of several weeks at the La Posta Astrogeophysical Observatory, which is located in the mountains about 70 miles east of San Diego, California, at an altitude of 1188 m MSL. Coordinates of the observatory are 116° 25' 6" west longitude and 32° 40' 39" north geodetic latitude (Bleiweiss and Wefer, 1975). We present spectral data based on a five hour long segment of a record that is representative of the lowest instrument noise consistently observed.

Figure 8 shows the spectral power density in the frequency range 5 X 10^{-4} Hz to 20 Hz characterizing performance of the instrument during a quiet period observed at night. We estimate the spectrum below 0.1 Hz using a standard fast Fourier Transform algorithm and average ten successive estimates made from 1/2 hour segments of the time series. We obtain spectral data at frequencies above 0.1 Hz using a real-time spectrum analyzer having an averaging capability.

For frequencies below 0.1 Hz, we assume a spectrum of the form $S(f) = S(f_o)(f_o/f)^{\gamma}$ and then use a least squares criterion to fit averaged spectral data to a straight line in logarithmic coordinates to obtain values of γ and $S(f_o)$. Values corresponding to the spectrum shown in Figure 8 are $\gamma = 1.3$ and $S(f_o) = 0.002$ $(pT/m)^2/Hz$ at $f_o = 1$ Hz, for $f<0.1$ Hz. Spectral power densities

* We use a low-pass filter having its half-power point at 0.3 Hz to preclude aliasing and digitally record on magnetic tape once a second to obtain data at frequencies below 0.1 Hz. We obtain spectral data at frequencies above 0.1 Hz using a real-time spectrum analyzer having an averaging capability.

in the frequency range 0.1 Hz to 20 Hz correspond to a white noise level of 0.03 $(pT/m)^2/Hz$. Additional estimates made near 10^2 Hz and 10^3 Hz correspond to the same white noise level.

We present spectra characterizing instrument performance during quiet times in order to demonstrate that the inherent noise spectrum of the gradiometer is in practice limited by the intrinsic noise spectrum of the SQUID sensor alone at frequencies below 0.1 Hz. Data* points in Figure 9 depict the spectrum of intrinsic noise of a torodial, point-contact type SQUID having the same design as that used in the gradiometer. The solid line delineates the spectrum of gradiometer noise shown in Figure 8. Figure 9 shows that the spectrum of gradiometer noise closely approaches that of the SQUID at frequencies below 0.1 Hz. Parameters characterizing the form of the SQUID spectrum have the values $\gamma = 1.1$ and $S(f_o) = 2.4 \times 10^{-3} (pT/m)^2/Hz$ at $f_o = 1$ Hz as compared to the values $\gamma = 1.3$ and $S(f_o) = 2.1 \times 10^{-3} (pT/m)^2/Hz$ at $f_o = 1$ Hz of the gradiometer spectrum.

At frequencies above 0.1 Hz, however, the gradiometer noise level is appreciably higher than the SQUID noise level. The increase in gradiometer white noise over that of the SQUID largely results from Johnson noise coming from the normal metal shield in the transformer. We expect the shield to increase the noise level by a factor of two or so, which is comparable to the observed increase of nearly a factor of four. Without an rfi transformer, we would expect to attain a white noise level limited by intrinsic white noise of the

* Data presented in Figures 9 and 10 are provided by courtesy of John Clarke and his research group at the University of California, Berkeley, California.

SQUID sensor. Presuming a maximum flux ratio of $(\phi_s/\phi_p)_n = 4.52 \times 10^{-3}$ without an rfi transformer (obtained from Equation 1b with $K_t = 1$), then, we would expect a white noise level for the gradiometer of about $10^{-3}(pT/m)^2/Hz$, which is comparable to the noise level of $3 \times 10^{-2}(pT/m)/\sqrt{Hz}$ reported by Wynn et al., (1975) that largely results from intrinsic noise of their sensor.

Although intrinsic noise of the SQUID sensor dominates the noise spectrum of the gradiometer below 0.1 Hz during quiet observational periods, we observe occasional increases in slope and level of spectra below 0.1 Hz that apparently are associated with semidiurnal effects. We expect to characterize sources of noise driven by fluctuating ambient conditions by spectrally analyzing fluctuations of ambient temperature and pressure and of the earth's magnetic field recorded at the field site.

B. INSTRUMENT IMPROVEMENT

Because intrinsic noise of its SQUID sensor limits instrument performance, replacing the torodial point-contact type SQUID in the instrument with a thin-film dc type SQUID (Clarke et al., 1975) is an immediate means of enhancing instrument performance. Measurements of noise spectra of the two types of SQUID sensors show that spectral density of the thin-film dc type, in units of ϕ_o^2/Hz, is appreciably smaller than spectral density of the torodial point-contact type at frequencies below about 0.1 Hz (Clarke, personal communication, 1975). Moreover, self-inductance of a thin-film dc type SQUID is about 1 nH compared to 0.05 nH for a torodial point-contact type. Equation 1b then tells us that coupling of flux to a thin-film dc type sensor is greater than coupling to a torodial point-contact type sensor, in the same superconducting circuit. Namely, equivalent noise energy in the pickup loops, ϕ_p^2/L_p, is proportional

to noise energy of the SQUID sensor, ϕ_s^2/L_s, for fixed values of the coupling coefficients K_s and K_t. The ratio ϕ_s^2/L_s provides a figure-of-merit for comparing performance of SQUID sensors (Classen, 1975).

Data points in Figure 10 depict the spectrum of intrinsic noise of a thin-film dc type SQUID in units of Φ_o^2/Hz marked on the right hand coordinate scale. The light dashed curve delineates the spectrum of intrinsic noise of a torodial point-contact type sensor, in units of Φ_o^2/Hz, as depicted by data points in Figure 9. The solid line marks the spectrum of inherent noise of the gradiometer in units of $(pT/m)^2$/Hz, marked on the left hand coordinate scale, as depicted by data points in Figure 8. The heavy dashed curve marks the spectrum of inherent noise expected of a gradiometer operating with a thin-film dc type SQUID. We obtain the expected gradiometer noise spectrum in units of $(pT/m)^2$/Hz from the spectrum of intrinsic noise of a thin-film dc type sensor in units of Φ_o^2/Hz by using the conversion factor 1.56×10^{-3} $\Phi_o/(pT/m)$, which accounts for the change in self-inductance of the SQUID in the superconducting circuit.

At frequencies below 10^{-3} Hz, then, intrinsic noise of the thin-film dc type SQUID limits expected performance of the gradiometer, and at frequencies above 10^{-3} Hz, Johnson noise from the normal metal shield in the rfi transformer limits performance. Figure 10 shows that the expected enhancement of instrument performance is substantial at frequencies below about 0.1 Hz. For example, in the frequency band from 0.001 to 0.01 Hz, RMS instrument noise is reduced from 0.17 pT/m to 0.017 pT/m, a tenfold enhancement of performance.

We suggest two improvements in instrument design -- one trivial and the other substantial. First, scoring aluminized Mylar layers wrapped around the interior vessel of the Dewar reduces strength of eddy currents excited in the superinsulation. Second, a triaxial superconducting magnetometer should be incorporated at the midpoint of the gradiometer axis both to provide more accurate means of balancing and aligning the gradiometer, and to afford measurement of the magnetic field as well as its gradients at a point.

Section VI

TECHNIQUES FOR SUPPRESSING NOISE FROM NEARBY MAGNETIC OBJECTS

Fluctuating gradients of magnetic fields resulting from ionospheric currents are too small to be directly observed at the ground. Nonetheless, ionospheric currents excite magnetization and eddy currents in magnetic objects near a gradiometer and so indirectly produce local, fluctuating gradients. Moreover, objects magnetized by the earth's magnetic field produce sharp, steady gradients in their vicinity. Slight, irregular movements of a gradiometer near magnetic objects, then, produce gradient fluctuations as well.*

Fluctuating gradients owing to nearby magnetic objects can mask ambient gradient fluctuations of interest. Consequently, we consider techniques for suppressing gradient fluctuations resulting from small, irregular movements of a gradiometer relative to a steady gradient field and from fluctuating magnetization currents.

As we have shown, gradients of a magnetic field at a point in free space are equivalent to the gradient field of a magnetic dipole located on a sphere of unit radius about the point. Changes in location, orientation, and moment of an equivalent dipole then describe gradient fluctuations owing to magnetic objects. Two techniques for suppressing fluctuations are available: (1) aligning the gradiometer to obtain a null response and (2) using a magnetic dipole to cancel gradients of an equivalent dipole.

* Because of residual gradiometer imbalance, irregular movements in a uniform magnetic field also produce gradient fluctuations, but the fluctuations are comparitively negligible for ambient gradients exceeding 10 pT/m.

A. SUPPRESSION OF NOISE FROM IRREGULAR MOVEMENTS

Small displacements of a gradiometer in a steady gradient field produce small changes in location, orientation, and moment of the equivalent dipole describing gradients of the ambient field in the neighborhood of the gradiometer. Changes in location result both from virtual rotations of the dipole accompanying small displacements at fixed gradiometer orientation and from actual gradiometer rotations, but changes in orientation and moment result from displacement alone.

From Equation 12a that gives gradients in a gradiometer basis in terms of the gradient field of a dipole, we find that the relation

$$G_{xo} + \delta G_x = R_o R_\delta (G_{yo} + \delta G_y) \tilde{R}_\delta \tilde{R}_o \tag{23a}$$

expresses gradients in the gradiometer basis following a small displacement from an initial point marked by subscript zero, where

$$\delta G_y = \frac{\delta g}{g_o} G_{yo} + \delta\chi G_y(g_o, \chi_o + \pi/2) \quad . \tag{23b}$$

The matrix R_δ represents an infinitesimal rotatio that we express in terms of angular deviations in location and orientation of the dipole by the sum

$$\begin{aligned} R_\delta = I &+ \delta\theta\cos\Omega_o \varepsilon_x - (\delta\phi\sin\theta_o\cos\Omega_o + \delta\theta\sin\Omega_o)\varepsilon_y \\ &+ \left[\delta\Omega + \delta\phi(\cos\theta_o - \sin\theta_o\sin\Omega_o)\right]\varepsilon_z \end{aligned} \tag{23c}$$

where

$$\varepsilon_x = \begin{bmatrix} 0 & 0 & 0 \\ 0 & 0 & -1 \\ 0 & 1 & 0 \end{bmatrix}, \quad \varepsilon_y = \begin{bmatrix} 0 & 0 & 1 \\ 0 & 0 & 0 \\ -1 & 0 & 0 \end{bmatrix}, \text{ and } \quad \varepsilon_z = \begin{bmatrix} 0 & -1 & 0 \\ 1 & 0 & 0 \\ 0 & 0 & 0 \end{bmatrix} \tag{23d}$$

From Equation 23a we then find that the relation

$$\begin{aligned} \delta G_x = {} & \frac{\delta g}{g_o} G_{xo} + \delta\chi G_x(\phi_o, \theta_o, \Omega_o; g_o, \chi_o + \pi/2) \\ & + (\delta\Omega \sin\theta_o \cos\phi_o - \delta\theta \sin\phi_o)(\varepsilon_x G_{xo} - G_{xo}\varepsilon_x) \\ & + (\delta\theta \cos\phi_o + \delta\Omega \sin\theta_o \sin\phi_o)(\varepsilon_y G_{xo} - G_{xo}\varepsilon_y) \\ & + (\delta\phi + \delta\Omega \cos\theta_o)(\varepsilon_z G_{xo} - G_{xo}\varepsilon_z) \end{aligned} \tag{24}$$

gives first order changes of gradients in the gradiometer basis following a small displacement in a steady gradient field, which is represented by the matrix G_{xo} at the initial point. Equation 24 shows that changes in gradients are proportional to the initial values represented by the matrix G_{xo}.

To suppress gradient fluctuations resulting from irregular motions, then, we first judiciously choose initial orientation of the gradiometer basis with respect to the equivalent dipole. We align the gradiometer so that the equivalent dipole lies along the $\hat{x}_1$ axis with its axis in the plane containing pick-up loops, which is normal to the $\hat{x}_2$ axis of the gradiometer basis. Namely, we take $\phi_o = 0$, $\theta_o = \pi/2$, and $\Omega_o = \pi/2$, so that

$$G_{xo} = g_o \begin{bmatrix} -2\cos\chi_o & 0 & \sin\chi_o \\ 0 & \cos\chi_o & 0 \\ \sin\chi_o & 0 & \cos\chi_o \end{bmatrix} . \tag{25}$$

Slight deviations in initial alignment give fluctuations of second order during irregular motions and so are negligible.

Gradient changes resulting from small displacements or rotations from the initial orientation are then given by the expression

$$\delta G_x = \frac{\delta g}{g_o} G_{xo} + \delta\chi G'_{xo} + \delta\Omega(\varepsilon_x G_{xo} - G_{xo}\varepsilon_x) + \delta\theta(\varepsilon_y G_{xo} - G_{xo}\varepsilon_y) + \delta\phi(\varepsilon_z G_{xo} - G_{xo}\varepsilon_z) \quad , \tag{26a}$$

where

$$G'_{xo} = g_o \begin{bmatrix} 2\sin\chi_o & 0 & \cos\chi_o \\ 0 & -\sin\chi_o & 0 \\ \cos\chi_o & 0 & -\sin\chi_o \end{bmatrix} \quad , \tag{26b}$$

$$\varepsilon_x G_{xo} - G_{xo}\varepsilon_x = g_o \begin{bmatrix} 0 & -\sin\chi_o & 0 \\ -\sin\chi_o & 0 & 0 \\ 0 & 0 & 0 \end{bmatrix} \quad , \tag{26c}$$

$$\varepsilon_y G_{xo} - G_{xo}\varepsilon_y = g_o \begin{bmatrix} 2\sin\chi_o & 0 & 3\cos\chi_o \\ 0 & 0 & 0 \\ 3\cos\chi_o & 0 & -2\sin\chi_o \end{bmatrix} \quad , \tag{26d}$$

and

$$\varepsilon_z G_{xo} - G_{xo}\varepsilon_z = g_o \begin{bmatrix} 0 & -3\cos\chi_o & 0 \\ -3\cos\chi_o & 0 & \sin\chi_o \\ 0 & \sin\chi_o & 0 \end{bmatrix} \quad . \tag{26e}$$

As a result, we see that changes in the transverse gradient, g_{23}, measured by the gradiometer result from effective rotations about the gradiometer axis alone; namely,*

* The same result is obtained by differentiating Equation 13 that gives the gradient response in terms of parameters specifying location, orientation, and moment of an equivalent dipole.

$$\delta g_{23} = \delta\phi g_o \sin\chi_o \ . \tag{27}$$

Magnitude of a gradient fluctuation is then the product of an effective angular deviation and a transverse gradient resulting from the component of the equivalent dipole along the gradiometer axis (the $\hat{x}_3$ axis). The effective angular deviation $\delta\phi$ is a sum of an angular deviation $\delta\phi_v$ owing to virtual rotation of the equivalent dipole accompanying displacement and an actual angular deviation $\delta\phi_a$ owing to rotation of the gradiometer basis.

To suppress gradient fluctuations resulting from effective rotations about the gradiometer axis, we position a dipole along the $\hat{x}_1$ axis of the gradiometer basis with its axis parallel to the $\hat{x}_3$ axis and adjust its moment so that it cancels the component of the equivalent dipole along the $\hat{x}_3$ axis. Specifically, we position the dipole so that $\phi_o^d = 0$, $\theta_o^d = \pi/2$, $\Omega_o^d = 3\pi/2$, and $\chi_o^d = \pi/2$ and adjust its moment so that $g_o^d = g_o \sin\chi_o$. Changes in the transverse gradient measured by the gradiometer that result from small displacements in the steady gradient field of the dipole are then expressed by the relation

$$\delta g_{23}^d = -\delta\phi^d g_o \sin\chi_o \ , \tag{28}$$

where $\delta\phi^d = \delta\phi_v^d + \delta\phi_a$.

Consequently, small displacements in the steady ambient field with the cancelling dipole in position give gradient changes expressed by the sum

$$\delta g_{23} + \delta g_{23}^d = (\delta\phi_v - \delta\phi_v^d) g_o \sin\chi_o \ . \tag{29}$$

Although angular deviations owing to actual rotation of the gradiometer are the same for both the equivalent dipole and the cancelling dipole and so cancel, angular deviations owing to virtual rotations accompanying displacement differ to the extent that curvature of the ambient field deviates locally from curvature of the cancelling dipole field.

Because we can position a dipole used to cancel gradients at a point at different distances from the point by adjusting its moment*, we can adjust the difference in angular deviations owing to virtual rotations accompanying small displacements. We place the dipole close to the point of cancellation, if the equivalent dipole representing the ambient gradient field rotates markedly during a small displacement, and far from the point, if it rotates slightly. Namely, we choose the distance from the point of cancellation to make curvatures of the dipole and ambient magnetic fields comparable.

Although initial misalignment of the cancelling dipole gives gradient fluctuations of second order in angular deviations and so is negligible for reasonably precise alignment, small displacements and/or rotations of the cancelling dipole itself relative to the ambient field produce additional gradient fluctuations of first order and so degrade its effectiveness. Fluctuations of the moment of the cancelling dipole, however, produce gradient fluctuations of second order. To be effective then, positioning of a dipole to cancel ambient transverse gradients must be steady with respect to the ambient field and reasonably precise, but its moment may fluctuate. Ideally, a cancelling dipole should be rigidly fixed to a magnetic object producing a local gradient field.

* The ratio m/r^4 is constant.

B. SUPPRESSION OF NOISE FROM FLUCTUATING MAGNETIZATION

In the absence of magnetic objects, the ambient magnetic field. $\vec{B}(t)$, is effectively uniform and comprises the earth's steady magnetic field, $\vec{B}_o$, and a small fluctuating magnetic field, $\vec{b}(t)$, resulting from electric currents in the ionosphere. A magnetic object distorts the ambient field and so produces steady gradients of the magnetic field in its vicinity as well as gradients that fluctuate as the uniform ambient field fluctuates. An object having a large magnetic permeability, for example, warps the surrounding magnetic field until resulting field lines are nearly normal to its surface.

Gradients of the magnetic field in the vicinity of a stationary magnetic object fluctuate as the undisturbed ambient field, which magnetizes the object, changes in strength and direction in response to ionosphere currents. Magnitudes of gradients are proportional to the strength of the ambient field divided by a characteristic length of an object and decrease with distance from an object as a power of its characteristic length divided by distance.

For example, a spherical iron shell magnetized by a uniform magnetic field, $\vec{B}(t)$, produces an induced magnetic field outside the shell that is described by the field of a magnetic dipole located at the center of the sphere. The dipole points along the uniform magnetizing field, and its moment $\vec{m}(t)$ is given by the expression

$$\vec{m}(t) = \frac{4\pi\chi}{\delta}\left[1 - \left(\frac{R^i}{R_o}\right)^3\right] R_o^3 \vec{B}(t) \ , \qquad (30a)$$

where

$$\delta = 3 + \chi \left[1 - \frac{(R_i/R_o)^3}{1+(3/2\chi)} \right] \quad . \tag{30b}$$

Here, R_o is the outer radius of the shell; R_i, its inner radius; and χ its magnetic susceptibility. Because magnetic susceptibility of iron is large ($\chi \sim 1000$), $\vec{m}(t) \cong 4\pi R_o^3 \vec{B}(t)$.

Gradients of the magnetic field surrounding an iron sphere, then, are everywhere described by the gradient field of a magnetic dipole that is fixed at the center of the sphere and changes its direction and moment in response to changes in direction and strength of the uniform ambient magnetic field. The equivalent dipole representing gradients at each point of the field is the actual dipole and so lies along a radial vector emanating from the center of the sphere.

Consequently, we find from Equation 13 that the transverse gradient measured by the gradiometer at a position defined by a radial vector $\vec{r}$ is expressed as

$$g_{23}(\vec{r},t) = g(t)\left\{\sin\chi(t)\left[\cos\Omega(t)\cos\phi\cos\theta - \sin\Omega(t)\sin\phi\cos2\theta\right] - \frac{3}{2}\cos\chi(t)\sin\phi\sin2\theta\right\} \quad , \tag{31a}$$

where

$$g(t) \cong \frac{3B(t)}{R_o}\left(\frac{R_o}{r}\right)^4 \tag{31b}$$

$\chi(t)$ and $\Omega(t)$ specify direction of the dipole axis with respect to the radial vector $\vec{r}$, and ϕ and θ specify direction of the radial vector in the gradiometer basis. Equation 31a tells us

that aligning the $\hat{x}_1$ axis of the gradiometer basis along a radial vector ($\phi = 0$ and $\theta = \pi/2$) gives a null response whatever the dipole orientation and so completely suppresses noise from fluctuating magnetization currents in the sphere. Slight misalignment of the gradiometer, however, gives the response

$$\Delta g_{23}(\vec{r},t) = g(t)\sin\chi(t)\left[\Delta\phi\sin\Omega(t) - \Delta\theta\cos\Omega(t)\right], \tag{31c}$$

where $\Delta\phi$ and $\Delta\theta$ specify misalignment of the $\hat{x}_1$ axis and radial vector $\vec{r}$.

Nonetheless, the fluctuating part of the earth's magnetic field is much smaller than the steady part, so that

$$g(t) = g_o + \delta g(t), \text{ with } \delta g(t)/g_o = b_{//}(t)/B_o \tag{32a}$$

$$\chi(t) = \chi_o + \delta\chi(t), \text{ with } \delta\chi(t) = \frac{(\hat{r} \times \vec{B}_o)}{B_o \sin\chi_o} \cdot \frac{(\vec{B}_o \times \vec{b}_\perp(t))}{B_o^2} \tag{32b}$$

and

$$\Omega(t) = \Omega_o + \delta\Omega(t), \text{ with } \delta\Omega(t)\sin\chi_o = \frac{(\hat{r} \times \vec{B}_o)}{B_o \sin\chi_o} \cdot \frac{\vec{b}_\perp(t)}{B_o} \tag{32c}$$

Here, χ_o and Ω_o give the direction of $\vec{B}_o$ with respect to $\vec{r}$,

$$g_o = \frac{3B_o}{R_o}\left(\frac{R_o}{r}\right)^4, \tag{32d}$$

$$\vec{b}_{//}(t) = \left[\frac{\vec{B}_o \cdot \vec{b}(t)}{B_o^2}\right]\vec{B}_o, \tag{32e}$$

which is the component of the fluctuating part of the field parallel to $\vec{B}_o$, and

$$\vec{b}_{\perp}(t) = \frac{\vec{B}_o \times (\vec{\omega} \times \vec{B}_o)}{B_o^2} \quad , \tag{32f}$$

which is the component perpendicular to $\vec{B}_o$. Consequently, allowing for slight misalignment, Equation 31c shows that gradient fluctuations resulting from fluctuating magnetization currents in an iron sphere are of second order and so negligible when the $\hat{x}_1$ axis of the gradiometer is aligned along a radial vector.

For an intricately shaped object, we surmise that an equivalent dipole describing gradients at a point near the object changes not only its orientation and moment but also its location as strength and direction of the earth's magnetic field fluctuates. Gradient fluctuations resulting from fluctuating magnetization currents are then, in effect, equivalent to fluctuations resulting from irregular motions. Fluctuating magnetization currents in an intricately shaped magnetic object produce virtual rotation of an equivalent dipole.

Aligning the gradiometer so that the equivalent dipole determined from the steady gradient field of a magnetic object lies along the $\hat{x}_1$ axis of the gradiometer basis with its axis in the plane containing pickup loops nullifies gradient fluctuations resulting from fluctuations of the dipole orientation and moment produced by fluctuations of the earth's magnetic field. Virtual rotations of the equivalent dipole produced by fluctuations of the earth's magnetic field then give gradient changes expressed by the relation

$$\delta g_{23} = \delta\phi_{vm} g_o \sin\chi_o \quad , \tag{33}$$

where $\delta\phi_{vm}$ is the apparent angle of rotation about the gradiometer axis.

Section VII

PRELIMINARY TESTS OF NOISE SUPPRESSION TECHNIQUES

Our field tests* of noise suppression techniques are necessarily preliminary because the wooden gimbal used to orient the gradiometer provides only vertical and horizontal axes of rotation and so both restricts gradiometer orientation (three axes of rotation provide unrestricted orientation) and limits precision of alignment to about 0.1 radian or a few degrees. We report results of tests of two techniques: (1) use of a current in a coil approximating a magnetic dipole to cancel the steady gradient field at a point near a magnetic object and (2) aligning the gradiometer to suppress gradient fluctuations from fluctuating magnetization currents in an iron sphere. In each case, we first summarily describe the technique, give a detailed procedure, and then present results of preliminary tests.

A. CANCELLING STEADY GRADIENTS

To cancel steady gradients at a point near a magnetic object, we place a coil at the position of an equivalent dipole corresponding to gradients at the point and adjust current in the coil to nullify the gradients. We determine positions of equivalent dipoles by measuring gradients in a fiducial basis, calculating corresponding eigenvalues and eigenvectors, and transforming to a description in terms of location, orientation, and moment of associated equivalent dipoles. After placing the coil at a position determined from gradients measured in the fiducial basis, we drive an oscillating current in the coil and adjust its location and

* We do tests at the La Posta Astrogeophysical Observatory located in the mountains about 70 miles east of San Diego, California. Coordinates of the observatory are 116° 25' 6" west longitude and 32° 40' 39" north geodetic latitude (Bleiweiss and Wefer, 1975).

orientation to obtain a null response at the gradiometer with the gradiometer basis aligned along principal axes of the ambient gradient field. We then tilt the gradiometer away from principal axes and adjust a steady current in the coil until rotating the gradiometer about its axis gives a null response.

1. Procedure

To determine the five independent steady gradients γ_{ij} defined in a fiducial basis $\{\hat{z}_i\}$, we rotate the gradiometer about each one of three axes forming a linearly independent triad. Rotating the gradiometer through an angle Ω about its axis gives the sinusoidal response expressed by the relation

$$g_{23} = U \cos \Omega - V \sin \Omega \tag{34a}$$

Amplitudes U and V depend on initial orientation of the gradiometer basis. Measuring amplitude and phase of the sinusoidal response developed during a complete rotation determines the coefficients U and V corresponding to an initial orientation.

For the three axes of rotation, we choose the $\hat{z}_3$ axis of the fiducial basis and two axes defined by the two sets of polar angles $(\theta,\pi/2)$ and $(\theta,0)$ with respect to the fiducial basis. When the gradiometer basis is initially coincident with the fiducial basis, coefficients U and V are equal to the gradients γ_{23} and γ_{13}, respectively. Rotating the gradiometer about its axis then, in effect, measures the gradients γ_{23} and γ_{13}. When the axis of the gradiometer is aligned with an axis of rotation defined by polar angles θ and $\pi/2$, the coefficients are given by the relations

$$U = \gamma_{23}\cos\theta - \frac{1}{2}(\gamma_{22}-\gamma_{33})\sin 2\theta \tag{34b}$$

and

$$V = \gamma_{13}\cos\theta - \gamma_{12}\sin\theta \tag{34c}$$

Rotating the gradiometer then gives a measure of γ_{12} and the difference $(\gamma_{22}-\gamma_{33})$, once γ_{23} and γ_{13} are determined. Finally, when the gradiometer axis is aligned along an axis of rotation defined by polar angles θ and 0, the coefficients are given by the relations

$$U = \gamma_{23}\cos\theta + \gamma_{12}\sin\theta \tag{34d}$$

and

$$V = \gamma_{13}\cos 2\theta + \frac{1}{2}(\gamma_{11}-\gamma_{33})\sin 2\theta \tag{34e}$$

Rotating the gradiometer then gives a measure of the difference $(\gamma_{11}-\gamma_{33})$, once γ_{23}, γ_{13}, and γ_{12} are determined. Because the sum of longitudinal gradients vanishes, the three rotations give a measurement of the independent gradients γ_{11}, γ_{33}, γ_{12}, γ_{13}, and γ_{23} defined in the fiducial basis.

From the five gradients, we determine three eigenvalues $(\lambda_1>\lambda_2>\lambda_3)$, corresponding eigenvectors $(\hat{e}_1, \hat{e}_2, \hat{e}_3)$, and three Euler angles (Φ, Θ, Ψ) that specify a rotation $R_p(\Phi, \Theta, \Psi)$ from a fiducial basis to the basis comprised of principal axes defined by the eigenvectors*. Namely, we establish the relation

$$G = R_p \Lambda \tilde{R}_p \tag{35}$$

that gives the matrix G describing gradients in the fiducial basis in terms of R_p and the diagonal matrix Λ whose elements are the eigenvalues λ_1, λ_2, and λ_3. Gradients in the fiducial basis, however, are also equal to gradients of the field of a magnetic dipole.

* The Appendix delineates calculation of eigenvalues, eigenvectors, and Euler angles from gradients of an ambient field.

The relation

$$G = R(\phi, \theta, \Omega)\tilde{Y}(\alpha)\Lambda Y(\alpha)\tilde{R}(\phi, \theta, \Omega) \tag{35a}$$

gives gradients of the field of a magnetic dipole located with respect to a fiducial basis by polar angles ϕ and θ defining direction of its position vector $\vec{r}$ and oriented with respect to the position vector by the azimuthal angle Ω and polar angle χ, as defined in Figure 4. The matrix $R(\phi, \theta, \Omega)$ represents three consecutive rotations, as defined by Equation 11a, that bring the fiducial basis into coincidence with the basis $\left\{\hat{y}_i\right\}$ defined in Figure 4. and

$$\tilde{Y}(\alpha) = \begin{bmatrix} \cos\alpha & 0 & -\sin\alpha \\ 0 & 1 & 0 \\ \sin\alpha & 0 & \cos\alpha \end{bmatrix} \tag{35b}$$

and represents a rotation through an angle $-\alpha$ about the $\hat{y}_2$ axis that brings the basis $\left\{\hat{y}_i\right\}$ into coincidence with principal axes of the gradient field of the dipole when $\tan 2\alpha = (2/3)\tan\chi$. Eigenvalues of the gradient field of a dipole equal eigenvalues of an ambient gradient field when

$$\tan\chi = \frac{\left|\lambda_1 \lambda_3\right|^{1/2}}{\lambda_2}, \quad 0<\chi<\pi \tag{35c}$$

and

$$g = \frac{\mu_o 3m}{4\pi r^4} = \left|\lambda_2^2 + \lambda_1 \lambda_3\right|^{1/2}, \tag{35d}$$

where m is the moment of the dipole and r, its distance from the field point.

Consequently, Equations 35 and 35a tell us that gradients of a dipole field equal gradients of an ambient field when location (ϕ, θ), orientation (χ, Ω), and moment of the dipole are determined by the relation

$$R_p(\phi, \theta, \Psi) = R(\phi, \theta, \Omega)\tilde{Y}(\alpha) \tag{36a}$$

together with Equations 35c and 35d. Polar angles ϕ_m and θ_m specifying direction of the dipole axis in the fiducial basis are determined by the relation

$$R(\phi, \theta, \Omega)Y(\chi) = Z(\phi_m + \pi/2)X(\theta_m), \tag{36d}$$

where matrices $Z(\psi)$ and $X(\psi)$ are given by Equations 11b and 11c.

From Equations 35a and 36a, we then find that gradients of the field of an arbitrarily positioned dipole are expressed in the basis comprised of principal axes of an ambient gradient field by the relation

$$\Gamma = Y_e\tilde{R}_e R\tilde{Y}\Lambda_d Y\tilde{R}R_e\tilde{Y}_e \quad , \tag{37a}$$

where elements of the diagonal matrix Λ_d are eigenvalues of the gradient field of the dipole and subscript e marks matrices corresponding to an equivalent dipole. If a dipole is near the position of an equivalent dipole, then $R = R_eR_\delta$, $Y = Y_eY_\delta$, and $\Lambda_d \cong (g/g_e)(\Lambda + \delta\Lambda)$, so that

$$\Gamma \cong (g/g_e)Y_eR_\delta\tilde{Y}_\delta\tilde{Y}_e(\Lambda + \delta\Lambda)Y_eY_\delta\tilde{R}_\delta\tilde{Y}_e \tag{37b}$$

where the ratio g/g_e gives magnitude of gradients of the dipole field relative to ambient gradients and $\delta\Lambda$ is proportional to $\delta\chi$.

The matrix product $Y_e R_\delta \tilde{Y}_\delta \tilde{Y}_e$ represents an infinitesimal rotation that we express in terms of angular deviations in location and orientation of the dipole by the sum

$$Y_e R_\delta \tilde{Y}_\delta \tilde{Y}_e = I + \delta\psi_x \varepsilon_x + \delta\psi_y \varepsilon_y + \delta\psi_z \varepsilon_z \quad , \tag{37c}$$

where

$$\delta\psi_x = \delta\phi(\cos\theta_e \sin\alpha_e + \sin\theta_e \sin\Omega_e \cos\alpha_e) + \delta\theta \cos\Omega_e \cos\alpha_e + \delta\Omega \sin\alpha_e \quad , \tag{37d}$$

$$\delta\psi_y = \delta\phi \sin\theta_e \sin\Omega_e - \delta\theta \sin\Omega_e - \delta\alpha \quad , \tag{37e}$$

$$\delta\psi_z = \delta\phi(\cos\theta_e \cos\alpha_e - \sin\theta_e \sin\Omega_e \sin\alpha_e) - \delta\theta \cos\Omega_e \sin\alpha_e + \delta\Omega \cos\alpha_e \quad , \tag{37f}$$

elementary matrices ε_x, ε_y, and ε_z are given by Equation 23d, and we find from Equation 36d that

$$\delta\Omega = (\delta\phi_m - \delta\phi)\cos\theta_e + \delta\theta_m \sin(\phi_e - \phi_{me}) \sin\theta_e \tag{37g}$$

and

$$\delta\chi = \delta\theta_m \left[\cos\theta_e \cos\Omega_e \sin(\phi_{me} - \phi_e) - \sin\Omega_e \cos(\phi_{me} - \phi_e)\right] - \delta\theta \sin\Omega_e + (\delta\phi_m - \delta\phi) \sin\theta_e \cos\Omega_e \tag{37h}$$

Consequently, we find from Equation 37b that

$$\Gamma \cong (g/g_e)(\Lambda + \delta\Lambda + \delta T) \quad , \tag{38a}$$

and, to first order in angular deviations, that the relation

$$(g/g_e)\delta T = (g/g_e)\begin{bmatrix} 0 & (\lambda_1-\lambda_2)\delta\psi_z & (\lambda_3-\lambda_1)\delta\psi_y \\ (\lambda_1-\lambda_2)\delta\psi_z & 0 & (\lambda_2-\lambda_3)\delta\psi_x \\ (\lambda_3-\lambda_1)\delta\psi_y & (\lambda_2-\lambda_3)\delta\psi_x & 0 \end{bmatrix} \tag{38b}$$

gives transverse gradients in the basis comprised of principal axes of an ambient gradient field. Specifically, the expression

$$g_{23} \cong (g/g_e)(\lambda_2-\lambda_3)\delta\psi_x \tag{38c}$$

gives response of the gradiometer when the gradiometer basis coincides with the basis comprised of principal axes of an ambient gradient field, and the expression

$$g_{23} = (g/g_e)\left[(\lambda_2-\lambda_3)\delta\psi_x\cos\psi - (\lambda_3-\lambda_1)\delta\psi_y\sin\psi\right] \tag{38d}$$

gives response when the gradiometer is rotated through an angle ψ about its axis. Equation 38b tells us that true alignment of a dipole at the position of an equivalent dipole gives a null response whatever the dipole moment. Moreover, large dipole moments provide means of discerning minute misalignment.

To position and align the moment of a coil approximating a magnetic dipole precisely at the location and orientation of an equivalent dipole of an ambient gradient field, then, we first align the gradiometer basis coincident with the basis comprised of principal axes of the ambient gradient field, as described subsequently, and place the coil at the location and orientation of an equivalent dipole determined from measurements of gradients in a fiducial basis. We then drive the coil with current oscillating at a frequency of say 5 Hz and adjust location and orientation of the coil until the peak at 5 Hz in the spectrum of gradiometer response (as displayed by a real-time spectrum analyzer) falls below the noise level of the instrument. The plane defined by the dipole axis, $\hat{m}$, and position vector, $\vec{r}$, is then normal to the eigenvector $\hat{e}_2$. Next, we rotate the gradiometer 90 degrees about its axis, so that pickup loops face the dipole, and again adjust location of the coil until the spectral peak falls below the level of instrument noise. Principal axes of the gradient field of the dipole are then coincident with principal axes of the ambient gradient field, so that the matrix δT vanishes, but the matrix $\delta\Lambda$ does not necessarily vanish. Finally, we return the gradiometer to the fiducial basis and adjust a steady current in the coil until rotating the gradiometer about its axis gives a minimum response so that $g/g_e = -1$. The response during rotation is then proportional to $g_e\delta\chi$.

To align the gradiometer basis precisely coincident with the basis comprised of principal axes of an ambient gradient field, we initially align the basis with principal axes determined from measurements of gradients in a fiducial basis, so that the matrix

$$\Gamma = \Lambda - \delta\tau \tag{39a}$$

represents gradients in the gradiometer basis, where elements of the diagonal matrix Λ are eigenvalues of the ambient gradient field and

$$\delta\tau = \begin{bmatrix} 0 & (\lambda_1-\lambda_2)\delta\tau_z & (\lambda_3-\lambda_1)\delta\tau_y \\ (\lambda_1-\lambda_2)\delta\tau_z & 0 & (\lambda_2-\lambda_3)\delta\tau_x \\ (\lambda_3-\lambda_1)\delta\tau_y & (\lambda_2-\lambda_3)\delta\tau_x & 0 \end{bmatrix} \tag{39b}$$

Angular deviations are given by the relations

$$\delta\tau_x = \delta\Phi\sin\Theta\sin\Psi + \delta\Theta\cos\Psi \tag{39c}$$

$$\delta\tau_y = \delta\Phi\sin\Theta\cos\Psi - \delta\Theta\sin\Psi \tag{39d}$$

and

$$\delta\tau_z = \delta\Phi\cos\Theta + \delta\Psi \tag{39e}$$

where $\delta\Phi$, $\delta\Theta$, and $\delta\Psi$ are deviations in the Euler angles Φ, Θ, and Ψ that define a rotation from the fiducial basis to the basis comprised of principal axes of the ambient gradient field.

Rotating the gradiometer about its axis through an angle ψ then gives the response expressed by the relation

$$g_{23}(\psi) = (\lambda_3-\lambda_2)\delta\tau_x\cos\psi - (\lambda_1-\lambda_3)\delta\tau_y\sin\psi \tag{40a}$$

Equation 40a tells us that true alignment of the gradiometer axis with the eigenvector $\hat{e}_3$ gives a null response during rotation of the gradiometer about its axis, so we adjust angular deviations $\delta\Phi$ and $\delta\Theta$ until rotation gives a null response.

Similarly, rotating about the $\hat{x}_2$ axis of the gradiometer basis gives the response expressed by the relation

$$g_{23}(\psi) = (\lambda_3-\lambda_2)\delta\tau_x\cos\psi + (\lambda_2-\lambda_1)\delta\tau_z\sin\psi \qquad (40b)$$

Equation 40b tells us that true alignment of the $\hat{x}_2$ axis of the gradiometer basis with the eigenvector $\hat{e}_2$ gives a null response during rotation and so affords means of adjusting the angular deviation $\delta\Psi$.

2. Results of Preliminary Tests

The wooden gimbal used to orient the gradiometer provides only vertical and horizontal axes of rotation and so precludes aligning the gradiometer basis coincident with the basis comprised of principal axes of an ambient gradient field. Although we can not use the present gimbal to test thoroughly the procedure outlined above for cancelling ambient gradients, our preliminary tests show that a steady current in a coil placed approximately in the position of an equivalent dipole reduces ambient gradients by about a factor of 100.

To facilitate positioning the coil, we first chose to cancel ambient gradients resulting from an iron sphere, which was placed 4.5 m north of the gradiometer and has a radius of 0.74 m. Magnitude of the earth's magnetic field is about 4.5×10^4 nT at the test site, so that the dipole induced at the center of the sphere by the earth's magnetic field produces gradients having magnitudes proportional to

$$g = \frac{3B}{R_o}\left(\frac{R_o}{r}\right)^4 = 133 \text{ nT/m}$$

The relation

$$g_{23} = g\left[\sin\chi\cos\Omega\cos\theta\cos\phi-(\sin\chi\sin\Omega\cos2\theta + \frac{3}{2}\cos\chi\sin2\theta)\sin\phi\right] \quad (41a)$$

gives the gradiometer response to the induced dipole, where polar angles ϕ and θ specify direction, in the gradiometer basis, of the position vector $\vec{r}$ pointing from the dipole to the gradiometer, as shown in Figure 4, and angles χ and Ω define direction of the dipole axis, which is parallel to the earth's magnetic field, with respect to the position vector. Because of rough terrain at the test site, the center of the sphere is somewhat above the center of the gradiometer, but we place the sphere so that the position vector and gradiometer axis lie approximately in a vertical plane containing the earth's magnetic field vector. Then $\Omega \cong 3\pi/2$, and so

$$g_{23} \cong \frac{1}{2}(\lambda_1-\lambda_3)\sin2(\theta-\alpha)\sin\phi \quad , \quad (41b)$$

where the expression

$$\lambda_1-\lambda_3 = g(4+5\cos^2\chi)^{1/2} \quad (41c)$$

gives the difference in eigenvalues λ_1 and λ_3 of gradients of the induced dipole field and the angle α, determined by the relation $\tan 2\alpha = (2/3)\tan\chi$, gives inclination of the eigenvector $\hat{e}_3$ to the position vector, as shown in Figure 11, and $\chi = \pi-(\phi_d+\theta_d)$. The local dip angle of the earth's magnetic field, ϕ_d, is about 55° at the site, and the dip angle of the position vector, θ_d, is about 5° or so.

Rotating the gradiometer about its axis ($0<\phi<2\pi$) and measuring amplitude of the response gives a gradient magnitude of 56 nT/m, and so we conclude from Equation 41b that $\theta-\alpha \cong 11^\circ$, which tells us that the gradiometer axis is tilted somewhat

from vertical. Because alignment procedures at the site are crude at present, we expect angular deviations of the order of 0.1 radians or a few degrees.

To cancel gradients of the induced dipole field, we place a coil about 5.6 m north of the gradiometer and align its axis parallel to the earth's magnetic field vector. The coil comprises 1000 turns of wire wound on an aluminum frame about 0.97 m in diameter. After making slight adjustments in lateral position and orientation of the coil, we find that a current of 0.6 A in the coil reduces amplitude of the response to rotation of the gradiometer about its axis from 56 nT/m to 0.49 nT/m, or by a factor of 100. For a current of 0.6 A, the moment of the coil is 444 A m^2, and so

$$g_c = \frac{3\mu_o m}{4\pi r^4} = 135 \text{ nT/m} ,$$

with r = 5.6 m, which is nearly equal to the strength of gradients produced by the sphere, g = 133 nT/m.

Because a magnetic dipole parallel to the earth's magnetic field at the center of an iron sphere describes the gradient field surrounding the sphere, placing a coil at the position of an equivalent dipole of the gradient field is straightforward. For irregularly shaped magnetic objects, however, determination of location and orientation of equivalent dipoles requires measurement of gradients in a fiducial basis. As a first test of cancellation techniques for irregularly shaped objects, we placed a collection of oil drums and steel planks approximately 5 m north of the gradiometer.

We define a fiducial basis by rotating the gradiometer about its axis, when vertical, until a null response is obtained, so that g_{23} vanishes in the fiducial basis. To measure gradients in the fiducial basis, we rotate the gradiometer first through an angle ϕ about its axis (the $\hat{x}_3$ axis of the gradiometer basis) and then through an angle θ about the $\hat{x}_2$ axis of the gradiometer basis, so that the expression

$$g_{23} = \left[\gamma_{12}\cos 2\phi - \tfrac{1}{2}(2\gamma_{11}+\gamma_{33})\sin 2\phi\right]\sin\theta - \gamma_{13}\sin\phi\cos\theta \qquad (42a)$$

gives its response in terms of gradients, γ_{ij}, in the fiducial basis and angles of rotation. Rotations about the gradiometer axis, $\theta = 0$, and about horizontal axes corresponding to $\phi = 0$ and $\phi = \pi/4$ then determine gradients γ_{13} and γ_{12} and the sum $2\gamma_{11} + \gamma_{33}$. Next, we rotate the gradiometer through an angle ψ about the $\hat{x}_1$ axis of the gradiometer basis, so that the expression

$$g_{23} = \tfrac{1}{2}(\gamma_{11} + 2\gamma_{33})\sin 2\psi \qquad (42b)$$

gives its response in terms of gradients in the fiducial basis and the angle of rotation and so determines the sum $\gamma_{11} + 2\gamma_{33}$. Since γ_{23} vanishes, the procedure measures the four nonvanishing gradients in the fiducial basis.

From gradients measured in the fiducial basis, we find, as described in the Appendix, location, orientation, and gradient strength g of the two pairs of equivalent dipoles corresponding to the collection of magnetic objects. The gradient strength of the objects is about 67 nT/m, and the plane containing axes of equivalent dipoles is no longer vertical as for the iron sphere but is tilted about 30° from vertical about the $\hat{x}_1$ axis of the fiducial basis.

Because the gimbal used to orient the coil provides only a horizontal axis of rotation, it precludes accurately aligning the axis of the coil in a tilted plane. Crude placement of the coil at the position of an equivalent dipole, however, reduced gradients by about a factor of 30.

B. ALIGNING FOR NULL RESPONSE

To suppress gradient fluctuations resulting from fluctuating magnetization currents in nearby magnetic objects, we orient the gradiometer so that an equivalent dipole corresponding to the steady gradient field of the objects lies along the $\hat{x}_1$ axis of the gradiometer basis with its axis in the plane containing pickup loops. To align the gradiometer, we begin by following the procedure described for cancelling steady gradients. Namely, we align the gradiometer basis coincident with the basis comprised of principal axes of the steady gradient field and precisely position a coil at the location and orientation of an equivalent dipole.

With a current oscillating in the coil, we then tilt the gradiometer about the $\hat{x}_2$ axis of the gradiometer basis and rotate it about its axis until a maximum response is attained so that pickup loops face the coil. Next, we point the axis of the coil directly toward the gradiometer and turn the gradiometer about the $\hat{x}_1$ axis of the gradiometer basis until a null response is obtained. The axis of the coil then lies along the $\hat{x}_2$ axis of the gradiometer basis.

Finally, we return the axis of the coil to its initial position and turn the gradiometer about its axis until a null response is obtained. The coil then lies along the $\hat{x}_1$ axis of the gradiometer basis with its axis in the plane containing pickup loops. The response then vanishes for every orientation of the coil.

1. Procedure

To align the gradiometer for a null response from a current oscillating in a coil positioned at the location and orientation of an equivalent dipole, we first align the gradiometer basis coincident with the basis comprised of principal axes and then turn the gradiometer through an angle $\pi/2 - \alpha$ about the $\hat{x}_2$ axis of the gradiometer basis, so that the coil then lies along the $\hat{x}_1$ axis of the gradiometer basis with its axis in the plane containing pickup loops. The matrix

$$R_a(\phi_a, \theta_a, \psi_a) = R_p(\Phi, \Theta, \Psi)\tilde{Y}(\pi/2 - \alpha) \tag{43a}$$

represents consecutive rotations of the gradiometer from a fiducial basis first to the basis comprised of principal axes (represented by R_p) and then about the $\hat{x}_2$ axis of the gradiometer basis through the angle $\pi/2 - \alpha$. Angles Φ, Θ, and Ψ are Euler angles specifying a rotation to the basis comprised of principal axes, and the angles ϕ_a, θ_a, and ψ_a are Euler angles specifying the rotation that aligns the gradiometer for a null response; namely,

$$R_a(\phi_a, \theta_a, \psi_a) = Z(\phi_a + \pi/2)X(\theta_a)Z(\psi_a) \tag{43b}$$

From Equation 36a that specifies location and orientation of an equivalent dipole in terms of Euler angles defining a rotation to a basis comprised of principal axes, we then find that

$$R_a(\phi_a, \theta_a, \psi_a) = R(\phi, \theta, \Omega)\tilde{Y}(\pi/2) \ , \tag{44a}$$

so that the relations

$$\cos\theta_a = \sin\theta\cos\Omega \tag{44b}$$

$$\sin\theta_a \sin(\phi - \phi_a) = -\sin\Omega \tag{44c}$$

$$\sin\theta_a \cos(\phi - \phi_a) = -\cos\theta\cos\Omega \tag{44d}$$

$$\cos\psi_a = \sin\theta\sin(\phi - \phi_a) \tag{44e}$$

and

$$\sin\psi_a = \cos\theta\sin\theta_a - \sin\theta\cos\theta_a\cos(\phi - \phi_a) \tag{44f}$$

give Euler angles ϕ_a, θ_a, and ψ_a in terms of angles ϕ, θ, and Ω that specify location and orientation of an equivalent dipole.

When the gradiometer is aligned for a null response, gradients are given by the relation

$$\Gamma = \tilde{R}_a G R_a \tag{45a}$$

where the relation

$$G = R(\phi,\ \theta,\ \Omega) G_y(g,\chi) \tilde{R}(\phi,\ \theta,\ \Omega) \tag{45b}$$

with $G_y(g,\chi)$ given by Equation 10a, gives gradients in the fiducial basis resulting from current in the coil positioned at the location and orientation of an equivalent dipole. For true alignment, then,

$$\Gamma_o = Y(\pi/2) G_y(g,\chi) \tilde{Y}(\pi/2) = g \begin{bmatrix} -2\cos\chi & 0 & -\sin\chi \\ 0 & \cos\chi & 0 \\ -\sin\chi & 0 & \cos\chi \end{bmatrix} \tag{45c}$$

where χ is the polar angle giving inclination of the axis of the coil to its position vector. Equation 45c shows that gra-

dients are then independent of the azimuthal angle Ω and that the gradiometer response vanishes whatever the polar angle χ and so vanishes for every orientation of the coil.

For misalignment of the gradiometer, $R_a = R_{ao}R_{a\delta}$, where $R_{a\delta}$ represents an infinitesimal rotation. We then find that

$$\Gamma = \Gamma_o - g\delta\Gamma_a \tag{46a}$$

where

$$\delta\Gamma_a = \delta A_x \begin{bmatrix} 0 & \sin\chi & 0 \\ \sin\chi & 0 & 0 \\ 0 & 0 & 0 \end{bmatrix} + \delta A_y \begin{bmatrix} -2\sin\chi & 0 & 3\cos\chi \\ 0 & 0 & 0 \\ 3\cos\chi & 0 & 2\sin\chi \end{bmatrix} - \delta A_z \begin{bmatrix} 0 & 3\cos\chi & 0 \\ 3\cos\chi & 0 & \sin\chi \\ 0 & \sin\chi & 0 \end{bmatrix} \tag{46b}$$

$$\delta A_x = \delta\phi\sin\theta_a\sin\psi_a + \delta\theta\cos\psi_a \quad , \tag{46c}$$

$$\delta A_y = \delta\phi\sin\theta_a\cos\psi_a - \delta\theta\sin\psi_a \quad , \tag{46d}$$

and

$$\delta A_z = \delta\phi\cos\theta_a + \delta\psi \quad . \tag{46e}$$

To make adjustments of $\delta\phi$ and $\delta\theta$, then, first we orient the gradiometer for a null response and turn it about its axis to obtain a maximum response from current oscillating in the coil, so that pickup loops face the coil. Its response is then given by

$$g_{23} = g\left[-\sin\chi + (\delta\phi\sin\theta_a\cos\psi_a - \delta\theta\sin\psi_a)3\cos\chi\right] \tag{47}$$

We then point the axis of the coil directly at the gradiometer so that $\chi \cong 0$ and adjust $\delta\phi$ and $\delta\theta$ to obtain a null response.

The axis of the coil then lies along the $\hat{x}_2$ axis of the gradiometer basis.

To adjust $\delta\psi$, we return the axis of the coil to its initial orientation and turn the gradiometer about its axis to obtain a null response. The coil then lies along the $\hat{x}_1$ axis of the gradiometer basis with its axis in the plane containing pickup loops. Finally, we point the axis of the coil in several directions to ensure that the response is null for every orientation of the coil.

2. Results of Preliminary Tests

Although we can not thoroughly test the alignment procedure outlined above for suppressing noise from fluctuating magnetization currents in magnetic objects because the gimbal used to orient the gradiometer precludes making the required alignments precisely, our preliminary tests show that crude alignment of the gradiometer reduces noise power from fluctuating magnetization currents in an iron sphere by a factor of about 100.

As a first test of noise suppression afforded by aligning a gradiometer for a null response, we placed an iron sphere, having a radius of 0.46 m, at distances of 3.7 m and 1.8 m north of the gradiometer. At each distance, we place the sphere so that the axis of the gradiometer and the position vector directed from the center of the sphere to the gradiometer lie approximately in a vertical plane containing the earth's magnetic field vector.

The magnetic dipole induced at the center of the sphere by the earth's magnetic field then gives a gradiometer response described by the relation

$$g_{23} \cong \frac{g}{2}(4 + 5\cos^2\chi)^{1/2}\sin 2(\theta - \alpha)\sin\phi \qquad (48a)$$

where ϕ and θ are polar angles specifying direction of the position vector in the gradiometer basis; the relation $\tan 2\alpha = (2/3)\tan\chi$ determines the angle α; and $\chi = \pi - (\phi_d + \theta_d)$, where ϕ_d is the local dip angle of the earth's magnetic field and θ_d, the dip angle of the position vector. The relation

$$g = \frac{3B}{R_o}\left(\frac{R_c}{r}\right)^4 \tag{48b}$$

gives gradient strength of the induced dipole, where $B = 4.5 \times 10^4$ nT is the strength of the earth's magnetic field at the site, R_o is the radius of the sphere, and r, its distance from the gradiometer. At the distance r = 3.7m, g = 70 nT/m, and at r = 1.8m, g = 1252 nT/m.

Rotating the gradiometer about its axis and measuring amplitude of the response gives a gradient magnitude of 7.8 nT/m, with r = 3.7m, and a magnitude of 136 nT/m, with r = 1.8m. The center of the sphere lies somewhat below the gradiometer in each case, $\theta_d \cong -5^o$, and so for $\phi_d = 55^o$, we conclude from Equation 48a that in each case $\theta - \alpha \cong 3^o$, which again tells us that the gradiometer axis is tilted somewhat from vertical and that $\theta = \pi/2 - \Delta\theta$ with $\Delta\theta \cong 10^o$.

To examine the affect of gradiometer alignment or suppressing noise from fluctuations in strength and direction of the dipole induced in the sphere that result from fluctuations in strength and direction of the earth's magnetic field, we express gradiometer response in terms of components of the fluctuating dipole in the gradiometer basis. Namely, we write the fluctuating gradiometer response as

$$\begin{aligned}\delta g_{23}(t) = {} & \delta g_1(t)\left(\frac{5}{4}\right)(\cos 2\theta - 1)\cos\theta\sin 2\phi \\ & + \delta g_2(t)\left(\frac{1}{4}\right)\left[5\cos 2\theta - 1 - 5(\cos 2\theta - 1)\cos 2\phi\right]\cos\theta \\ & - \delta g_3(t)\left(\frac{1}{2}\right)(5\cos 2\theta + 3)\sin\theta\sin\phi \quad ,\end{aligned} \tag{49a}$$

where

$$\delta g_i(t) = g\left[\frac{b_i(t)}{B}\right] , \tag{49b}$$

and $b_i(t)$ are components of the fluctuating part of the earth's magnetic field in the gradiometer basis. For $\theta = \pi/2 - \Delta\theta$, then, Equation 49a tells us that

$$\delta g_{23}(t) \cong \delta g_3(t)\sin\phi + \frac{\Delta\theta}{2}\left[\delta g_1(t)5\sin 2\phi + \delta g_2(t)(3-5\cos 2\phi)\right] \tag{49c}$$

Moreover, Equation 48a shows that rotating the gradiometer about its axis until response to steady gradients vanishes gives the zero position for the angle ϕ. For $\phi = 0$, response to gradient fluctuations is suppressed; namely,

$$\delta g_{23}(t) \cong -\delta g_2(t)\Delta\theta , \tag{50a}$$

and for $\phi = \pi/2$, response to gradient fluctuation is unsuppressed; namely,

$$\delta g_{23}(t) \cong \delta g_3(t) + 4\delta g_2(t)\Delta\theta \tag{50b}$$

To investigate the effect of suppressing noise by aligning a gradiometer for a null response, then, we compare spectra of gradiometer response for the two alignments $\phi = 0$ and $\phi = \pi/2$ with the iron sphere placed 1.8m north of the gradiometer. Figure12a shows a spectrum obtained for the alignment $\phi = \pi/2$, and Figure12b shows a spectrum obtained the following day for the alignment $\phi = 0$. The heavy solid line in each figure delineates the spectrum of inherent instrument noise observed in a magnetically quiet environment, as shown in Figure 8 . Heavy broken lines delineate the spectrum expected without

effective suppression, which we determine from spectra of fluctuating components of the earth's magnetic field reported by Davidson, 1964, by using Equation 49b and presuming that variations in direction of the fluctuating magnetic field are isotropic. Light broken lines mark spectra expected with noise power reduced by a factor $(\Delta\theta)^2$, as specified by Equation 50a, with $\Delta\theta = 0.1$ radians.

From Figures 12a and 12b, we first observe that spectral density of estimated spectra increases with decreasing frequency at about the same rate as spectral density of magnetic field fluctuations; namely, spectral densities are proportional to $(1/f)^{2.6}$ (Davidson, 1964). Next, we see that magnitudes of observed spectra, in both cases, are about at the level expected when gradient fluctuations are reduced by a factor $(\Delta\theta)^2$ with $\Delta\theta = 0.1$ radians. Finally, the expected increase in level of observed spectra for $\phi = \pi/2$ is not evident in Figure 12a.

Equation 50b then suggests the conclusion that the vertical component of the fluctuating magnetic field is suppressed at the test site. The conclusion is consistent with data from magnetic observatories (Campbell, 1975) that show the vertical component of magnetic field fluctuations at mid latitudes is appreciably smaller than the horizontal component.

The slight increase in level at high frequencies of the observed spectrum shown in Figure 12b results from a class Pc 5 micropulsation event (Campbell, 1967; Saito, 1969) evident in the time series record shown in Figure 13. Pulsations begin at about 0400 hrs (PST) on 6 February 1976 and continue for $\sim$5000 seconds as a damped sinusoidal oscillation having a period of roughly 500 seconds. Maximum peak-to-peak amplitude of the pulsation is about 350 nT.

Spectra of gradiometer response observed when the iron sphere is placed 3.7 m north of the gradiometer are indistinguishable from spectra observed in a magnetically quiet environment. Moving the sphere from 1.8 m to 3.7 m reduces noise power by a factor of $(3.7/1.8)^8$ or about 300, and so we expect spectral levels comparable to inherent noise of the instrument.

Section VIII
OPERATION AT THE OCEANOGRAPHIC TOWER

Our field tests show that the construct of an equivalent dipole provides a useful means of describing response of the gradiometer to ambient gradients that are sensibly constant over the distance separating pickup loops (25 cm). Preliminary tests of noise suppression techniques, developed by describing gradiometer response in terms of an equivalent dipole, demonstrate reduction of noise power by a factor of 100 using crude means of aligning the gradiometer and suggest that reduction of noise is limited by alignment precision alone. By improving alignment to a precision of 10^{-3} radians or 0.05 degrees, we expect to reduce noise power by a factor of 10^{6}.

Here, we use the construct of an equivalent dipole to estimate stability and alignment required to suppress noise enough to afford certain measurement of fluctuating gradients of magnetic fields generated above the surface by oceanic internal waves passing the oceanographic tower operated by the Naval Undersea Center. The tower is located about one mile offshore near San Diego, California in water 18 m deep. Although internal waves passing the tower provide a well characterized and readily accessible source for first measurements of gradients of magnetic fields generated by internal waves, magnetization currents in the steel structure of the tower produce steady as well as fluctuating local gradients that make the task of measuring fluctuating gradients from internal waves an exacting one.

In what follows, we first describe gradients of the steady magnetic field near the tower, give typical spectra of fluctuating gradients expected from internal waves passing the

tower, and then specify stability and alignment required to afford certain measurement of fluctuating gradients from internal waves.

A. GRADIENTS OF THE STEADY MAGNETIC FIELD NEAR THE TOWER

To obtain requisite information for assessing effects of gradients resulting from magnetization currents in the tower structure, we used a fluxgate gradiometer to measure the steady gradient field in the vicinity of the tower (Gillespie and Podney, 1976). We measured steady gradients at nine positions due west of the tower in a vertical plane containing its centerline. The pair of coordinates (Z_2, Z_3) specify a position, where the coordinate Z_2 gives its horizontal distance in meters due west of the centerline of the tower and the coordinate Z_3, its height in meters above the ocean bottom. The water depth is about 18 m.

Table I lists eigenvalues $(\lambda_1, \lambda_2, \lambda_3)$ and polar angles $(\phi_1, \theta_1; \phi_2, \theta_2; \phi_3, \theta_3)$ giving directions of a set of eigenvectors $(\hat{e}_1, \hat{e}_2, \hat{e}_3)$ of the steady gradient field at the nine positions. Figure 14 defines the fiducial basis used to reckon directions of eigenvectors. The $\hat{z}_3$ axis is directed vertically downward; the $\hat{z}_1$ axis, northward; and the $\hat{z}_2$ axis, eastward. Table I shows that the eigenvector $\hat{e}_2$ points nearly northward and 10 to 20 degrees above horizontal. The plane containing axes of equivalent dipoles, which is normal to $\hat{e}_2$, is then tilted 10 to 20 degrees about a horizontal axis pointing eastward and so is close to a vertical plane of symmetry of the tower structure. The structure comprises four steel pilings set in a square array aligned north-south and east-west.

TABLE I

EIGNEVALUES λ_1, λ_2, AND λ_3 (IN UNITS OF nT/m) AND POLAR ANGLES (IN DEGREES) OF THE EIGENVECTOR SET ($\hat{e}_1$, $\hat{e}_2$, $\hat{e}_3$)

(z_2,z_3)	λ_1	λ_2	λ_3	ϕ_1	θ_1	ϕ_2	θ_2	ϕ_3	θ_3
(22.2,25.1)	345	-121	-224	276.2	85.4	4.6	104.4	23.4	15.2
(22.4,23.1)	344	-115	-229	277.1	80.5	5.3	100.9	47.3	14.5
(22.7,20.9)	326	-101	-224	275.7	75.6	1.0	107.6	42.9	23.1
(19.2,25.4)	538	-233	-305	276.3	88	5.9	99.4	18.1	9.6
(19.4,22.9)	524	-222	-302	276	81.2	2.3	112.7	25.8	24.5
(19.7,20.7)	501	-181	-321	276.9	74.6	3.3	102.6	55.7	20.1
(16.2,25.1)	897	-380	-518	277.3	89	6.9	112.5	9.6	22.5
(16.4,23.1)	870	-338	-532	276.5	81.6	4.4	104.2	36.2	16.6
(16.7,20.8)	792	-290	-502	277	75.2	0.9	111.8	38.5	26.8

Table II lists parameters specifying location, orientation, and gradient strength of the equivalent dipole corresponding to the set of eigenvectors ($\hat{e}_1$, $\hat{e}_2$, $\hat{e}_3$) at each position. It shows that the position vector locating equivalent dipoles lies in the vertical plane of symmetry of the tower structure ($\phi \cong 90^{o}$). Figure 15 depicts location and orientation in the plane of symmetry of the equivalent dipole for each position. Dashed lines indicate locations of dipole images. Lengths of vectors indicating orientation of dipole axes are proportional to respective dipole moments. Gradient strength, g, of equivalent dipoles decreases with increasing horizontal distance, Z_2, from the tower centerline in proportion to Z_2^{-n} with n = 2.55.

In a vertical plane of symmetry of the tower structure, then, gradients from magnetization currents in the structure are represented by gradients of a dipole located in the plane of symmetry. Asymmetry of the superstructure of the tower, however, tilts the axis of the equivalent dipole a few degrees out of the plane of symmetry.

B. SPECTRA OF FLUCTUATING GRADIENTS EXPECTED FROM INTERNAL WAVES PASSING THE TOWER

Magnetic fields generated above the surface by progressive waves in a stratified ocean are circularly polarized in a vertical plane normal to wave crests, and their magnitudes decrease exponentially with height, h, above the surface as e^{-kh}, where k denotes wave number (Podney, 1975). As a result, gradients parallel to wave crests vanish, and the matrix (Podney, 1976)

$$G(h,\vec{r},t;\vec{k},\omega) = g(\vec{k},\omega)e^{-kh}\begin{bmatrix} \sin(\omega t-\vec{k}\cdot\vec{r}+\eta) & 0 & \cos(\omega t-\vec{k}\cdot\vec{r}+\eta) \\ 0 & 0 & 0 \\ \cos(\omega t-\vec{k}\cdot\vec{r}+\eta) & 0 & -\sin(\omega t-\vec{k}\cdot\vec{r}+\eta) \end{bmatrix} \quad (51)$$

TABLE II

PARAMETERS DEFINING LOCATION, ORIENTATION, AND GRADIENT STRENGTH OF THE EQUIVALENT DIPOLE

(Z_2,Z_3)	g,nT/m	χ	Ω	ϕ	θ	ϕ_m	θ_m
(22.2,25.1)	249	118.9	255.6	89.4	70.3	215.8	163.3
(22.4,23.1)	255	116.7	259.1	92	73.5	227.9	165.4
(22.7,20.9)	252	113.8	252.4	87	77.5	212.9	159.6
(19.2,25.4)	333	134.7	260.6	93.5	75.2	260	149
(19.4,22.9)	330	132.3	247.3	89	82	242.2	140.2
(19.7,20.7)	357	120.4	257.4	91.5	81.7	244.8	154.9
(16.2,25.1)	567	132.2	247.5	90.2	74.2	237.6	146.8
(16.4,23.1)	591	124.9	255.8	91.1	77.2	242.8	154.2
(16.7,20.8)	561	121.2	248.2	88	82.7	230.1	148.5

represents gradients at a height h above the surface in a basis having its $\hat{z}_3$ axis pointing vertically downward; its $\hat{z}_1$ axis, in the direction of wave propagation $\hat{k}$; and its $\hat{z}_2$ axis, parallel to wave crests. The scalar $g(\vec{k},\omega)$ gives the strength of gradients generated at the surface by a wave having a frequency ω and wave vector $\vec{k}$, and $\eta(\vec{k})$ is a phase shift.

From Equations 51 and 12b, we conclude that an equivalent dipole representing gradients generated at a point above the surface by an ocean wave circles a sphere of unit radius about the point on a great circle path in a vertical plane normal to wave crests. The axis of the dipole is tangent to the sphere in a vertical plane normal to wave crests, $\chi = \pi/2$ and $\Omega = \pi/2$, and circles the sphere at a frequency equal to one half the wave frequency; namely, $2\theta(t) = \omega t - \vec{k}\cdot\vec{r} + \eta$. Its moment is proportional to wave amplitude.

For surface waves, the relation

$$g(\vec{k},\omega) = \xi(\vec{k},\omega)\left(\frac{\mu_o \sigma \omega}{4}\right) B \left[(1+f)^2 \sin^2\phi_d + (1-f)^2 \cos^2\phi_d \cos^2\theta_h\right]^{1/2} \qquad (52a)$$

gives the strength of gradients generated at the surface by a surface wave that has a wave height $\xi(\vec{k},\omega)$ and heads at an angle θ_h east of magnetic north. Here, B denotes magnitude of the earth's magnetic field; ϕ_d, its dip angle; σ, the electrical conductivity of seawater ($\sim$4 mhos/m); and

$$f = \frac{kDe^{-kD}}{\sinh kD} \quad , \qquad (52b)$$

where D denotes water depth. The relation

$$\cot\eta = -\left(\frac{1-f}{1+f}\right)\cot\phi_d \cos\theta_h \qquad (52c)$$

gives the phase shift.

For internal waves, the relation

$$g_n(\vec{k},\omega) = \xi_n(d,\vec{k},\omega)\left(\frac{\mu_o\sigma\omega}{2}\right)B(\sin^2\phi_d+\cos^2\phi_d\cos^2\theta_{h,n})^{1/2} I_n(d,k) \qquad (53a)$$

gives the strength of gradients generated at the surface by an nth mode internal wave that has a displacement $\xi_n(d,\vec{k},\omega)$ at a depth $d(0<d<D)$ and heads at an angle $\theta_{h,n}$ east of magnetic north. Here,

$$I_n(d,k) = \frac{1}{\Phi_n(d,k)}\int_o^D \Phi_n(\zeta,k)e^{-k\zeta}kd\zeta \quad , \qquad (53b)$$

where $\Phi_n(\zeta,k)$ is an eigenfunction giving the profile of an nth mode wave. Eigenfunctions vanish at the surface and bottom of an ocean and are orthonormal with respect to the weight function $N^2(z)$; namely; $\Phi_n(0,k) = \Phi_n(D,k) = 0$, and

$$\int_o^D \Phi_n(\zeta,k)\Phi_m(\zeta,k)N^2(\zeta)d\zeta = \delta_{nm} \quad , \qquad (53c)$$

where $N(z)$ is the Brunt-Väisäla frequency profile of a thermocline. The relation

$$\tan \eta_n = -\cot\phi_d\cos\theta_{h,n} \qquad (53d)$$

gives the phase shift.

We use Equation 53a to estimate spectra of fluctuating gradients expected from internal waves. It shows that strength of gradients generated at the surface is proportional to wave displacement at depth and that the coefficient depends on a weighted integral of an eigenfunction over depth, as expressed by Equation 53b. From spectral measurements of isotherm displacements at the top of the thermocline together with the measured thermocline profile, then, we compute spectra of fluctuating gradients expected from internal waves passing the tower.* The waves pass the tower in packets of long-crested first-mode waves running close to due east, so $\theta_h \cong \pi/2$. Magnitude of the earth's magnetic field at the tower is about 47,200 nT and its dip angle is about 61° (Gillespie and Podney, 1976).

Figure 1 shows three typical spectra of transverse gradients expected 7 m above the surface from internal waves passing the tower compared to the inherent noise spectrum of the instrument. Spectra shown in Figure 1 give the expected spectral response when pickup loops of the gradiometer face in the direction of wave propagation or, more specifically, when the $\hat{x}_1$ axis of the gradiometer basis is parallel to wave crests. As is evident, spectral densities of fluctuating gradients expected from internal waves are well above the level of instrument noise.

* Fluctuating gradients from surface waves are neglibly small at frequencies of internal waves at the tower.

C. ALIGNMENT AND STABILITY REQUIREMENTS

We plan to jut the gradiometer over water on a rigid nonmagnetic cantilever extending horizontally 25 meters from the centerline of the tower in a vertical plane of symmetry. The gradient field of a dipole located in the plane of symmetry and having a gradient strength, g, of about 200 nT/m or 2 X 10^5 pT/m gives gradients at the position of the gradiometer from magnetization currents in the tower structure. We represent fluctuations in response of the gradiometer, which result both from fluctuations in its position and orientation and from fluctuations in magnetization currents in the tower, in terms of fluctuations in location, orientation, and gradient strength of the dipole.

1. Alignment

Without aligning the gradiometer to suppress noise from fluctuating magnetization currents in the tower, we expect a spectral density of fluctuating gradients, N_I, given by the relation

$$N_I(f) = g^2\left[b(f)/B\right]^2 = 1.25 \text{ X } 10^{-4}(1/f)^{2.6}(\text{pT/m})^2/\text{Hz} \ , \qquad (54a)$$

where the relation

$$b^2(f) = 6.31 \text{ X } 10^{-6}(1/f)^{2.6} \quad (\text{nT})^2/\text{Hz} \qquad (54b)$$

gives the spectral density of magnetic field fluctuations owing to changing ionospheric currents as reported by Davidson, 1964. We see from Figure 1 and Equation 54a, then, that gradient fluctuations from fluctuating magnetization currents in the tower mask gradient fluctuations expected from internal waves unless the gradiometer is aligned to suppress gradient fluctuations from magnetization currents in the tower.

By aligning the gradiometer for a null response with a precision of 0.01 radians or 0.6 degrees, however, we reduce the spectral density of gradient fluctuations owing to fluctuating magnetization currents in the tower by a factor of 10^{-4}, which then puts it below the level of instrument noise. We align for a null response by orienting the gradiometer so that the dipole representing gradients of magnetization currents in the tower is located along the $\hat{x}_1$ axis of the gradiometer basis with its axis in the plane containing pickup loops. The plane containing pickup loops is then close to a vertical plane of symmetry of the tower structure.

In order to align the gradiometer for a null response and at the same time to face pickup loops in the direction of internal wave propagation, we choose the plane of symmetry so that internal waves cross the plane at nearly normal incidence. Namely, we extend the cantilever from either the north or the south side of the tower. Aligning the gradiometer for a null response to suppress gradient fluctuations from fluctuating magnetization currents in the tower then gives a near maximum response to gradient fluctuations from internal waves as well.

2. Stability

When the gradiometer is aligned for a null response, it responds only to displacements and changes in orientation that produce an effective rotation about the gradiometer axis of the equivalent dipole representing gradients from magnetization currents in the tower. Namely, the relation

$$g_{23}(t) = \delta\phi(t)\ g\ \sin\chi \tag{55}$$

then gives gradient fluctuations resulting from irregular motions, where $\delta\phi(t)$ is the effective angle of rotation about the gradiometer axis, g is the gradient strength of the equivalent dipole, and the angle χ gives inclination of its axis to the position vector locating the dipole in the gradiometer basis. Our measurements give $g = 2 \times 10^5$ pT/m and $\chi = 115^o$. From Equation 55a, we then expect a spectral density of fluctuating gradients resulting from irregular motion, N_s, given by the relation

$$N_s(f) = 0.77\Phi(f) \quad (pT/m)^2/Hz \quad , \tag{55b}$$

where $\Phi(f)$ is a spectral density of fluctuations in the effective angle of rotation about the gradiometer axis, in units of (seconds of arc)^2/Hz.

To keep spectral density of gradient fluctuations from irregular motions at the level of instrument noise in the bandwidth of gradient fluctuations expected from internal waves, nominally 2×10^{-3} Hz to 5×10^{-3} Hz, the cantilever must limit angular deviations of effective rotations about the gradiometer axis to a few seconds of arc or about 10^{-5} radians in the bandwidth. We require, then, that structural design of the cantilever limit rotational and translational fluctuations of the instrument relative to the tower to 10^{-5} radians (2 seconds of arc) and 0.1 mm in the bandwidth of gradient fluctuations expected from internal waves. A displacement of 0.1 mm at a radius of 25 m gives an angular deviation of about 1 second of arc.

3. Cantilever Design

Figure 16 shows an elevation and top view of the structural design developed by Mechanics Research, Inc. (Haire and Van Lerberg, 1976) to give the requisite stability under wave, wind, and thermal loads expected during operations at the tower. The cantilever is a four-sided truss space frame extending about 20 meters from the

face of the tower. An 8 m base section made of tubular aluminum attaches to the tower supports, and a 12 m outer section made of a fiberglass laminate supports the instrument at the tip of the cantilever. The instrument Dewar fits in a fiberglass gimbal mount whose three independent axes of rotation provide means of orienting the gradiometer axis as necessary. A catwalk running the length of the cantilever provides access to the instrument.

Section IX
CONCLUSION

At present, we describe the response of a superconducting magnetic gradiometer in terms of the magnetic field and its gradients at the midpoint of the gradiometer axis. The description is a useful approximation provided gradients of the ambient magnetic field are sensibly constant over the length of the gradiometer axis. The part of the response proportional to the magnetic field at the midpoint results from slight differences in area and orientation of the loops forming the pick-up circuit of the gradiometer and vanishes for a perfectly balanced gradiometer. The part proportional to a gradient of the magnetic field at the midpoint depends of five independent elements of a matrix representing gradients of the ambient magnetic field at the midpoint.

To concisely describe the gradient response, we use the five elements to define location, orientation, and moment of an equivalent magnetic dipole that gives gradients at the midpoint equal to gradients of the ambient field. Constructing an equivalent dipole lets us visualize the response to ambient gradients. For example, the gradient field of a dipole fluctuating about a mean location, orientation, and moment represents fluctuating gradients from nearby magnetic objects. A dipole circling a sphere of unit radius about the midpoint on a great circle path in a vertical plane normal to wave crests represents gradients from an ocean wave. A swarm of dipoles circling the sphere represents gradients from a field of random waves.

Results of preliminary tests of gradiometer response are consistent with the description based on a first order approximation. Nonetheless, the results are not precise enough to delimit the range of validity of the first order description. We plan further tests using more accurate gimbals and alignment procedures both to determine a more precise description of gradiometer response and to mark limits of validity of the first order description.

ACKNOWLEDGEMENTS

We greatly appreciate unstinting and diligent efforts of James Buxton during field tests as well as his valuable contributions and thoughtful criticism throughout the course of the work. We gratefully acknowledge the work of John Clarke and his research group at the University of California, Berkeley, California, who provided the data presented in Figures 9 and 10 depicting the spectrum of intrinsic noise of SQUID sensors. We are especially grateful to Spencer Buckner both for his diligent and artful work evident in the design and construction of the gradiometer probe and for providing values of the parameters in the superconducting circuit shown in Figure 2b. We thank Philip Selwyn for providing computations required to estimate spectra of gradients expected from internal waves passing the tower as shown in Figure 1 and Richard Ziemer for providing spectra of isotherm displacements.

Timely and unstinting support provided by the Ocean Measurements Group of the Naval Undersea Center, under the direction of Dale Good, together with the hospitable assistance of the staff of the La Posta Astrogeophysical Observatory, directed by Max Bleiweiss, makes our field testing possible and continues to be invaluable.

REFERENCES

Bleiweiss, M. P. and F. L. Wefer, La Posta astrogeophysical observatory, Sol. Phys. 43, 253, 1975

Campbell, W., Geomagnetic Pulsations, in Physics of Geomagnetic Phenomena, Vol., II, edited by S. Matsushita and W. Campbell, chap. IV-4, Academic Press, New York, 1967

Campbell, W., An analysis of spectra of geomagnetic variations having periods from 5 min. to 4 hrs., J. Geophys. Res., 1975 (submitted Sept. 1974)

Classen, J., Coupling considerations for SQUID devices, J. Appl. Phys., 46, 2268, 1975

Clarke, J., Josephson junction detectors, Science 184, 1235, 1974

Clarke, J., W. M. Goubau, and M. B. Ketchen, A thin-film dc SQUID with low noise and drift, Appl. Phys. Letters, 27, 155, 1975

Cox, C. S., Internal waves, in The Sea, vol. 1 part 2, edited by M. N. Hill, chap. 22, Part II, John Wiley, New York, 1962

Davidson, M., Average diurnal characteristics of geomagnetic power spectrums in the period range 4.5 to 1000 seconds, J. Geophys. Res., 69, 5116-5119, 1964

Gillespie, G. and W. Podney, The magnetic field and magnetic field gradients of the NUC oceanographic research tower, Physical Dynamics, Inc. Rept. No. PDL-76-109, 1976

Haire, A. M. and D. Van Lerberg, Gradiometer support structure, Mechanics Research, Inc., Repts. No. MRI-2882-TR1, March, 1976 and MRI-2882-TR2, June 1976

La Fond, E. C., Internal waves, in The Sea, vol. 1 part 2, edited by M. N. Hill, chap. 22, Part I, John Wiley, New York, 1962

Podney, W., Electromagnetic fields generated by ocean waves, J. Geophys. Res., 80, 2977-2990, 1975

Podney, W., Spectra of magnetic field gradients generated over oceans by ocean waves, Physical Dynamics, Inc., Rept. No. PD-76-108, 1976

Saito, T., Geomagnetic Pulsations, Space Sci. Rev., 10, 319-412, 1969

Winant, C. and J. Olson, The vertical structure of coastal currents, Deep-Sea Research, 23, p. 925, 1976

Wynn, W. M., C. P. Frahm, P. J. Carroll, R. H. Clark, J. Willhoner, and M. J. Wynn, Advanced superconducting gradiometer/magnetometer arrays and a novel signal processing technique, IEEE Trans. Magn., MAG-11, 701, 1975

Ziemer, R. and G. Gillespie, Planning for the ARPA/OWEX internal wave magnetic sensing experiment, Physical Dynamics, Inc. Rept. No. PD-SN-76-112, 1976

Ziemer, personal communication, 1976

Zimmerman, J., J. Appl. Phys., 42, 4483, 1971

Zimmerman, J. and N. Frederick, Miniature ultrasensitive superconducting magnetic gradiometer and its use in cardiography and other applications, Appl. Phys. Letters 19, 16, 1971

FIGURE CAPTIONS

Figure 1 Three typical spectra of fluctuating gradients of magnetic fields expected 7 m above the surface from internal waves passing the oceanographic tower operated by the Naval Undersea Center as compared to the inherent noise spectrum of the instrument. Spectra are estimates based on spectral measurements of isotherm displacements made during August 1972. Serial numbers marking spectra tell the month, day, and local time at the beginning of corresponding time series; for example, 08211540 means August 21 at 15:40 hours (PST).

Figure 2a Illustration of the instrument showing Dewar construction and principal components of the gradiometer probe. A wrapping of alternating layers of fiber glass cloth and aluminized Mylar, which is not shown, insulates the interior vessel. The Dewar stands 48" high, is 26" in diameter, and weighs about 250 lbs.

Figure 2b Diagram of the superconducting circuit of the gradiometer. Two coplanar pickup loops, having a combined self inductance L_p, are oppositely wound in series and connected to the primary winding (having a self inductance L_1) of a transformer containing a normal metal shield between its superconducting windings that attenuates radio frequency interference (rfi). The secondary winding of the transformer has a self inductance L_2 and is connected to a field coil, having a self inductance L_f, that couples flux to a superconducting quantum interference device (SQUID). The SQUID has a self inductance L_s and is driven by a tank circuit connected to room temperature electronics. The rfi transformer, SQUID, and tank circuit are encapsulated in a superconducting shield. A super current I_1 flows in the pickup circuit, and a super current I_2, in the coupling circuit.

Figure 3 Geometry of pickup loops comprising an axis of a superconducting magnetic gradiometer. Centers of the two pickup loops are separated by a distance 2s, and their areas are A_1 and A_2. Normals to the plane of each loop are directed along unit vectors $\hat{n}_1$ and $\hat{n}_2$, and radial vectors $\vec{\rho}_1$ and $\vec{\rho}_2$ locate points within a loop contour. The gradiometer basis $\{\hat{x}_i\}$ is fixed midway between centers of the loops and is located with respect to a fiducial basis by the vector $\vec{R}$.

Figure 4 Vector diagram depicting location and orientation of a magnetic dipole, $\vec{m}$, with respect to the gradiometer basis $\{\hat{x}_i\}$. Polar angles ϕ and θ specify direction of the position vector $\vec{r}$ locating the dipole. The polar angle χ and azimuthial angle Ω specify direction of the dipole axis with respect to the position vector. The $\hat{y}_3$ axis of the basis $\{\hat{y}_i\}$ points along the position vector; the $\hat{y}_2$ axis, along $\hat{r} \times \hat{m}$; and the $\hat{y}_1$ axis, along $(\hat{r} \times \hat{m}) \times \hat{r}$.

Figure 5 Record of gradiometer response during a clockwise rotation followed by a counter clockwise rotation about its axis. Rotations are made stepwise in sixteen increments of 22.5°, pausing at positions numbered 1 through 16 that correspond to numbered positions in Figure 6. Spikes mark movements between incremental positions, and flats mark values recorded while pausing.

Figure 6 Orientation of positions 1 through 16 with respect to magnetic north. Rotations begin with the $\hat{x}_2$ axis of the gradiometer basis pointing northward and proceed through positions 1, 2, 3, ..., 16, 1 during a clockwise rotation and through positions 1, 16, 15, ..., 2, 1 during a counter clockwise rotation.

Figure 7 Signature of hysteresis observed during rotation at an imbalance somewhat less than 10^{-5} m^{-1}. The trace records gradiometer response during a stepwise oscillation of the $\hat{x}_2$ axis of the gradiometer basis about position 5 marked in Figure 6, beginning with a clockwise movement to position 7. Numbered flats mark values recorded while dwelling at corresponding positions. Spikes mark movements between positions in the sense denoted by vertical arrows.

Figure 8 Data depicting the noise spectrum of the gradiometer operating in a magnetically quiet environment. We use a calibration of 4.5 mV/(pT/m) to obtain spectral density in units of $(pT/m)^2/Hz$, marked on the left hand coordinate scale, and a calibration of 12.7 V/ϕ_o to obtain spectral density in units of ϕ_o^2/Hz, marked on the right hand coordinate scale. Points marked by a circular dot ● represent data obtained from digital records. Points marked by a triangular dot ▼ represent data obtained from a real-time spectrum analyzer. Error bars mark limits corresponding to two standard deviations.

Figure 9 Data depicting the spectrum of intrinsic noise of the SQUID sensor compared to the noise spectrum of the gradiometer operating in a magnetically quiet environment. The left hand coordinate scale gives spectral density in units of $(pT/m)^2/Hz$, and the right hand scale, in units of ϕ_o^2/Hz. The conversion factor is $3.5 \times 10^{-4} \phi_o/(pT/m)$. The solid line delineates the spectrum of inherent gradiometer noise shown in Figure 8, as represented by the spectral form $S(f) = (2.1 \times 10^{-3})/f^{1.3} (pT/m)^2/Hz$, for $f<0.1$ Hz, and $S(f) = 0.03(pT/m)^2/Hz$, for $f>0.1$ Hz.

Figure 10 Expected enhancement of instrument performance from use of a thin-film dc type SQUID sensor. Data points depict the spectrum of intrinsic noise of a thin-film dc type SQUID in units of Φ_o^2/Hz marked on the right hand coordinate scale, and the heavy dashed line marks a corresponding expected spectrum of gradiometer noise in units of $(pT/m)^2$/Hz marked on the left hand coordinate scale. The light dashed curve delineates the spectrum of intrinsic noise of a torodial point-contact type sensor as used in the instrument, in units of Φ_o^2/Hz, and the solid line marks the corresponding spectrum of inherent gradiometer noise in units of $(pT/m)^2$/Hz.

Figure 11 Magnetic dipole describing the induced gradient field at a radial position $\vec{r}$ outside an iron sphere magnetized by the earth's magnetic field. Eigenvectors $\hat{e}_1$ and $\hat{e}_3$ mark principal axes in a meridian plane for several values of the angle $\chi = \pi - (\phi_d + \theta_d)$. The dip angle, ϕ_d, of the earth's magnetic field at the site is about 55^o, and the dip angle θ_d, of the position vector, $\vec{r}$, is $\pm 5^o$ or so. The angle α between eigenvector $\hat{e}_3$ and the position vector is about 68^o for $\theta_d = 0$ and $\phi_d = 55^o$.

Figure 12a Spectrum of gradient fluctuations from an iron sphere placed 1.8 m north of the gradiometer with pickup loops facing nominally north-south so that $\phi = \pi/2$. The corresponding time series, called POSTA 9, begins 4 February 1976 at 16:22 hours (PST) and ends 5 February 1976 at 09:40 hours (PST). The heavy solid line delineates the spectrum of inherent instrument noise shown in Figure 8, and light and heavy dashed lines mark spectra expected with and without suppression of noise, respectively, owing to aligning for a null response.

Figure 12b Spectrum of gradient fluctuations from an iron sphere placed 1.8 m north of the gradiometer with pickup loops facing nominally east-west so that $\phi = 0$. The corresponding time series, called POSTA 10, begins 5 February 1976 at 15:15 hours (PST) and ends 6 February 1976 at 16:37 hours (PST). The heavy solid line delineates the spectrum of inherent instrument noise shown in Figure 8, and light and heavy dashed lines mark spectra expected with and without suppression of noise, respectively, owing to aligning for a null response.

Figure 13 Section of time series record POSTA 10 showing a class Pc 5 micropulsation event recorded on 6 February 1976. Pulsations begin at about 0400 hours (PST) and continue for ~5 00 seconds as a damped sinusoidal oscillation having a period of roughly 500 seconds. (Gradient magnitudes marked on the left hand coordinate scale are relative to an arbitrary zero.)

Figure 14 Fiducial basis $\{\hat{z}_i\}$ used to define measurements of gradients in the vicinity of the oceanographic tower. The $\hat{z}_3$ axis points vertically downward; the $\hat{z}_1$ axis, northward; and the $\hat{z}_2$ axis, eastward. Polar angles (ϕ_1, θ_1; ϕ_2, θ_2; ϕ_3, θ_3) specifying directions of the set of eigenvectors ($\hat{e}_1$, $\hat{e}_2$, $\hat{e}_3$) at each position are listed in Table I. Eigenvector $\hat{e}_2$ points nearly northward and 10° to 20° above horizontal, and eigenvector $\hat{e}_1$ points nearly due west and 5° to 15° below horizontal.

Figure 15 Location and orientation in the vertical plane of symmetry of an equivalent dipole for gradients at each position near the oceanographic tower. Heavy dashed lines mark locations of dipole images. Lengths of vectors indicating orientation of dipoles are proportional to respective dipole moments and decrease with increasing horizontal distance,

Z_2, from the tower centerline in proportion to Z_2^{-n} with n = 2.55. Coordinates (Z_2, Z_3) specify a position: Z_2 gives its horizontal distance in meters due west of the centerline of the tower and Z_3 gives its height in meters above the ocean bottom. Positions are nominally spaced at 2 m intervals vertically and 3 m intervals horizontally.

Figure 16 Elevation and top view of the cantilever support for the gradiometer.

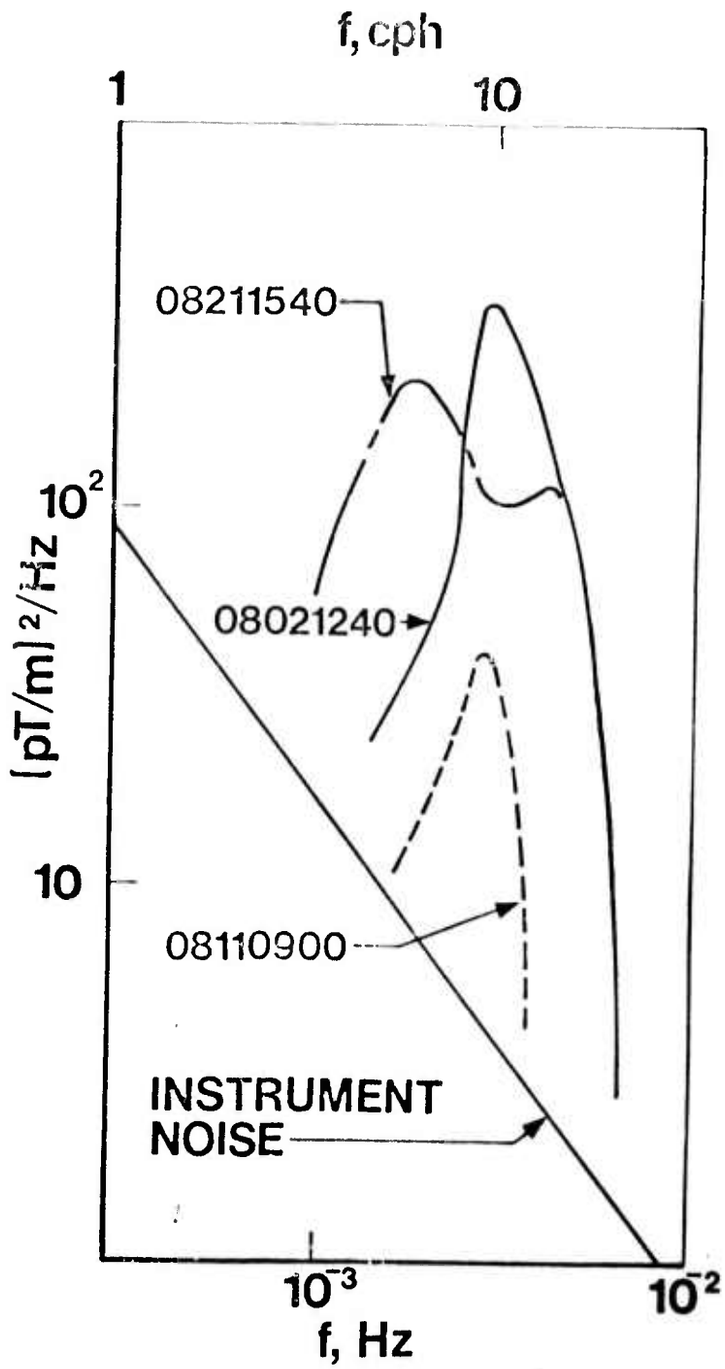
f, cph
1
10
08211540
08021240
08110900
INSTRUMENT
NOISE
10^2
10
$(pT/m)^2/Hz$
10^{-3}
10^{-2}
f, Hz

FIGURE 1

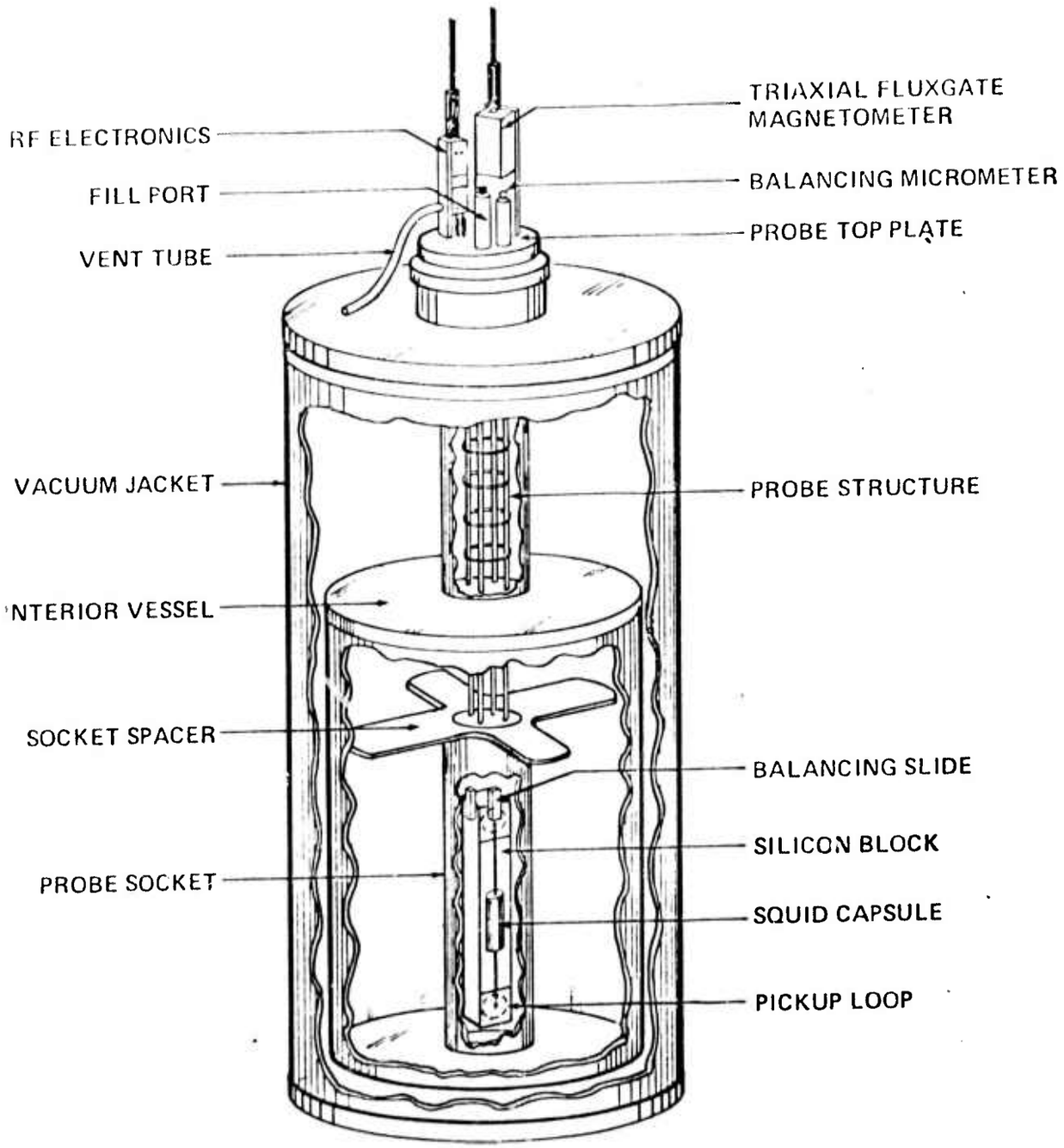
TRIAXIAL FLUXGATE MAGNETOMETER
RF ELECTRONICS
BALANCING MICROMETER
FILL PORT
PROBE TOP PLATE
VENT TUBE
VACUUM JACKET
PROBE STRUCTURE
NTERIOR VESSEL
SOCKET SPACER
BALANCING SLIDE
SILICON BLOCK
PROBE SOCKET
SQUID CAPSULE
PICKUP LOOP

FIGURE 2a

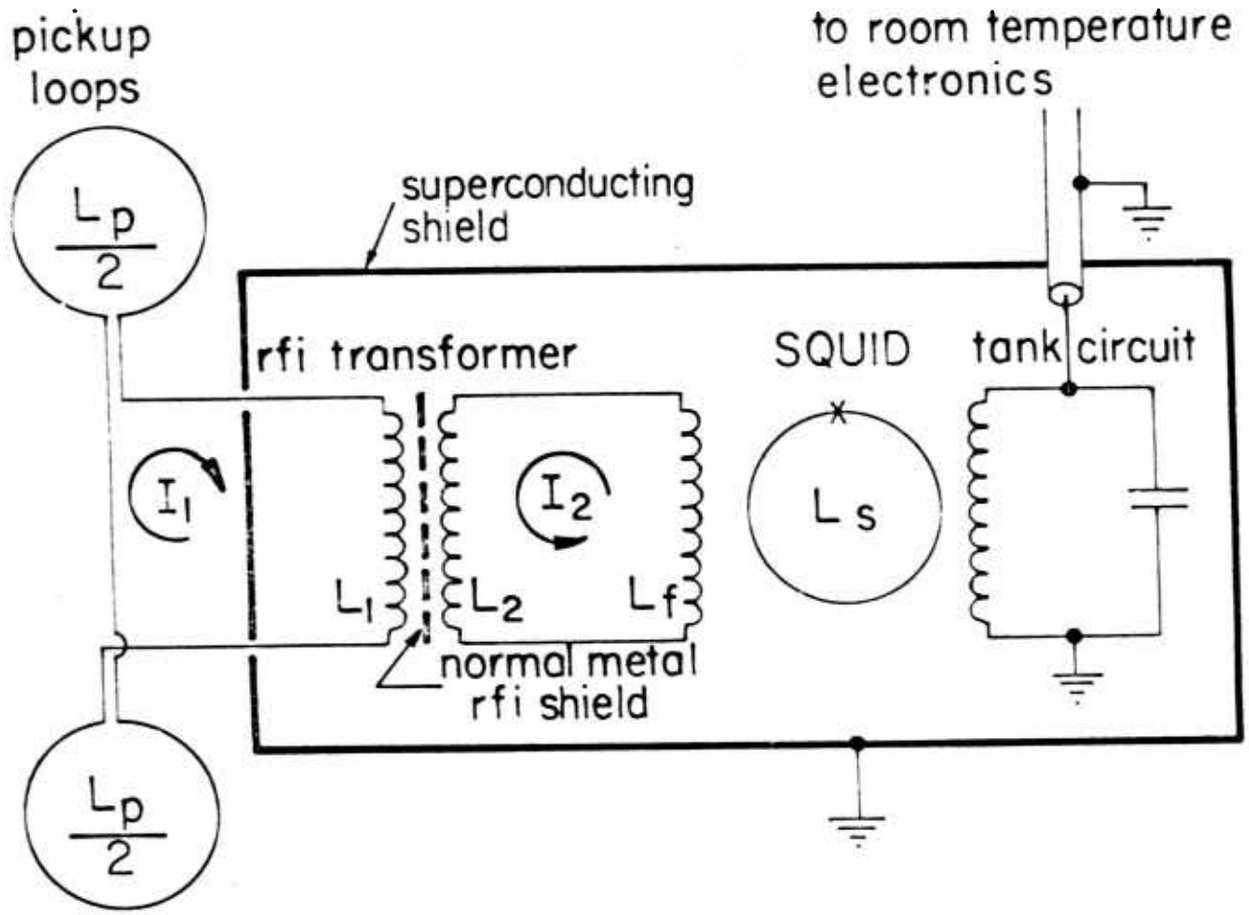
pickup
loops
$\frac{L_p}{2}$
superconducting
shield
to room temperature
electronics
rfi transformer
SQUID
tank circuit
I_1
I_2
L_s
L_1
L_2
L_f
normal metal
rfi shield
$\frac{L_p}{2}$

FIGURE 2b

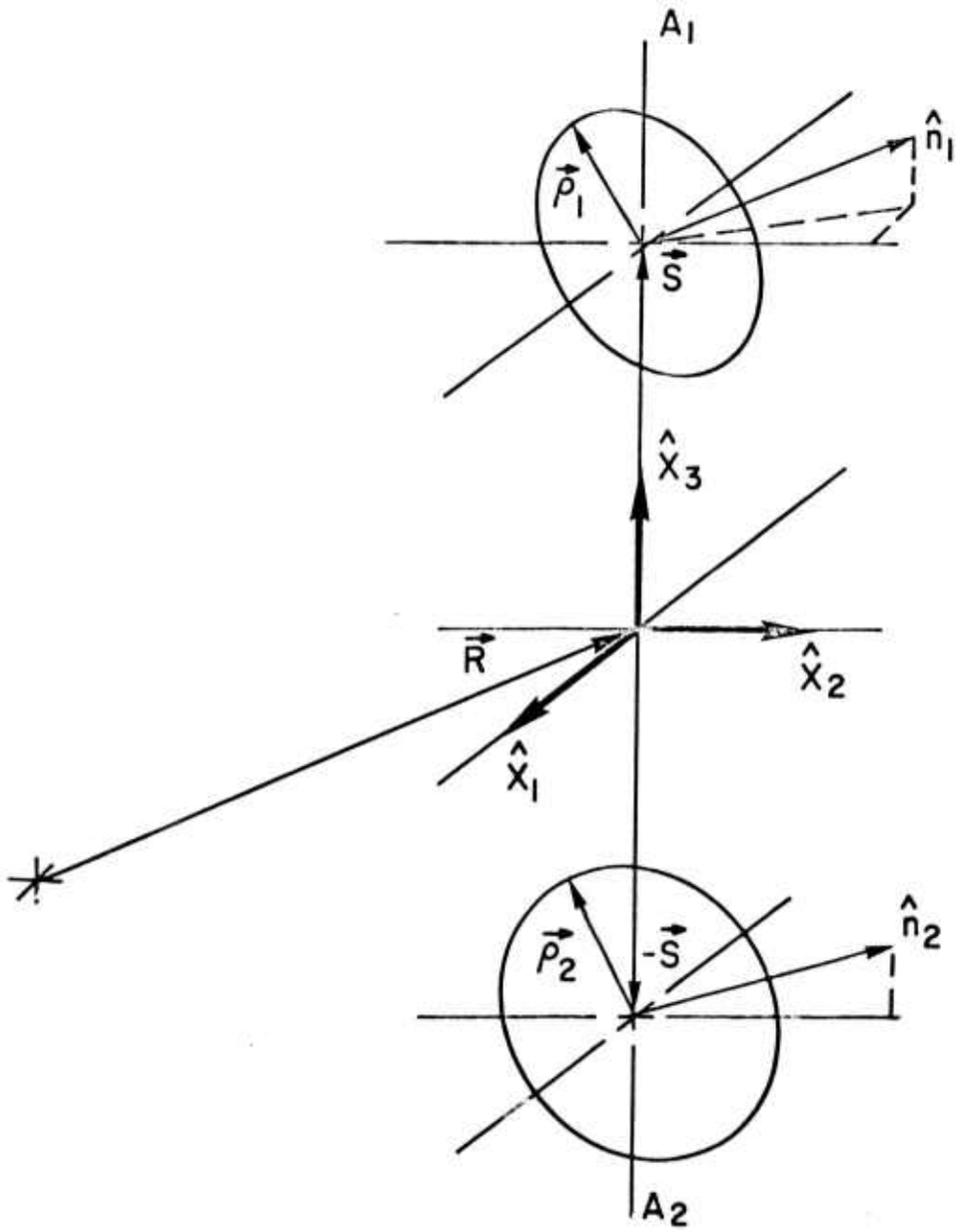
A1
$\hat{n}_1$
$\vec{\rho}_1$
$\vec{S}$
$\hat{X}_3$
$\vec{R}$
$\hat{X}_2$
$\hat{X}_1$
$\vec{\rho}_2$
$-\vec{S}$
$\hat{n}_2$
A2

FIGURE 3

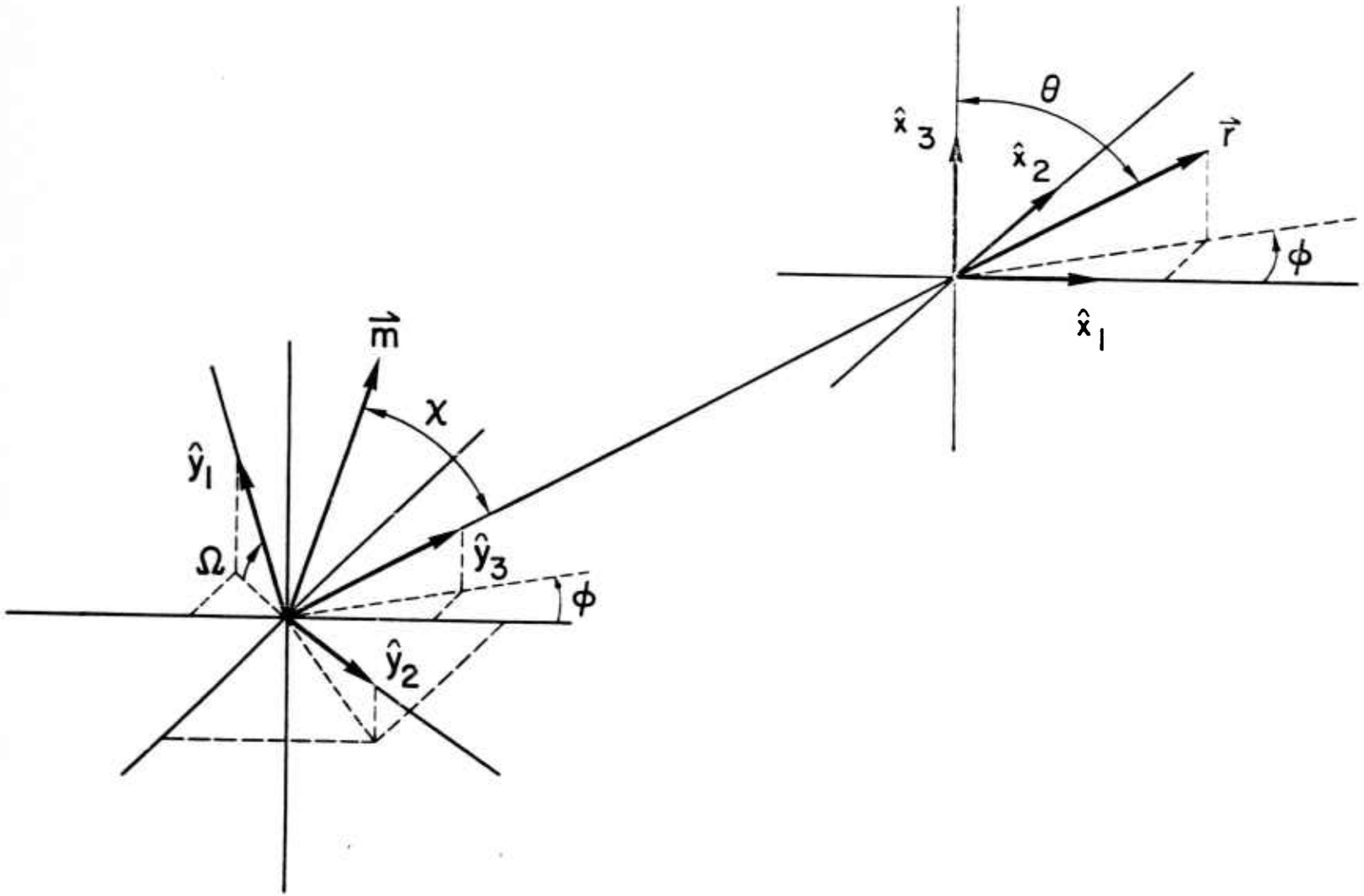

FIGURE 4

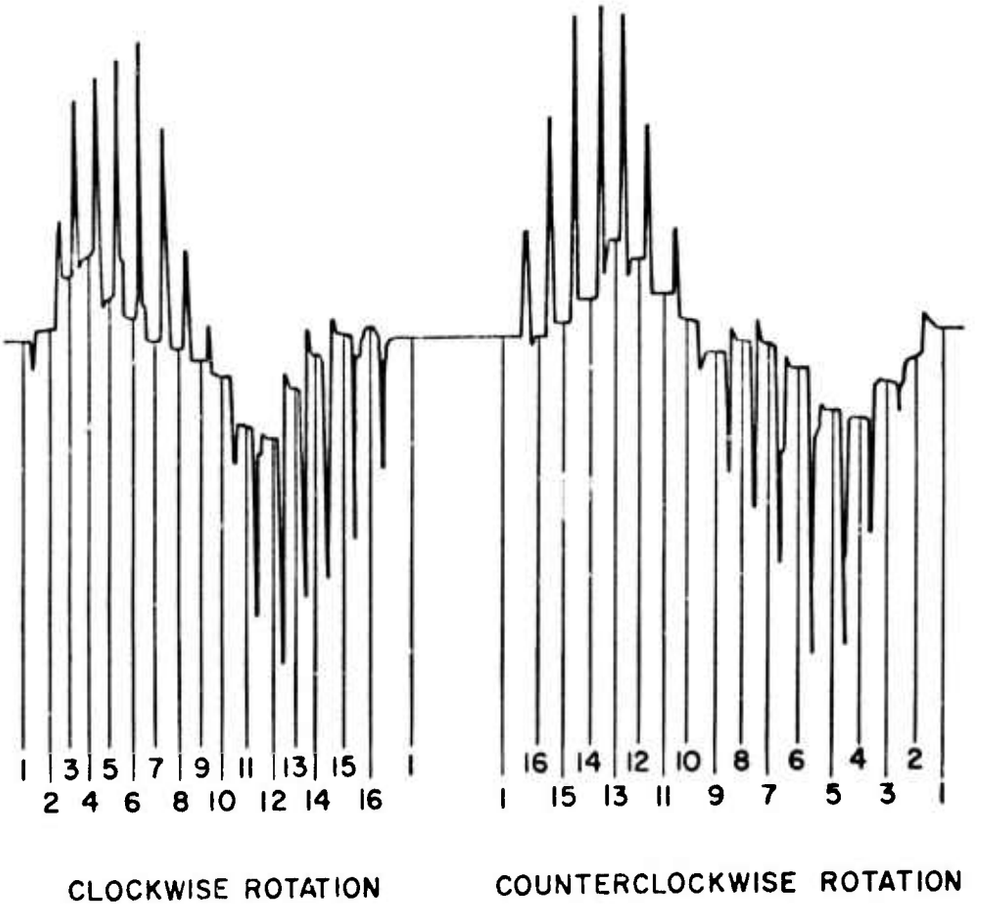
1 3 5 7 9 11 13 15 1
2 4 6 8 10 12 14 16
16 14 12 10 8 6 4 2
1 15 13 11 9 7 5 3 1
CLOCKWISE ROTATION
COUNTERCLOCKWISE ROTATION

FIGURE 5

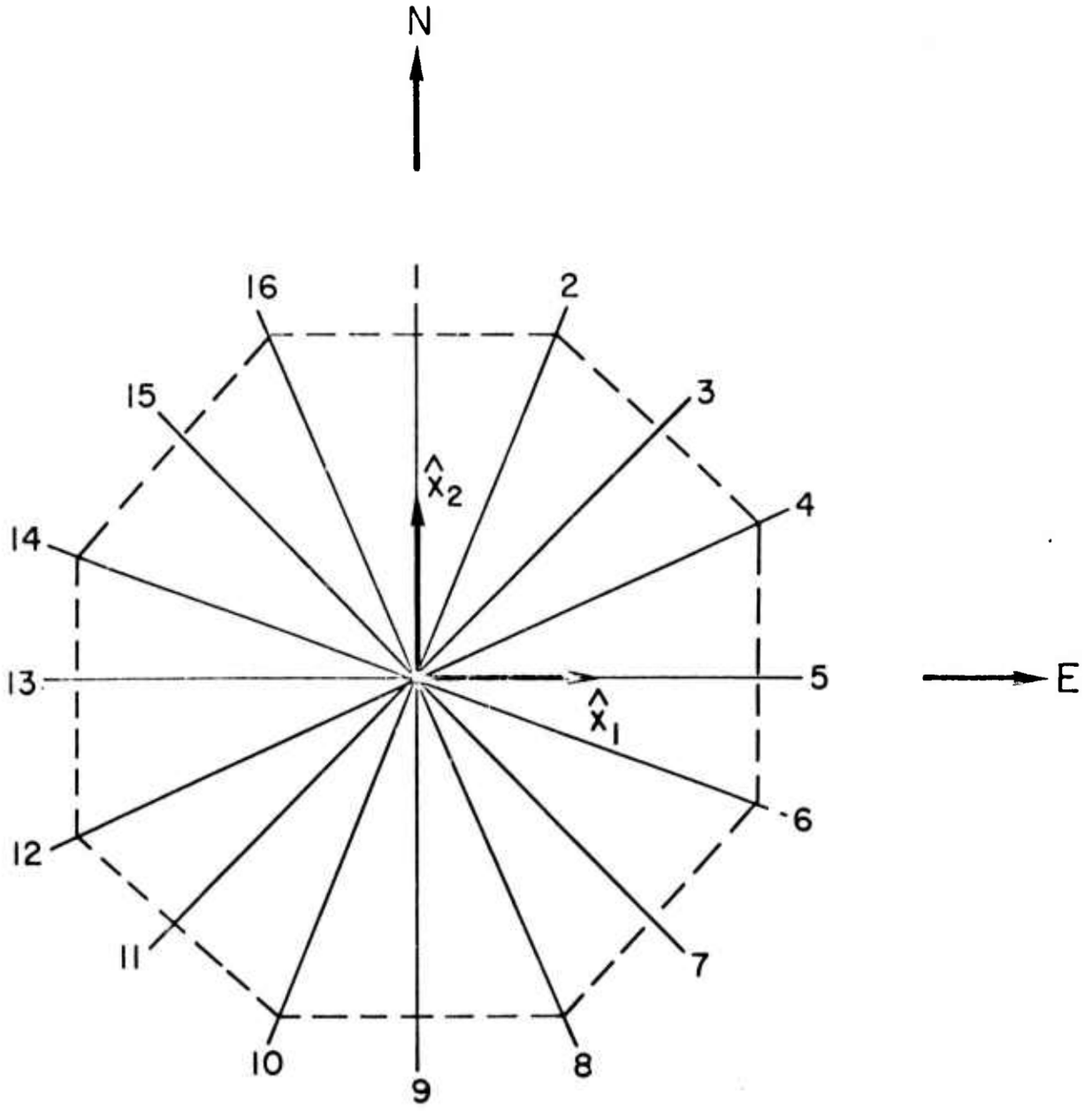

FIGURE 6

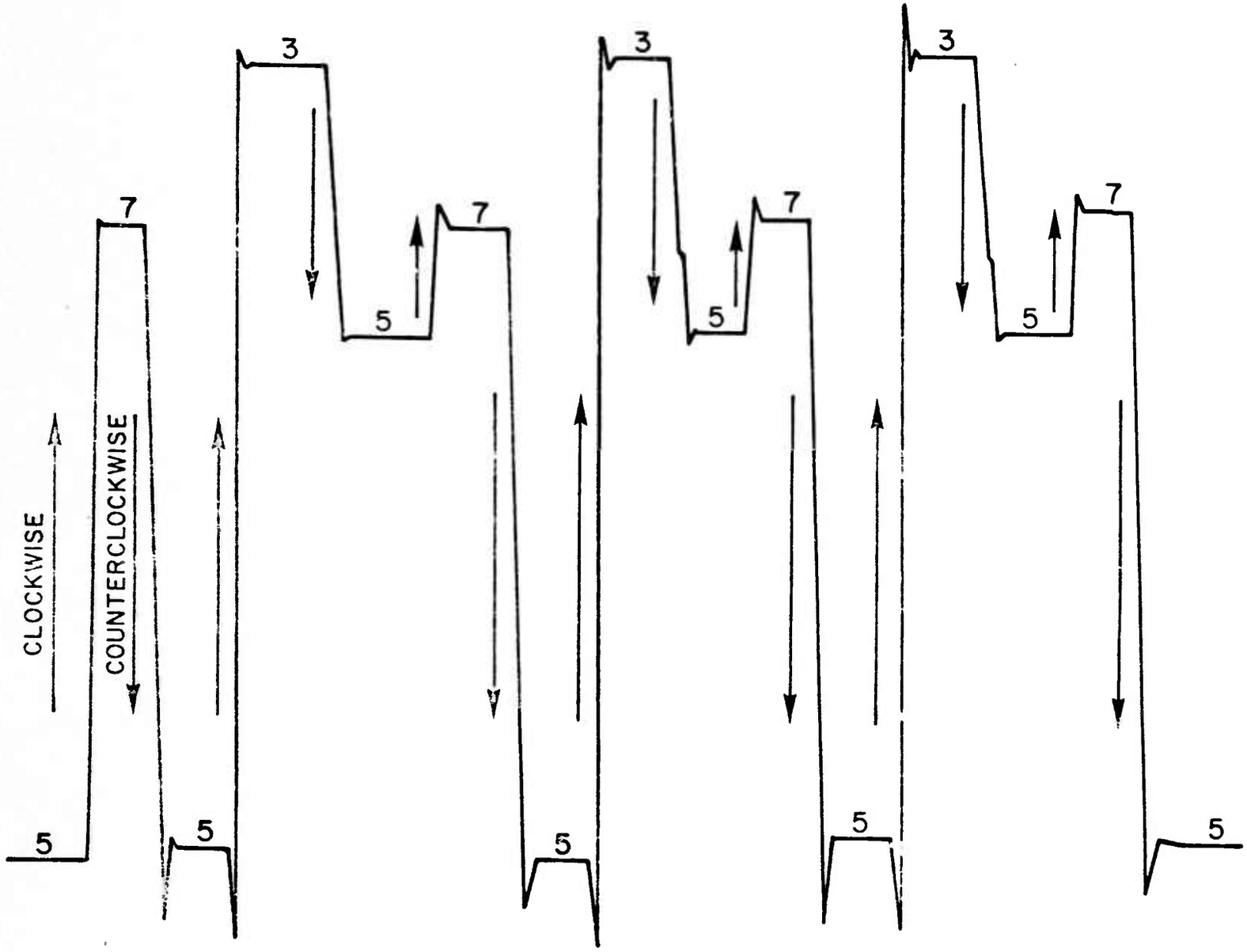

FIGURE 7

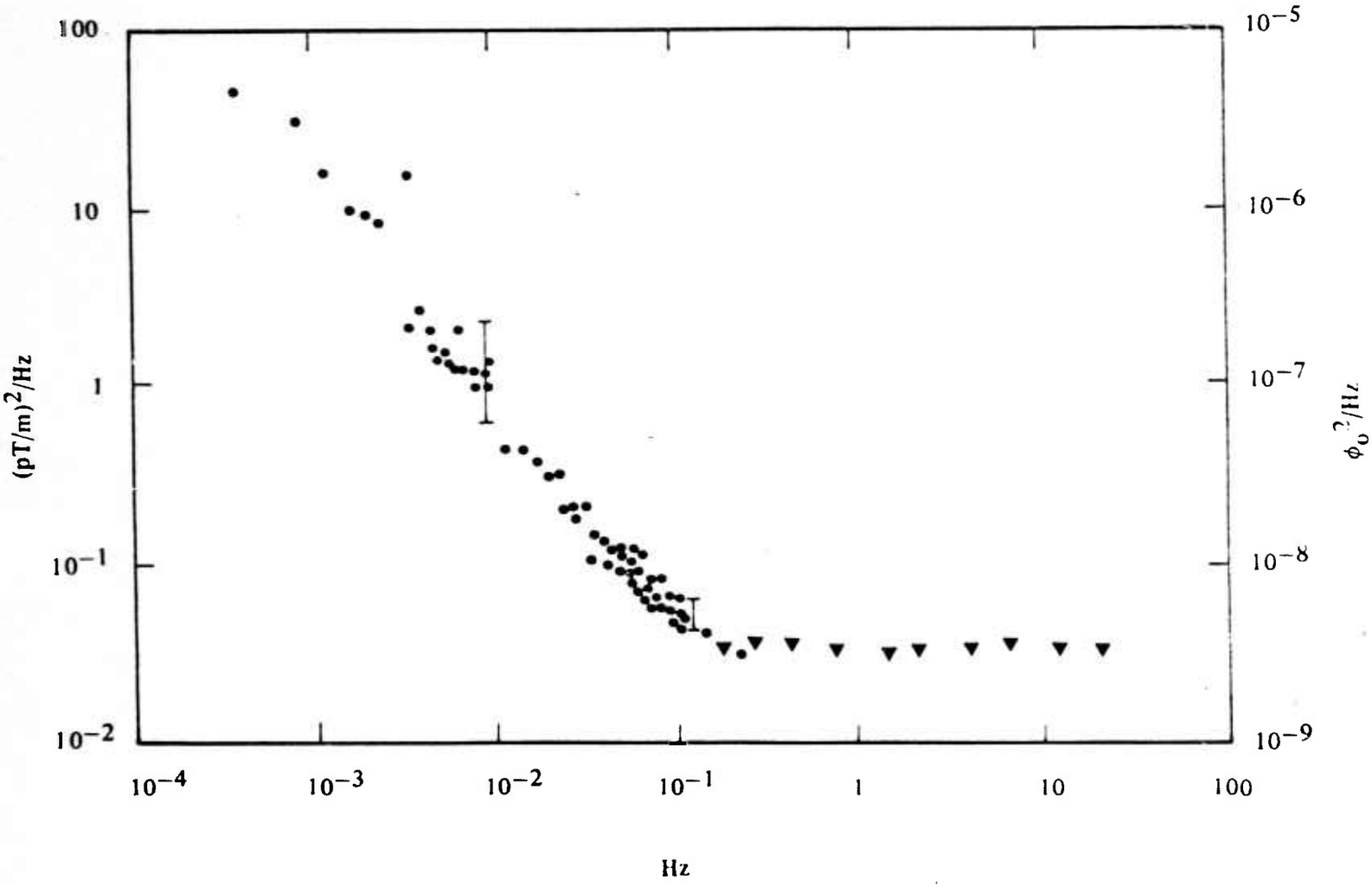
100
10
1
10^{-1}
10^{-2}
$(pT/m)^2/Hz$
10^{-5}
10^{-6}
10^{-7}
10^{-8}
10^{-9}
ϕ_0^2/Hz
10^{-4}
10^{-3}
10^{-2}
10^{-1}
1
10
100
Hz

FIGURE 8

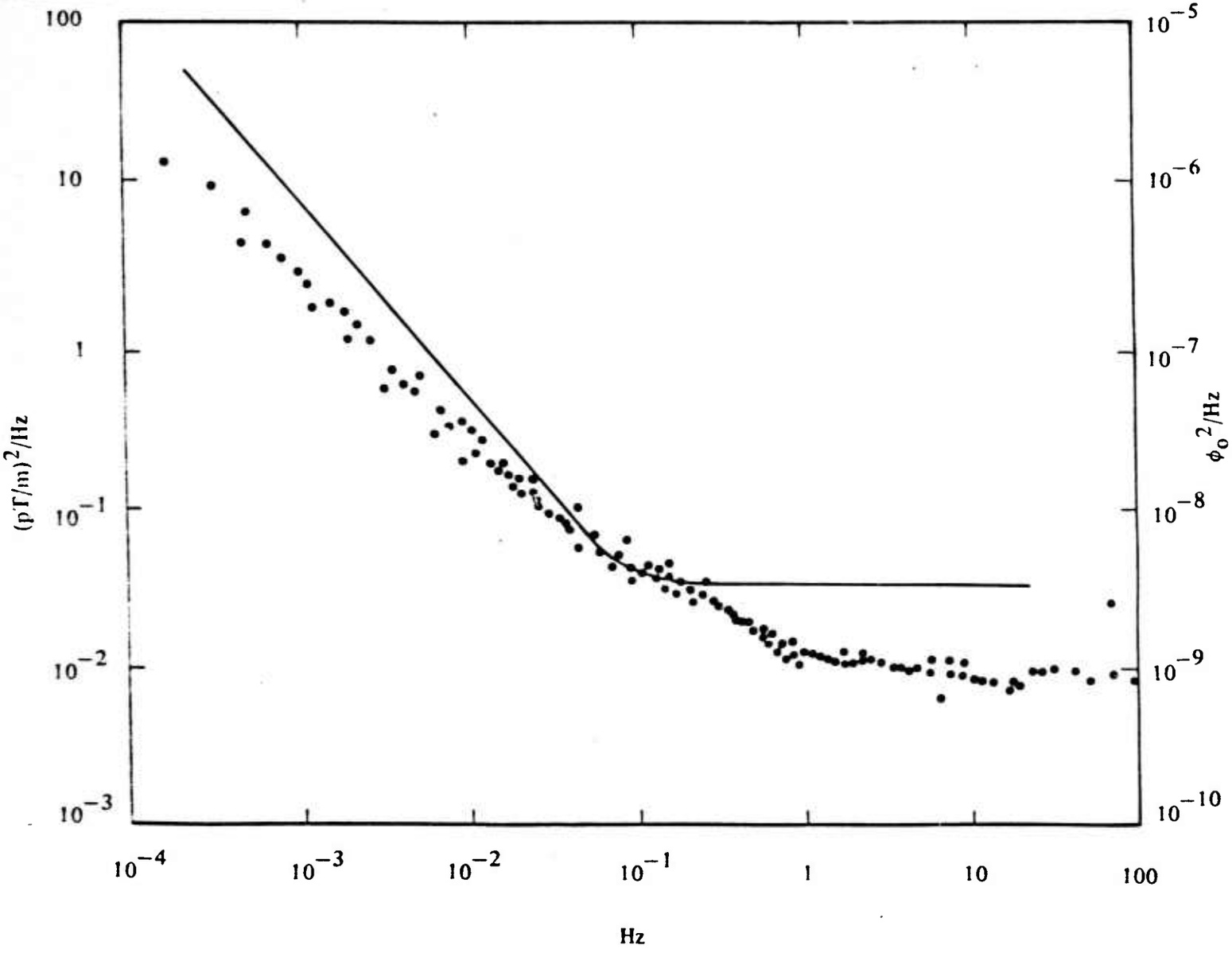
100
10
1
10^{-1}
10^{-2}
10^{-3}
$(p\Gamma/m)^2/Hz$
10^{-4}
10^{-3}
10^{-2}
10^{-1}
1
10
100
Hz
10^{-5}
10^{-6}
10^{-7}
10^{-8}
10^{-9}
10^{-10}
ϕ_o^2/Hz

FIGURE 9

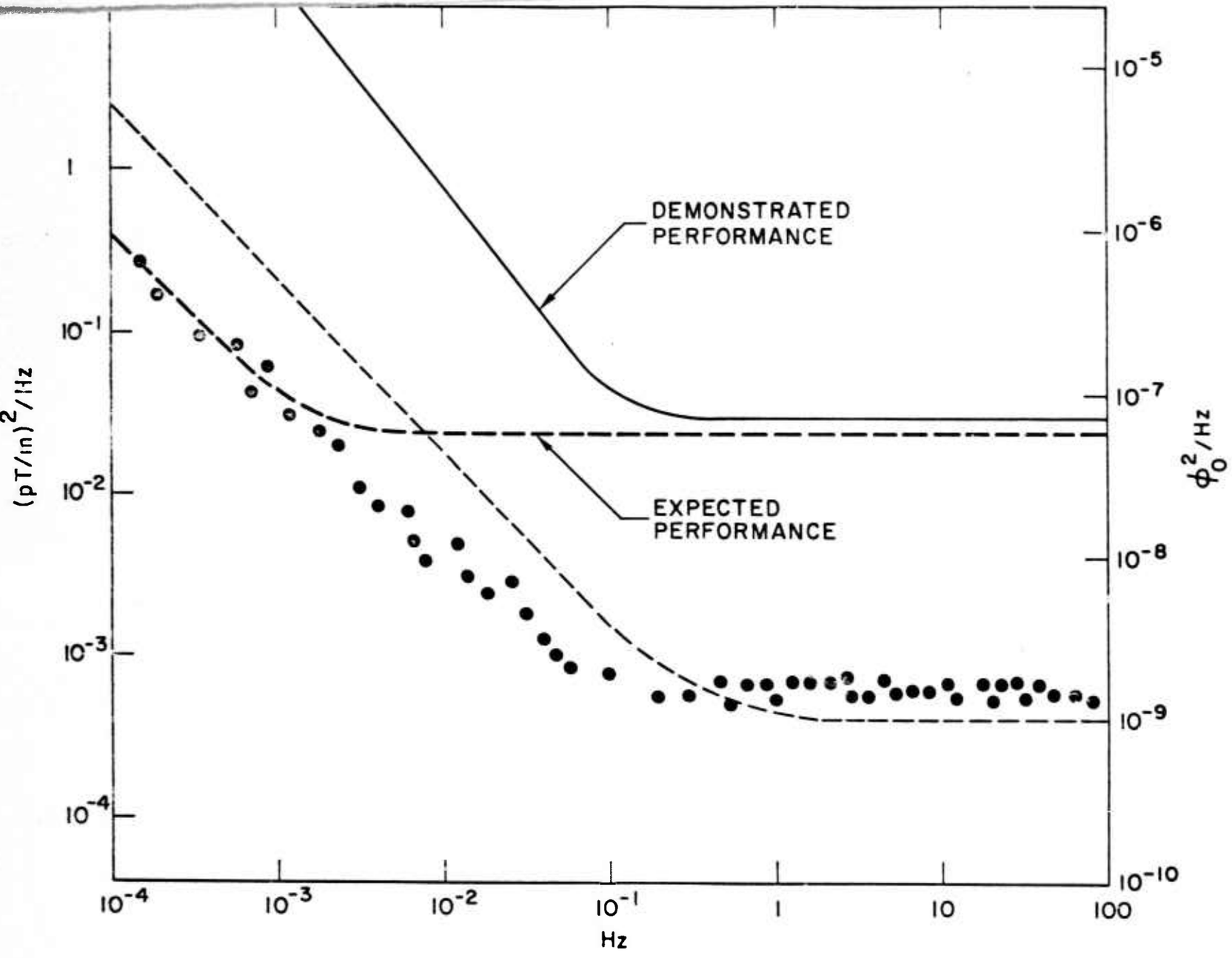
DEMONSTRATED
PERFORMANCE
EXPECTED
PERFORMANCE
(pT/in)^2/Hz
ϕ_0^2/Hz
Hz
1
10^{-1}
10^{-2}
10^{-3}
10^{-4}
10^{-5}
10^{-6}
10^{-7}
10^{-8}
10^{-9}
10^{-10}
10
100

FIGURE 10

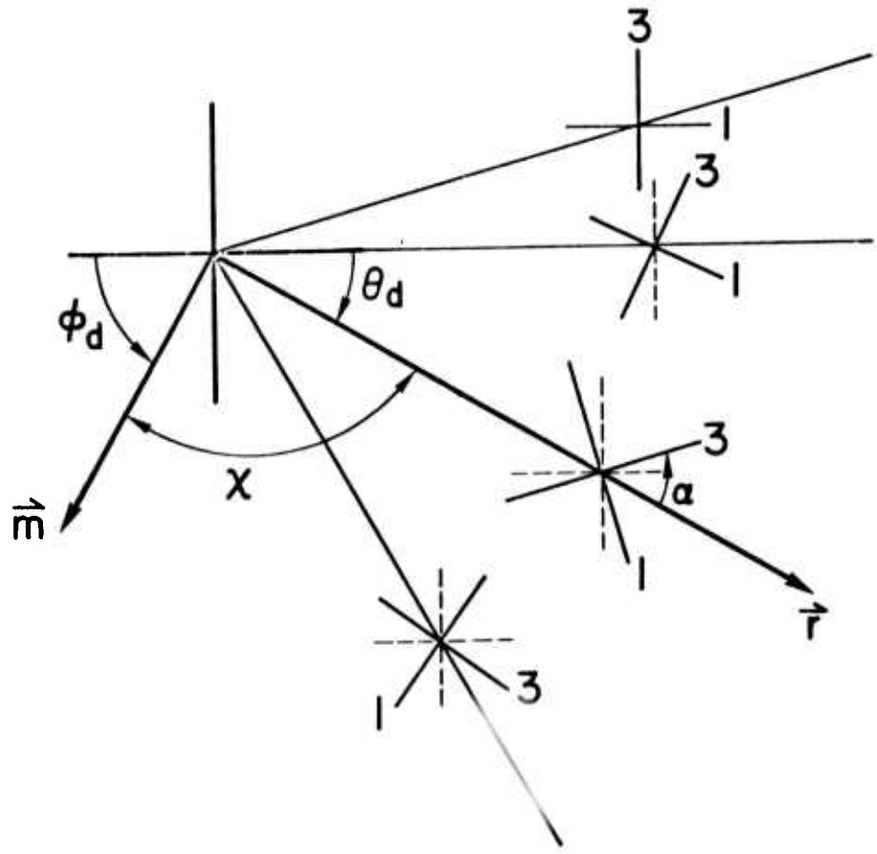

FIGURE 11

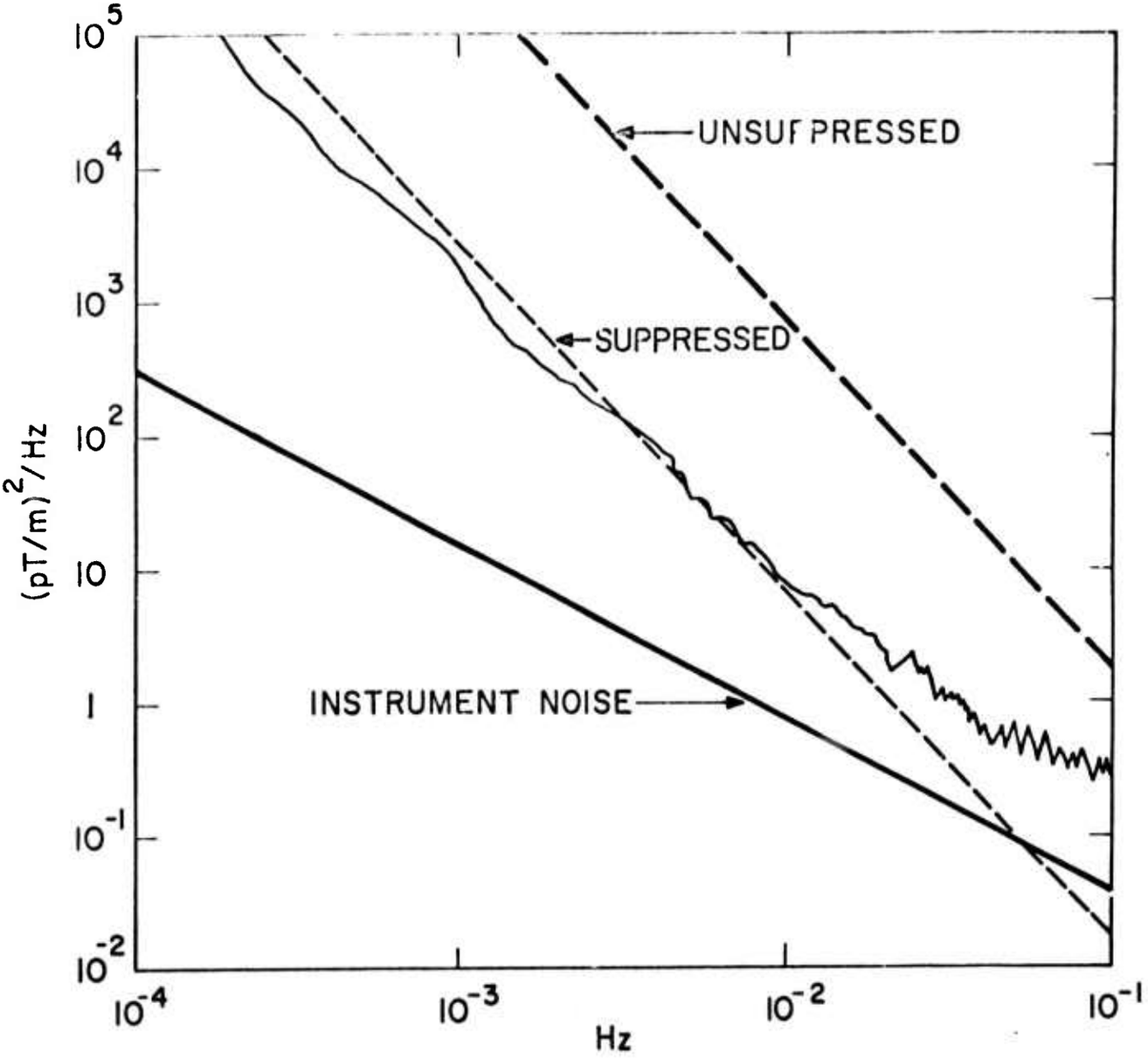
10^5
10^4
10^3
10^2
10
1
10^{-1}
10^{-2}
$(pT/m)^2/Hz$
UNSUPPRESSED
SUPPRESSED
INSTRUMENT NOISE
10^{-4}
10^{-3}
10^{-2}
10^{-1}
Hz

FIGURE 12a

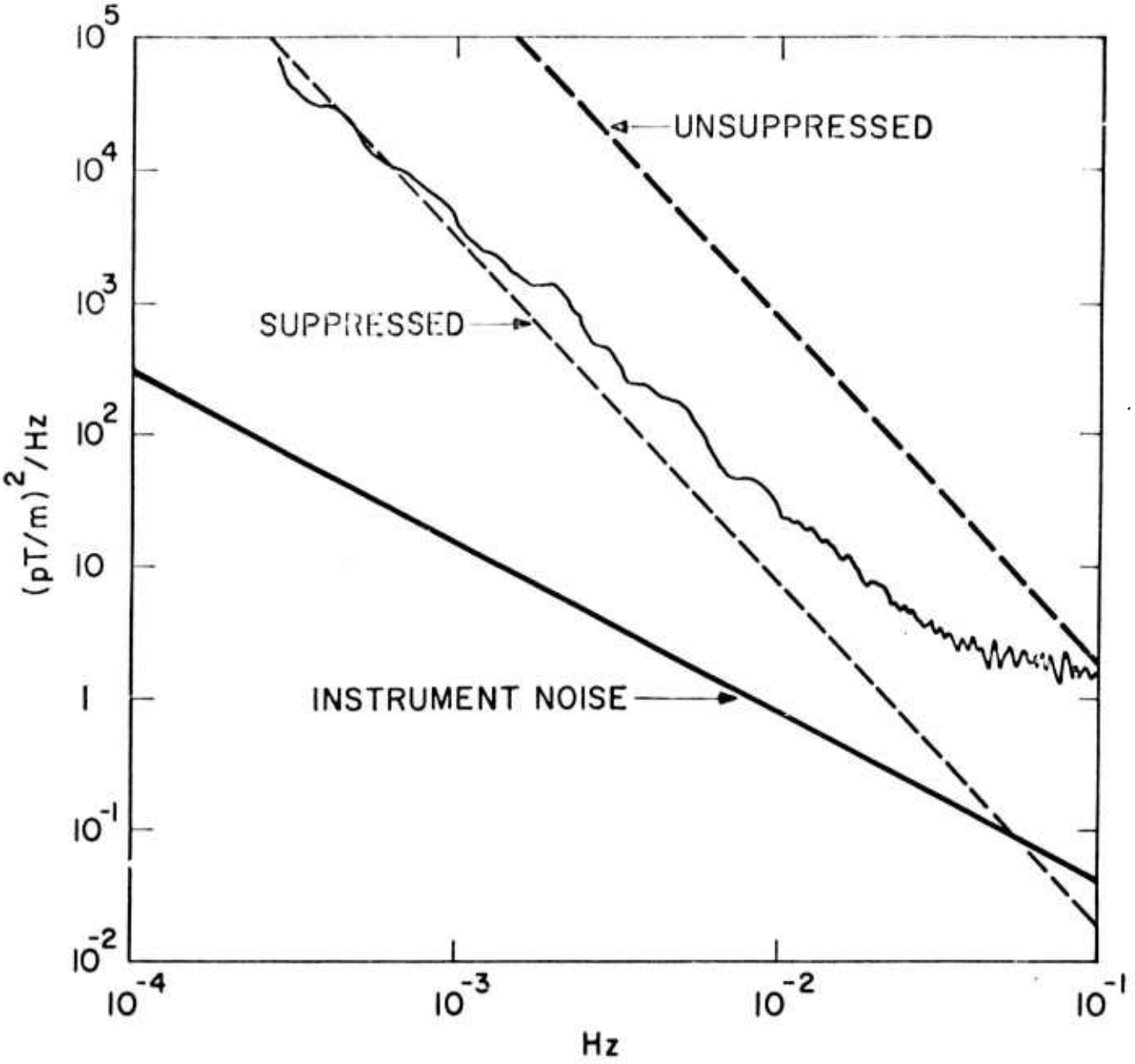
10^5
10^4
10^3
10^2
10
1
10^{-1}
10^{-2}
$(pT/m)^2/Hz$
UNSUPPRESSED
SUPPRESSED
INSTRUMENT NOISE
10^{-4}
10^{-3}
10^{-2}
10^{-1}
Hz

FIGURE 12b

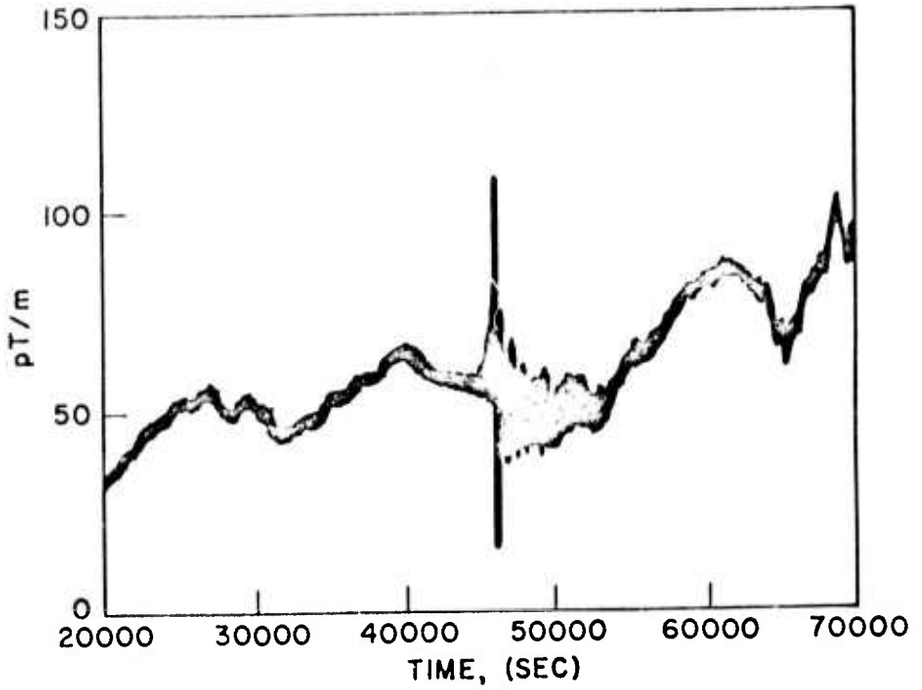

FIGURE 13

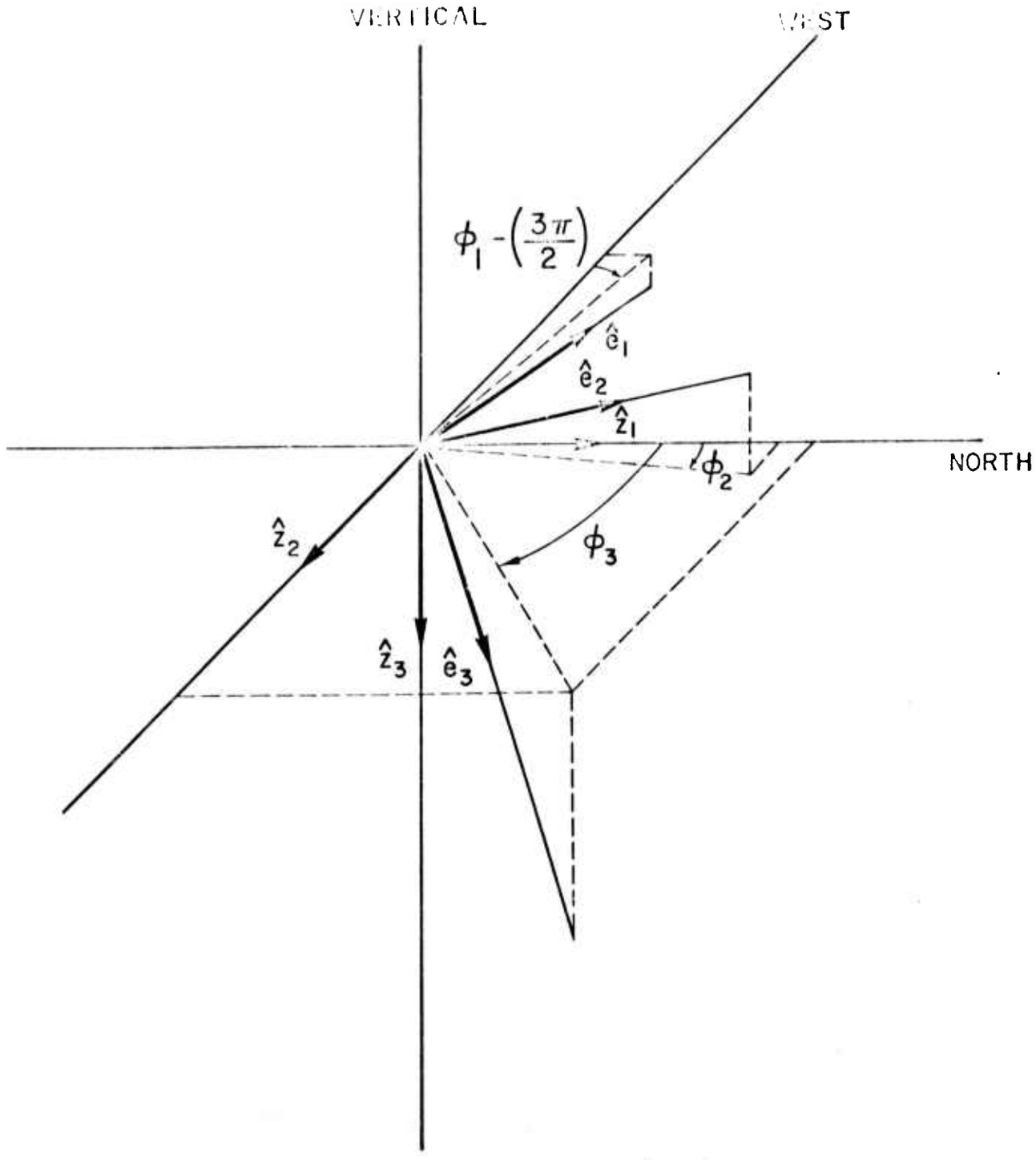
VERTICAL
WEST
NORTH
$\phi_1 - \left(\frac{3\pi}{2}\right)$
$\hat{e}_1$
$\hat{e}_2$
$\hat{z}_1$
ϕ_2
$\hat{z}_2$
ϕ_3
$\hat{z}_3$
$\hat{e}_3$

FIGURE 14

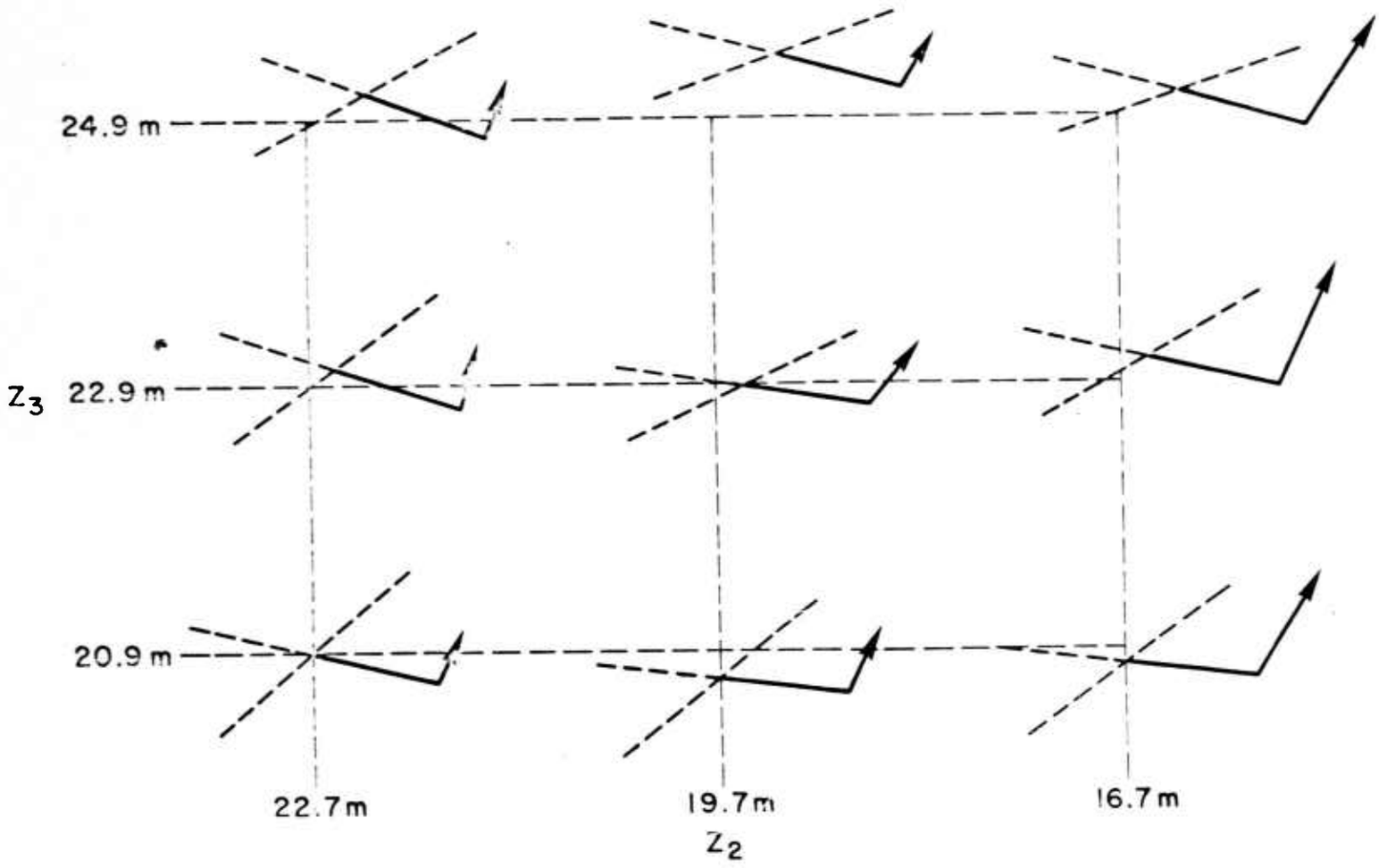

FIGURE 15

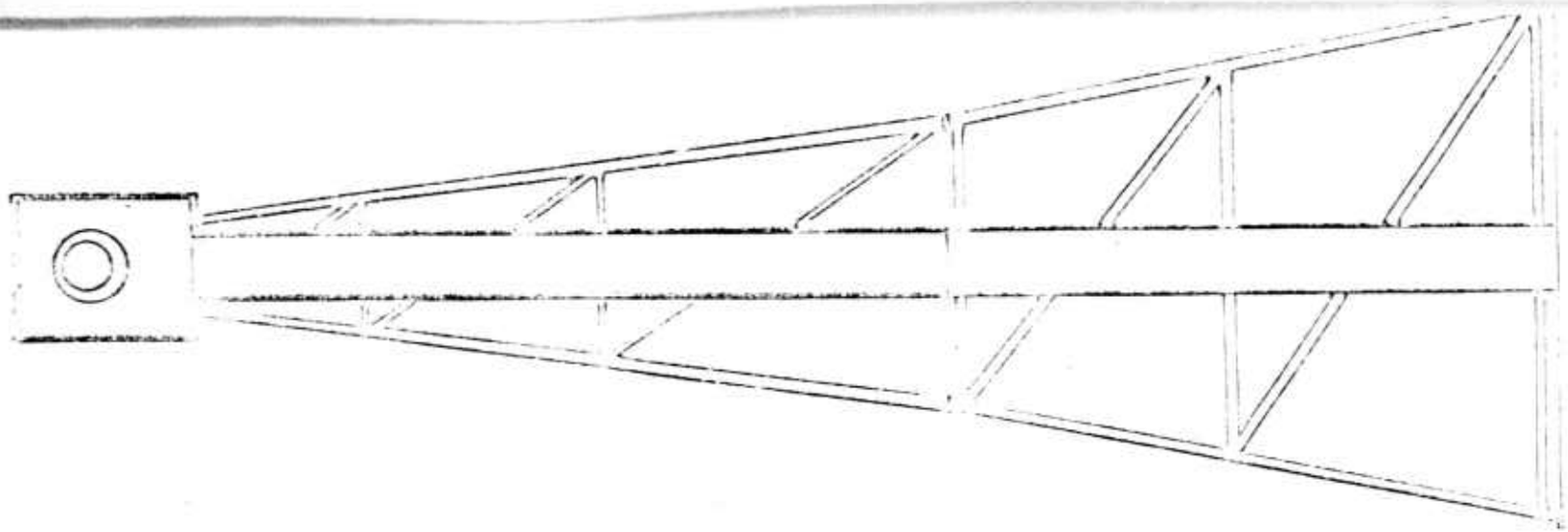

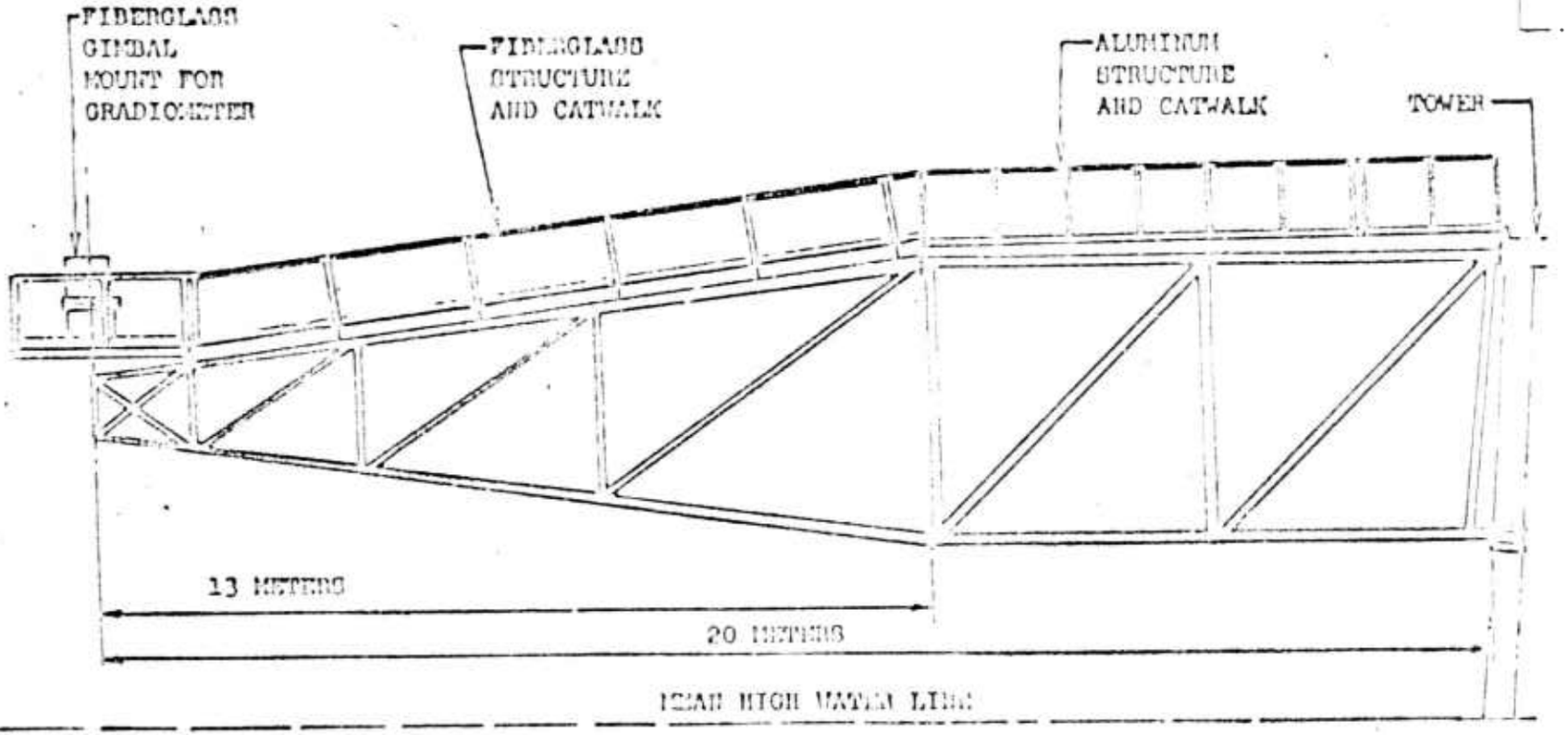
FIBERGLASS
GIMBAL
MOUNT FOR
GRADIOMETER
FIBERGLASS
STRUCTURE
AND CATWALK
ALUMINUM
STRUCTURE
AND CATWALK
TOWER
13 METERS
20 METERS
MEAN HIGH WATER LINE

APPENDIX

GRADIENTS OF MAGNETIC FIELDS IN FREE SPACE

We represent gradients of a magnetic field, $\vec{b}(\vec{R},t)$, by a matrix G having elements $g_{ij}(\vec{R},t)$, where

$$g_{ij} = \hat{x}_i \cdot \vec{\nabla} (\hat{x}_j \cdot \vec{b}), \qquad (i,j = 1,2,3) \tag{1a}$$

in an orthogonal basis $\left\{ \hat{x}_i \right\}$. An element g_{ij} represents the gradient in a direction $\hat{x}_i$ of the component of magnetic field in a direction $\hat{x}_j$. The relation

$$\Gamma(\hat{u},\hat{v}) = \sum_{i,j} g_{ij} u_i v_j \ , \tag{1b}$$

then, gives the gradient in a direction $\hat{u}$ of the component of magnetic field in a direction $\hat{v}$, where u_i and v_i are components of the unit vectors $\hat{u}$ and $\hat{v}$ in the basis $\left\{ \hat{x}_i \right\}$. We express $\Gamma(\hat{u},\hat{v})$ as a matrix product by using the relation

$$\Gamma(\hat{u},\hat{v}) = \tilde{U} G V \ , \tag{1c}$$

where U and V are column matrices representing unit vectors $\hat{u}$ and $\hat{v}$, respectively, and tilde marks a transposed matrix.

Equation 1a shows that the sum of diagonal elements of a gradient matrix vanishes because the divergence of a magnetic field vanishes. Moreover, the vector identity

$$g_{ij} - g_{ji} = (\hat{x}_i \times \hat{x}_j) \cdot (\vec{\nabla} \times \vec{b}) \tag{2}$$

tells us that matrices representing gradients of an irrotational magnetic field are symmetric; namely, $\tilde{G} = G$.

A magnetic field in free space is both nondivergent and irrotational and so is the gradient of a harmonic function, ψ; namely, $\vec{b} = \vec{\nabla}\psi$, where $\nabla^2\psi = 0$. Consequently, gradients of a magnetic field in free space are represented by a symmetric matrix that has a vanishing trace*, whose elements are given by

$$g_{ij} = \frac{\partial^2\psi}{\partial x_i \partial x_j} \tag{3}$$

Only five of the nine elements of a matrix representing gradients of a magnetic field in free space, then, are independent.

An axis of a perfect gradiometer that is aligned in a direction $\hat{x}_i$ and senses the component of magnetic field in a direction $\hat{x}_j$ measures the element g_{ij} of a gradient matrix. A gradiometer comprising two orthogonal axes that measure longitudinal elements g_{11} and g_{22} together with three mutually orthogonal axes that measure transverse elements g_{12}, g_{13}, and g_{23}, then, determines gradients of a magnetic field in free space in the orthogonal basis defined by its axes. Because of Equation 1b, matrix elements measured in the gradiometer basis in turn determine gradients in every direction $\hat{u}$ of the component of magnetic field in any direction $\hat{v}$.

A. GRADIOMETER ROTATIONS

As a gradiometer rotates, matrix elements measured in the gradiometer basis change continuously. We describe gradiometer rotations by a matrix R that represents a rotation from a basis $\{\hat{x}_i\}$ to a basis $\{\hat{y}_i\}$.

* The trace of a matrix is the sum of its diagonal elements.

The matrix R is orthogonal*, and its elements are given by

$$r_{ij} = \hat{x}_i \cdot \hat{y}_j . \tag{4}$$

For a vector represented by a column matrix U_x in a basis $\{\hat{x}_i\}$, the relation

$$U_y = \tilde{R} U_x \tag{5a}$$

gives its representation U_y in a basis $\{\hat{y}_i\}$, where R represents rotation from the basis $\{\hat{x}_i\}$ to the basis $\{\hat{y}_i\}$. Because the matrix product expressed by Equation 1c is invariant, we find that the relation

$$G_y = \tilde{R} G_x R \tag{5b}$$

specifies the matrix G_y representing gradients of a magnetic field in a basis $\{\hat{y}_i\}$ in terms of their representation G_x in a basis $\{\hat{x}_i\}$. Elements of a gradient matrix measured in one basis then determine the gradient matrix in every other basis obtained by rotating the gradiometer.

We express a matrix representing a rotation as the product of three matrices representing three successive, independent rotations through the Eulerian angles Φ, Θ, and Ψ defined in Figure A1 by the product (Indritz, 1963)

* The relation $\tilde{R}R = R\tilde{R} = I$, where I denotes the unit matrix, defines an orthogonal matrix.

$$R(\phi, \theta, \psi) = Z(\phi)\ X(\theta)\ Z(\psi) \tag{6a}$$

where

$$Z(\phi) = \begin{bmatrix} \cos\phi & -\sin\phi & 0 \\ \sin\phi & \cos\phi & 0 \\ 0 & 0 & 1 \end{bmatrix} \tag{6b}$$

and represents a rotation through an angle ϕ about a z-axis, and

$$X(\theta) = \begin{bmatrix} 1 & 0 & 0 \\ 0 & \cos\theta & -\sin\theta \\ 0 & \sin\theta & \cos\theta \end{bmatrix} \tag{6c}$$

and represents a rotation through an angle θ about an x-axis. We note that $\tilde{Z}(\phi) = Z(-\phi)$ and $\tilde{X}(\theta) = X(-\theta)$, so that $\tilde{R}(\phi, \theta, \psi) = R(-\psi, -\theta, -\phi)$.

A rotation specified by Euler angles ϕ, θ, and ψ, however, is equivalent to rotation through an angle ϕ about some axis specified by polar angles ϕ_o and θ_o with respect to the fiducial basis (Goldstein, 1959). Namely,

$$Z(\phi) = \tilde{P}(\phi_o, \theta_o)R(\phi, \theta, \psi)P(\phi_o, \theta_o) \quad , \tag{7a}$$

so that

$$R(\phi_o, \theta_o; \phi) = P(\phi_o, \theta_o)Z(\phi)\tilde{P}(\phi_o, \theta_o) = R(\phi, \theta, \psi) \quad , \tag{7b}$$

where $P(\phi_o, \theta_o) = Z(\phi_o + \pi/2)X(\theta_o)$ and represents a rotation from the fiducial basis to a basis having its z-axis aligned with the axis of rotation. From Equation 7b we find that angles ϕ_o, θ_o, and ϕ are expressed in terms of Eulerian angles specifying the same rotation by the relations

$$\phi_o = \frac{\Phi - \Psi}{2} \tag{8a}$$

$$\tan \theta_o = \frac{\tan \Theta/2}{\sin\left(\frac{\Phi + \Psi}{2}\right)} \tag{8b}$$

and

$$\cos \phi/2 = \cos \Theta/2 \cos\left(\frac{\Phi + \Psi}{2}\right) \tag{8c}$$

To make the dependence on the angle of rotation ϕ explicit, we write a rotation matrix as the sum

$$R(\phi_o, \theta_o; \phi) = E_1(\phi_o, \theta_o) + E_2(\phi_o, \theta_o)\cos\phi + Q(\phi_o, \theta_o)\sin\phi \tag{9a}$$

where

$$E_1(\phi_o, \theta_o) = P(\phi_o, \theta_o)\varepsilon_x\varepsilon_z\varepsilon_y\tilde{P}(\phi_o, \theta_o) , \tag{9b}$$

$$E_2(\phi_o, \theta_o) = I - E_1(\phi_o, \theta_o) , \tag{9c}$$

and

$$Q(\phi_o, \theta_o) = P(\phi_o, \theta_o)\varepsilon_z\tilde{P}(\phi_o, \theta_o) \tag{9d}$$

with

$$\varepsilon_x = \begin{bmatrix} 0 & 0 & 0 \\ 0 & 0 & -1 \\ 0 & 1 & 0 \end{bmatrix} \quad \varepsilon_y = \begin{bmatrix} 0 & 0 & 1 \\ 0 & 0 & 0 \\ -1 & 0 & 0 \end{bmatrix} \text{ , and } \varepsilon_z = \begin{bmatrix} 0 & -1 & 0 \\ 1 & 0 & 0 \\ 0 & 0 & 0 \end{bmatrix}$$

The matrix Q corresponds to a sum of differential rotations about x,y, and z axes of the fiducial basis, as expressed by the expansion

$$Q(\phi_o, \theta_o) = \varepsilon_x \sin\theta_o \cos\phi_o + \varepsilon_y \sin\theta_o \sin\phi_o + \varepsilon_z \cos\theta_o, \quad (10a)$$

and for an infinitesimal rotation $\Delta\phi$,

$$R(\phi_o, \theta_o; \Delta\phi) = I + Q(\phi_o, \theta_o)\Delta\phi \quad (10b)$$

Having presented means for describing gradiometer rotations, we now investigate changes in gradient signals produced by changes in orientation of a gradiometer. We first consider rotation about an axis of the gradiometer basis and then about an arbitrary axis.

1. Rotation about a gradiometer axis

Naming of axes of a gradiometer basis is arbitrary, and so we call the axis of rotation the z-axis. Following rotation of a gradicmeter through an angle ϕ about its z-axis, the gradient matrix measured in the gradiometer basis, $\Gamma(\phi)$, is expressed in terms of its initial value G by the relation

$$\Gamma(\phi) = \tilde{Z}(\phi) G Z(\phi) \ . \quad (11a)$$

Consequently, its elements γ_{ij} are given in terms of their initial values g_{ij}, by the relations

$$\gamma_{11} = -g_{33}/2 + \left[g_{12}^2 + (g_{11}+g_{33}/2)^2 \right]^{1/2} \cos 2(\phi_1 - \phi) \quad (12a)$$

$$\gamma_{22} = -g_{33}/2 - \left[g_{12}^2 + (g_{11}+g_{33}/2)^2 \right]^{1/2} \cos 2(\phi_1 - \phi) \quad (12b)$$

$$\gamma_{33} = g_{33} \quad (12c)$$

$$\gamma_{12} = \left[g_{12}^2 + (g_{11}+g_{33}/2)^2 \right]^{1/2} \sin 2(\phi_1 - \phi) \quad (12d)$$

$$\gamma_{13} = (g_{13}^2 + g_{23}^2)^{1/2}\sin(\phi_2 + \phi) \tag{12e}$$

and

$$\gamma_{23} = (g_{13}^2 + g_{23}^2)^{1/2}\cos(\phi_2 + \phi) \tag{12f}$$

where

$$\tan 2\phi_1 = g_{12}/(g_{11} + g_{33}/2) \tag{12g}$$

and

$$\tan \phi_2 = g_{13}/g_{23} \tag{12h}$$

We observe that the longitudinal gradient γ_{33} is constant, that longitudinal gradients γ_{11} and γ_{22} vary sinusoidally about the mean value $(g_{11} + g_{22})/2$, and that transverse gradients vary sinusoidally about zero. As a result, we can always find a null position for a transverse gradient by rotating a gradiometer about any one of its axes, since specification of a z-axis is arbitrary. We can not find a null position for longitudinal gradients unless $g_{12}^2 \geqslant g_{11}g_{22}$, $g_{23}^2 \geqslant g_{22}g_{33}$, or $g_{13}^2 \geqslant g_{11}g_{33}$. Because the sum of diagonal elements vanishes, however, at least two of the conditions are satisfied.*

2. Rotation about an arbitrary axis

During rotation of a gradiometer about an axis other than one of its three mutually perpendicular axes, each element

* Nonetheless, determination of a null position for longitudinal gradients is impractical because mean values of sinusoidal oscillations are experimentally indeterminant.

of the gradient matrix oscillates about a nonzero mean value. Oscillations are a sum of sinusoids having arguments ϕ and 2ϕ, where ϕ is the angle of rotation. Amplitudes of sinusoidal oscillations depend on initial orientation of the gradiometer and polar angles ϕ_o and θ_o specifying the axis of rotation with respect to its initial orientation.

The relation

$$\Gamma(\phi_o, \theta_o; \phi) = \tilde{R}(\phi_o, \theta_o; \phi)GR(\phi_o, \theta_o; \phi) \tag{13a}$$

gives the gradient matrix obtained by rotating a gradiometer through an angle ϕ about an axis specified by polar angles ϕ_o and θ_o with respect to its initial orientation in terms of the initial value G. When the rotation matrix $R(\phi_o, \theta_o; \phi)$ is expressed explicitly in terms of the rotation angle by Equation 9a, we find that $\Gamma(\phi_o, \theta_o; \phi)$ is expressed as a sum of sinusoids with arguments ϕ and 2ϕ by the relation

$$\begin{aligned}\Gamma(\phi_o, \theta_o; \phi) = {} & E_1GE_1 + 1/2(E_2GE_2 - QGQ) + 1/2(E_2GE_2 + \\ & QGQ)\cos 2\phi + 1/2(E_2GQ - QGE_2)\sin 2\phi + \\ & (E_1GE_2 + E_2GE_1)\cos\phi + (E_1GQ - QGE_1)\sin\phi ,\end{aligned} \tag{13b}$$

where matrices $E_1(\phi_o, \theta_o)$, $E_2(\phi_o, \theta_o)$, and $Q(\phi_o, \theta_o)$ are given by Equations 9b, 9c, and 9d.

Because mean values and amplitudes of sinusoidal components depend on polar angles ϕ_o and θ_o and on the initial matrix G, we can not always find a null position for transverse gradients by rotating a gradiometer about an axis

other than one of its three mutually perpendicular axes. Nonetheless, for axes of rotation lying within a narrow cone about a gradiometer axis, defined by $\theta_o \ll 1$ for a z-axis, we find from Equation 9a that

$$R(\phi_o, \theta_o; \phi) \cong Z(\phi)\left|I + \theta_o E(\phi_o, \phi)\right| \quad , \quad \theta_o \ll 1 \, , \tag{14a}$$

where

$$E(\phi_o, \phi) \cong \left|\sin(\phi-\phi_o)+\sin\phi_o\right| \varepsilon_x + \left|\cos(\phi-\phi_o)-\cos\phi_o\right| \varepsilon_y , \tag{14b}$$

so that

$$\Gamma(\phi_o, \theta_o; \phi) \cong \Gamma(\phi) + \theta_o \left|\Gamma(\phi)E(\phi_o, \phi)-E(\phi_o, \phi)\Gamma(\phi)\right| , \tag{14c}$$

where $\Gamma(\phi)$ is given by Equation 11a. We conclude from Equation 14c that transverse gradients vanish during rotation of a gradiometer about an axis lying within a narrow cone about any one of its three mutually perpendicular axes.

3. Infinitesimal rotations

For an infinitesimal rotation through an angle $\Delta\phi$ about an axis specified by polar angles ϕ_o and θ_o, we find from Equations 13a and 10b that the differential of the gradient matrix is given by

$$\Gamma(\phi_o, \theta_o; \Delta\phi) - G = \Delta\phi \left[GQ(\phi_o, \theta_o) - Q(\phi_o, \theta_o)G\right] \, , \tag{15a}$$

where the matrix $Q(\phi_o, \theta_o)$ is expressed as a sum of differential rotations about x,y and z axes of the fiducial basis by Equation 10a. From Equations 15a and 10a, we then find that differentials of the matrix elements are given by

$$\Delta g_{11} = 2(g_{12}\,\Delta\phi_z - g_{13}\,\Delta\phi_y) \tag{15b}$$

$$\Delta g_{22} = 2(g_{23}\,\Delta\phi_x - g_{12}\,\Delta\phi_z) \tag{15c}$$

$$\Delta g_{33} = 2(g_{13}\,\Delta\phi_y - g_{23}\,\Delta\phi_x) \tag{15d}$$

$$\Delta g_{12} = g_{13}\,\Delta\phi_x - g_{23}\,\Delta\phi_y + (g_{22} - g_{11})\Delta\phi_z \tag{15e}$$

$$\Delta g_{13} = -g_{12}\,\Delta\phi_x + (g_{11} - g_{33})\Delta\phi_y + g_{23}\Delta\phi_z \tag{15f}$$

and

$$\Delta g_{23} = (g_{33} - g_{22})\Delta\phi_x + g_{12}\,\Delta\phi_y - g_{13}\Delta\phi_z \tag{15g}$$

where

$$\Delta\phi_x = \Delta\phi \sin\theta_o \cos\phi_o \tag{15h}$$

$$\Delta\phi_y = \Delta\phi \sin\theta_o \sin\phi_o \tag{15i}$$

and

$$\Delta\phi_z = \Delta\phi \cos\theta_o \tag{15j}$$

A. PRINCIPAL AXES OF A GRADIENT FIELD

Because a gradient matrix is both real and symmetric, it is diagonal in an orthogonal basis comprised of principal axes with diagonal elements or eigenvalues λ_1, λ_2, and λ_3. Since the trace of a gradient matrix vanishes, $\lambda_1 + \lambda_2 + \lambda_3 = 0$. The diagonal matrix Λ and a matrix R specifying rotation from a gradiometer basis to the basis comprised

of principal axes determine the matrix G measured in a gradiometer basis; namely, $\Lambda = \tilde{R}GR$, so that $G = R\Lambda\tilde{R}$. As a result, two eigenvalues and three Euler angles specifying orientation of principal axes with respect to a gradiometer basis are a set of five independent scalars that determine gradients measured in a gradiometer basis.

If orientation of both the gradiometer basis and principal axes is specified with respect to an arbitrary fiducial basis by matrices R_g and R_p, respectively, then $R_p = R_g R$, and so $G = \tilde{R}_g R_p \Lambda \tilde{R}_p R_g$. On the one hand, if principal axes are taken as the fiducial basis, then $R_p = I$ and $G = \tilde{R}_g \Lambda R_g$, and on the other hand, if the gradiometer basis is taken as the fiducial basis, then $R_g = I$ and $G = R_p \Lambda \tilde{R}_p$. For a gradiometer aligned along principal axes, $R_g = R_p$ and so $G = \Lambda$. Transverse gradients then vanish, and longitudinal gradients equal the eigenvalues λ_1, λ_2, and λ_3.

Eigenvalues of a gradient matrix are roots of the characteristic equation

$$\det(G - \lambda I) = (\lambda - \lambda_1)(\lambda - \lambda_2)(\lambda - \lambda_3) = 0 \qquad (16a)$$

or

$$\lambda^3 - \lambda(g_{11}^2 + g_{33}^2 + g_{11}g_{33} + g_{12}^2 + g_{13}^2 + g_{23}^2) - \det G = 0 \qquad (16b)$$

Roots of the characteristic equation are ordered, and we name them so that $\lambda_1 > \lambda_2 > \lambda_3$. Because the sum of eigenvalues vanishes, at least one root is positive and one is negative, so that λ_1 and λ_3 are, respectively, the greatest positive root and smallest negative root of the characteristic equation.

Direction cosines of corresponding eigenvectors $\hat{e}_k$, which define directions of principal axes, form the columns of the matrix R specifying rotation from a gradiometer basis to the basis comprised of principal axes; namely, $r_{ik} = \hat{x}_i \cdot \hat{e}_k$. Elements of the kth column of R are a solution of the system of three homogenous equations

$$\sum_j g_{ij} r_{jk} = \lambda_k r_{ik} , \quad i = 1,2,3 , \tag{17}$$

obtained from the matrix equation GR = RΛ. The characteristic equation assures existence of a solution.

Consequently, we find from Equation 17 that polar angles ϕ_k and θ_k specifying the direction of $\hat{e}_k$ with respect to the gradiometer basis are determined by the relations

$$\tan\theta_k \cos\phi_k = \frac{g_{13}(\lambda_k - g_{22}) + g_{12}g_{23}}{(\lambda_k - g_{11})(\lambda_k - g_{22}) - g_{12}^2} \tag{18a}$$

and

$$\tan\theta_k \sin\phi_k = \frac{g_{23}(\lambda_k - g_{11}) + g_{12}g_{13}}{(\lambda_k - g_{11})(\lambda_k - g_{22}) - g_{12}^2} \tag{18b}$$

We observe that polar angles $\phi_k' = \phi_k + \pi$ and $\theta_k' = \pi - \theta_k$ as well as ϕ_k and θ_k are solutions of Equations 18a and 18b for each eigenvalue, so that both $\hat{e}_k$ and $-\hat{e}_k$ are eigenvectors corresponding to eigenvalue λ_k, as is also evident from Equation 17. Because the sense of an eigenvector is indeterminant, we can combine three eigenvectors in eight ways to form eight orthogonal bases comprised of principal axes. Four of the eight bases are right-handed, and four are left-handed. We exclude left-handed bases and find that four right-handed, orthogonal bases comprised of principal axes

are defined by the four sets of eigenvectors: $(\hat{e}_1, \hat{e}_2, \hat{e}_3)$, $(\hat{e}_1, -\hat{e}_2, -\hat{e}_3)$, $(-\hat{e}_1, -\hat{e}_2, \hat{e}_3)$, and $(-\hat{e}_1, \hat{e}_2, -\hat{e}_3)$.

To determine a first set of eigenvectors, we choose $\hat{e}_1$ and $\hat{e}_3$ so that $0 \leqslant \theta_1 \leqslant \pi/2$ and $0 \leqslant \theta_3 \leqslant \pi/2$ and require right-handedness, namely that $\hat{e}_2 = \hat{e}_3 \times \hat{e}_1$, so that

$$\cos \theta_2 = \sin \theta_3 \sin \theta_1 \sin(\phi_1 - \phi_3) \tag{19}$$

From Equations 18a and 18b, we then find a unique set of polar angles $(\phi_1, \theta_1; \phi_2, \theta_2; \phi_3, \theta_3)$ defining directions of the set of eigenvectors $(\hat{e}_1, \hat{e}_2, \hat{e}_3)$. Polar angles defining directions of the other three sets of eigenvectors are then directly determined. For example, polar angles for the set $(\hat{e}_1, -\hat{e}_2, -\hat{e}_3)$ are given by the set $(\phi_1, \theta_1; \phi_2 + \pi, \pi - \theta_2; \phi_3 + \pi, \pi - \theta_3)$.

By expressing elements r_{ik} of the matrix R specifying rotation from the gradiometer basis to the basis defined by the set of eigenvectors $(\hat{e}_1, \hat{e}_2, \hat{e}_3)$ in terms of Euler angles Φ, Θ, and Ψ, we find that the Euler angles specifying the rotation are determined by the relations

$$\Phi = \phi_3 + \pi/2 , \tag{20a}$$

$$\Theta = \theta_3 , \tag{20b}$$

$$\cos\Psi = \sin\theta_1 \sin(\phi_1 - \phi_3) , \tag{20c}$$

and

$$\sin\Psi = \sin\theta_2 \sin(\phi_3 - \phi_2) . \tag{20d}$$

Euler angles specifying rotation from the gradiometer basis to bases defined by the sets of eigenvectors $(\hat{e}_1, -\hat{e}_2, -\hat{e}_3)$, $(-\hat{e}_1, -\hat{e}_2, \hat{e}_3)$, and $(-\hat{e}_1, \hat{e}_2, -\hat{e}_3)$ are given in terms of those of the first set by the sets $(\Phi + \pi, \pi - \Theta, \pi - \Psi)$, $(\Phi, \Theta, \pi + \Psi)$, and $(\Phi + \pi, \pi - \Theta, 2\pi - \Psi)$, respectively.

As we show subsequently, eigenvalues of a gradient field at a point are equal to eigenvalues of the gradient field produced by a magnetic dipole located on a sphere of unit radius about the field point. Because four sets of eigenvectors correspond to the same set of eigenvalues, a magnetic dipole located at any one of four positions on the unit sphere produces the same magnetic field gradients at the field point.

C. GRADIENT FIELD OF A MAGNETIC DIPOLE

We examine the gradient field of a magnetic dipole both to illustrate means of describing gradients of magnetic fields in free space and to provide the basis for demonstrating that gradients of a magnetic field at a point in free space are equal to gradients produced by a magnetic dipole located on a sphere of unit radius about the point.

The gradient of the harmonic function

$$\psi = \frac{-\mu_o \vec{m}\cdot\vec{r}}{4\pi\, r^3}\ , \quad \mu_o = 4\pi \times 10^{-7}\ \text{H/m}\ , \tag{21a}$$

gives, in MKS units, the magnetic field produced at a position $\vec{r}$ by a magnetic dipole of moment $\vec{m}$. The relation

$$\vec{b} = \vec{\nabla}\psi = \frac{\mu_o m}{4\pi\, r^3}\left[2(\hat{m}\cdot\hat{r})\hat{r} - \hat{r} \times (\hat{m} \times \hat{r})\right]\ , \tag{21b}$$

then, expresses the magnetic field $\vec{b}$ as a sum of components parallel and perpendicular to the unit vector $\hat{r}$, where $\hat{r} = \vec{r}/r$ and $\hat{m} = \vec{m}/m$. Equation 21b tells us that the magnetic field produced at a position $\vec{r}$ by a dipole of strength m is a sum of fields produced by one dipole of strength $m \cos\chi$ directed along $\vec{r}$ and another of strength $m \sin\chi$ directed perpendicular to $\vec{r}$, where $\cos\chi = \hat{m}\cdot\hat{r}$.

To examine gradients of the magnetic field of a dipole, we consider the gradient field in three right-handed, orthogonal bases: (1) a basis $\{\hat{x}_i\}$ with its $\hat{x}_3$ axis aligned along the dipole axis $\hat{m}$, which we call the dipole basis; (2) a basis $\{\hat{y}_i\}$ with its $\hat{y}_3$ axis aligned along the position vector $\vec{r}$, which we call the position-vector basis; and (3) a basis $\{\hat{z}_i\}$ with its $\hat{z}_3$ axis aligned in an arbitrary direction.

1. Dipole basis

We choose a basis $\{\hat{x}_i\}$ with the $\hat{x}_3$ axis directed along the dipole axis $\hat{m}$; the $\hat{x}_2$ axis, along $\hat{m} \times \hat{r}$; and the $\hat{x}_1$ axis, along $(\hat{m} \times \hat{r}) \times \hat{m}$. From Equation 3 and the harmonic potential function of a dipole expressed by Equation 21a, then, we find that the matrix G_x representing gradients of the magnetic field of a dipole in the basis $\{\hat{x}_i\}$ is expressed as

$$G_x = g \begin{bmatrix} \cos\chi(1 - 5\sin^2\chi) & 0 & \sin\chi(1 - 5\cos^2\chi) \\ 0 & \cos\chi & 0 \\ \sin\chi(1 - 5\cos^2\chi) & 0 & \cos\chi(-2 + 5\sin^2\chi) \end{bmatrix}, \qquad (22a)$$

where $\cos\chi = \hat{m}\cdot\hat{r}$ and

$$g = \frac{\mu_o}{4\pi}\left(\frac{3m}{r^4}\right) \tag{22b}$$

We then find, from Equation 16b, that its eigenvalues are given by

$$\lambda_1 = \frac{g}{2}\left|(4 + 5\cos^2\chi)^{1/2} - \cos\chi\right| \tag{23a}$$

$$\lambda_2 = g\cos\chi \tag{23b}$$

and

$$\lambda_3 = \frac{-g}{2}\left|(4 + 5\cos^2\chi)^{1/2} + \cos\chi\right| \tag{23c}$$

Figure A2 delineates λ_1/g, λ_2/g, and λ_3/g as functions of χ and shows that λ_1 is positive, λ_3 is negative, and λ_2 is positive for $0<\chi<\pi/2$ and negative for $\pi/2<\chi<\pi$.

Moreover, the set of Euler angles $(\pi/2, \Theta, \pi/2)$, where $\Theta = \chi + \alpha$ and

$$\tan 2\alpha = (2/3)\tan\chi \qquad (0<\alpha<\pi/2) \tag{24a}$$

specifies a rotation from the dipole basis to the basis comprised of principal axes defined by the set of eigenvectors $(\hat{e}_1, \hat{e}_2, \hat{e}_3)$, as illustrated in Figure A3. The angle α between the eigenvector $\hat{e}_3$ and the position vector $\vec{r}$ ranges from 0 to $\pi/2$ as χ ranges from 0 to π. The relation

$$\tan\beta = (1/2)\tan\chi \tag{24b}$$

determines the angle β between the magnetic field vector and the position vector, which ranges from 0 to π and as χ ranges from 0 to π.

The sets of Euler angles $(3\pi/2, \pi - \theta, \pi/2)$, $(\pi/2, \theta, 3\pi/2)$, and $(3\pi/2, \pi - \theta, 3\pi/2)$ specify rotations to bases defined by the sets of eigenvectors $(\hat{e}_1, -\hat{e}_2, -\hat{e}_3)$, $(-\hat{e}_1, -\hat{e}_2, \hat{e}_3)$, and $(-\hat{e}_1, \hat{e}_2, -\hat{e}_3)$, respectively. Figure A4 depicts orientation of principal axes, marked by eigenvectors $\hat{e}_1$ and $\hat{e}_3$, for several values of the angle χ. Principal axes corresponding to eigenvalues λ_1 and λ_3 lie in a meridian plane of the dipole, the plane defined by the dipole axis and the position vector, and the principal axis corresponding to eigenvalue λ_2 is normal to a meridian plane.

2. Position-vector basis

We next choose an orthogonal basis $\{\hat{y}_i\}$ in which the $\hat{y}_3$ axis is directed along $\vec{r}$ and orientation of the dipole is specified by polar angles Ω and χ, as shown in Figure A5. The matrix $R(\Omega, \chi)$ defined by

$$R(\Omega, \chi) = Z(\Omega + \pi/2)X(\chi)Z(\pi/2) \tag{25}$$

specifies a rotation that brings the basis $\{\hat{y}_i\}$ into coincidence with the basis $\{\hat{x}_i\}$.

Consequently, the relation

$$G_y = R(\Omega, \chi)G_x\tilde{R}(\Omega, \chi) \tag{26a}$$

determines the matrix G_y representing gradients of a dipole field in the basis $\{\hat{y}_i\}$ in terms of their representation

G_x in the basis $\{\hat{x}_i\}$, as given by Equation 22a. We then find that

$$G_y = g \begin{bmatrix} \cos\chi & 0 & \sin\chi\cos\Omega \\ 0 & \cos\chi & \sin\chi\sin\Omega \\ \sin\chi\cos\Omega & \sin\chi\sin\Omega & -2\cos\chi \end{bmatrix} \tag{26b}$$

Expression 26b tells us that longitudinal gradients in the basis $\{\hat{y}_i\}$ result from a dipole of strength m cos χ directed along $\hat{y}_3$ and that transverse gradients result from dipoles of strength m sin χ cos Ω and m sin χ sin Ω directed along the $\hat{y}_1$ and $\hat{y}_2$ axes, respectively. Eigenvalues and corresponding principal axes, of course, are the same as given before. The set of Euler angles $(\Omega + \pi/2, -\alpha, -\pi/2)$, however, specifies rotation from the position-vector basis to the basis comprised of principal axes defined by the set of eigenvectors $(\hat{e}_1, \hat{e}_2, \hat{e}_3)$.

3. Arbitrary basis

Finally, we choose an arbitrary orthogonal basis $\{\hat{z}_i\}$ in which orientation of the dipole is specified by polar angles ϕ_m and θ_m and direction of the position vector is specified by polar angles ϕ_r and θ_r, as shown in Figure A6. The matrix $R(\phi_r, \theta_r)$ defined by

$$R(\phi_r, \theta_r) = Z(\phi_r + \pi/2)X(\theta_r) \tag{27a}$$

specifies a rotation that brings the basis $\{\hat{z}_i\}$ into coincidence with the basis $\{\hat{y}_i\}$ defined in Figure A5 provided

$$\cos\Omega \sin\chi = \sin\theta_m \sin(\phi_m - \phi_r) \tag{27b}$$

$$\sin\Omega \sin\chi = \sin\theta_r\cos\theta_m - \cos\theta_r\sin\theta_m\cos(\phi_m - \phi_r) \tag{27c}$$

and

$$\cos\chi = \cos\theta_r\cos\theta_m + \sin\theta_r\sin\theta_m\cos(\phi_m - \phi_r) \tag{27d}$$

The relation

$$G_z = R(\phi_r, \theta_r)R(\Omega, \chi)G_x\tilde{R}(\Omega, \chi)\tilde{R}(\phi_r, \theta_r) , \tag{28a}$$

then, determines the matrix G_z representing gradients of a dipole field in an arbitrary basis $\left\{\hat{z}_i\right\}$ in terms of their representation G_x in the basis $\left\{\hat{x}_i\right\}$. As a result, we find that

$$\begin{aligned} G_z = {} & g\cos\chi\left[I - 3/2\ A_1(\phi_r, \theta_r)\right] \\ & + g\sin\chi\left[\cos\Omega\ A_2(\phi_r, \theta_r) - \sin\Omega\ A_3(\phi_r, \theta_r)\right], \end{aligned} \tag{28b}$$

where I denotes the unit matrix,

$$A_1(\phi_r, \theta_r) = \begin{bmatrix} 2\cos^2\phi_r\sin^2\theta_r & \sin2\phi_r\sin^2\theta_r & \cos\phi_r\sin2\theta_r \\ \sin2\phi_r\sin^2\theta_r & 2\sin^2\phi_r\sin^2\theta_r & \sin\phi_r\sin2\theta_r \\ \cos\phi_r\sin2\theta_r & \sin\phi_r\sin2\theta_r & 2\cos^2\theta_r \end{bmatrix} \tag{28c}$$

$$A_2(\phi_r, \theta_r) = \begin{bmatrix} -\sin2\phi_r\sin\theta_r & \cos2\phi_r\sin\theta_r & -\sin\phi_r\cos\theta_r \\ \cos2\phi_r\sin\theta_r & \sin2\phi_r\sin\theta_r & \cos\phi_r\cos\theta_r \\ -\sin\phi_r\cos\theta_r & \cos\phi_r\cos\theta_r & 0 \end{bmatrix} \tag{28d}$$

and

$$A_3(\phi_r, \theta_r) = \begin{bmatrix} \cos^2\phi_r\sin2\theta_r & (1/2)\sin2\phi_r\sin2\theta_r & \cos\phi_r\cos2\theta_r \\ (1/2)\sin2\phi_r\sin2\theta_r & \sin^2\phi_r\sin2\theta_r & \sin\phi_r\cos2\theta_r \\ \cos\phi_r\cos2\theta_r & \sin\phi_r\cos2\theta_r & -\sin2\theta_r \end{bmatrix} \tag{28e}$$

In an arbitrary basis, then, either of two sets of four independent angles, $(\phi_r, \theta_r; \Omega, \chi)$ or $(\phi_r, \theta_r; \phi_m, \theta_m)$, and the scale factor g determine gradients of the magnetic field of a dipole. Because five independent matrix elements determine gradients of a magnetic field in free space, gradients at a point in free space are equivalent to the gradient field of a magnetic dipole located on a sphere of unit radius about the point. By requiring $G = G_z$ for a matrix representing gradients of a magnetic field, we can in principle determine a set of four angles $(\phi_r, \theta_r; \phi_m, \theta_m)$, which specify location and orientation of a dipole, and a scale factor g by solving the system of five equations obtained by equating matrix elements. Choosing a unit radius in the scale factor g then determines the strength of an equivalent dipole. Nonetheless, the direct approach soon becomes fouled by algebra, and we choose another approach to obtain equivalent dipoles of a gradient field in free space.

D. EQUIVALENT DIPOLES OF A GRADIENT FIELD

We seek location, orientation, and strength of a magnetic dipole that produces gradients, represented by a matrix G_d, at a point in free space that are the same as gradients represented by a matrix G; namely, we ask that the differential matrix ΔG vanish, where $\Delta G = G - G_d$. If elements of a matrix vanish in one basis, they vanish in all bases, and so we require elements of the differential matrix to vanish in a basis in which G is diagonal.

The relations

$$G_d = R_d \Lambda_d \tilde{R}_d \tag{29a}$$

and

$$G = R \Lambda \tilde{R} \tag{29b}$$

express matrices G_d and G in terms of their respective diagonal matrices Λ_d and Λ and matrices R_d and R that specify rotations from a fiducial basis to bases comprised of their respective principal axes. Rotation to principal axes of the dipole field is the resultant of two consecutive rotations expressed by the matrix product

$$R_d = RR_\delta \ , \tag{29c}$$

where R_δ represents a rotation from principal axes of the gradient field represented by G to principal axes of the gradient field of the dipole. Consequently, we express the differential matrix ΔG as

$$\Delta G = R(\Lambda - R_\delta \Lambda_d \tilde{R}_\delta)\tilde{R} \tag{29d}$$

Expression 29d tells us that the differential matrix vanishes if both the principal axes of the two gradient fields coincide, $R_\delta = I$, and their eigenvalues are equal, $\Lambda_d = \Lambda$.

1. Dipole orientation and location

To determine orientation and location of an equivalent dipole, then, we first find eigenvalues $(\lambda_1, \lambda_2, \lambda_3)$ of the gradient field represented by the matrix G and a corresponding set of Euler angles Φ, θ, and Ψ that specify rotation from a fiducial basis to principal axes defined by the set of eigenvectors $(\hat{e}_1, \hat{e}_2, \hat{e}_3)$. Namely, we use Equations 16b, 18a, 20a, 20b, 20c, and 20d to find the set of five independent scalars $(\lambda_1, \lambda_3, \Phi, \Theta, \Psi)$ from the five independent elements $(g_{11}, g_{33}, g_{12}, g_{13}, g_{23})$ of the matrix G. We recall that the set of Euler angles specifies one of four possible rotations to a basis comprised of principal axes because the sense of an

eigenvector is indeterminant.

Because eigenvalues of the matrix G are ordered ($\lambda_1 > \lambda_2 > \lambda_3$) and their sum vanishes, we find from Equations 23a, 23b, and 23c that they are equal to eigenvalues of the gradient field of a dipole at a position for which

$$\tan \chi = \frac{/\lambda_1 \lambda_3/^{1/2}}{\lambda_2} \quad , \; 0 < \chi < \pi \tag{30a}$$

and

$$g = \frac{\mu_o 3m}{4\pi r^4} = /\lambda_2^2 + \lambda_1 \lambda_3/^{1/2} \tag{30b}$$

The set of five scalars (g, χ, Φ, Θ, Ψ), then, specifies the gradient field represented by the matrix G.

Figure A7 shows orientation and location of the dipole $\vec{m}_1$ that produces a gradient field whose eigenvalues are λ_1, λ_2, and λ_3 and whose principal axes coincide with the set of eigenvectors ($\hat{e}_1$, $\hat{e}_2$, $\hat{e}_3$). The dipole axis and position vector $\vec{r}_1$ lie in the plane normal to the eigenvector $\hat{e}_2$. Equation 30a determines the angle χ between the dipole axis and position vector, and Equation 30b, magnitude of the dipole moment. Dashed lines in Figure A7 delineate orientation and location of dipoles that produce gradient fields, having eigenvalues λ_1, λ_2, and λ_3, whose principal axes coincide with the sets of eigenvectors ($\hat{e}_1$, $-\hat{e}_2$, $-\hat{e}_3$), ($-\hat{e}_1$, $\hat{e}_2$, $-\hat{e}_3$), and ($-\hat{e}_1$, $-\hat{e}_2$, $\hat{e}_3$) as noted. As is evident, the four equivalent dipoles lie in the plane normal to the eigenvector $\hat{e}_2$, and they form the two pairs ($\vec{m}_1$, $\vec{r}_1$; $-\vec{m}_1$, $-\vec{r}_1$) and ($\vec{m}_2$, $\vec{r}_2$; $-\vec{m}_2$, $-\vec{r}_2$) with the first pair associated with the eigenvector $\hat{e}_2$ and the second, with the eigenvector $-\hat{e}_2$.

We observe from Figure A7 that column matrices

$$M_p = \begin{bmatrix} \sin(\alpha+\chi) \\ 0 \\ \cos(\alpha+\chi) \end{bmatrix} \quad \text{and} \quad \rho_p = \begin{bmatrix} -\sin\alpha \\ 0 \\ -\cos\alpha \end{bmatrix} \tag{31}$$

give direction cosines of the dipole axis and position vector $\vec{m}$ and $\vec{r}$, respectively, in the basis defined by the set of eigenvectors $(\hat{e}_1, \hat{e}_2, \hat{e}_3)$. Consequently, in the fiducial basis the matrices $M = RM_p$ and $\rho = R\rho_p$ give orientation and location of the dipole whose principal axes, defined by the eigenvectors $(\hat{e}_1, \hat{e}_2, \hat{e}_3)$, coincide with those of the gradient field represented by the matrix G. The matrix R describes rotation from the fiducial basis to principal axes of G as specified by the Euler and angles Φ, Ψ, and Θ.

In the fiducial basis, we then find that polar angles ϕ_m and θ_m defining direction of the dipole $\vec{m}_1$ are determined by the relations

$$\cos\theta_m = \cos\Theta \cos(\alpha+\chi) + \sin\Psi \sin\Theta \sin(\alpha+\chi) \tag{32a}$$

$$\sin\theta_m \cos(\phi_m-\Psi) = \cos\Psi \sin(\alpha+\chi) \tag{32b}$$

and

$$\sin\theta_m \sin(\phi_m-\Phi) = \sin\Psi \cos\Theta \sin(\alpha+\chi) - \sin\Theta \cos(\alpha+\chi) \tag{32c}$$

and that polar angles ϕ_r and θ_r defining direction of the position vector $\vec{r}_1$ are determined by the relations

$$-\cos\theta_r = \cos\Theta \cos\alpha + \sin\Psi \sin\Theta \sin\alpha \tag{32d}$$

$$-\sin\theta_r \cos(\phi_r-\Phi) = \cos\Psi \sin\alpha \tag{32e}$$

and

$$-\sin\theta_r \sin(\phi_r - \Phi) = \sin\Psi \cos\Theta \sin\alpha - \sin\theta\cos\alpha \ . \qquad (32f)$$

Equations 32a through 32f give a prescription for transforming the set of five scalars $(g, \chi, \Phi, \Psi, \Theta)$ to the set $(g, \phi_r, \theta_r, \phi_m, \theta_m)$ that specifies the gradient field represented by the matrix G in terms of the gradient field of its equivalent dipole $\vec{m}_1$ located at position $\vec{r}_1$. The set $(g, \pi+\phi_r, \pi-\theta_r, \pi+\phi_m, \pi-\theta_m)$ corresponds to the equivalent dipole $-\vec{m}_1$ located at position $-\vec{r}_1$. We obtain the set $(g, \phi_r', \theta_r', \phi_m', \theta_m')$ corresponding to the equivalent dipole $\vec{m}_2$ located at position $\vec{r}_2$ by adding π to the angle Ψ in Equations 32a through 32f. Finally, the set $(g, \pi+\phi_r', \pi-\theta_r', \pi+\phi_m', \pi-\theta_m')$ corresponds to the equivalent dipole $-\vec{m}_2$ located at $-\vec{r}_2$.

2. Alignment errors

A dipole placed at the position of an equivalent dipole cancells gradients at the corresponding field point. Because positioning is imperfect, however, errors in aligning a cancelling dipole leave residual gradients at the field point. We describe residual gradients resulting from errors in alignment in terms of infinitesimal rotation of principal axes from true alignment and infinitesimal deviation of eigenvalues from true values.

The matrix

$$R_\delta = I + \Delta\phi Q(\phi_o, \theta_o) \qquad (33)$$

specifies an infinitesimal rotation from principal axes of the gradient field represented by the matrix G through an angle $\Delta\phi$ about an axis specified by polar angles ϕ_o and θ_o with respect to the principal axes, where $Q(\phi_o, \theta_o)$ is

expressed by Equation 10a. Eigenvalues of the gradient field of the cancelling dipole deviate from those of the gradient field represented by the matrix G by an amount $\Delta\Lambda_d = \Lambda_d - \Lambda$.

From Equation 29d, we then find that the relation

$$\Delta G \doteq R \left| -\Delta\Lambda_d + \Delta\phi(\Lambda Q - Q\Lambda) \right| \tilde{R} \tag{34a}$$

gives residual gradients resulting from alignment errors. The difference in eigenvalues results from deviations in the scale factor, Δg, and in the angle χ as expressed by the relation

$$\Delta\Lambda_d = \Lambda\left(\frac{\Delta g}{g}\right) + \frac{\partial\Lambda_d}{\partial\chi}\ \Delta\chi \quad . \tag{34b}$$

In the basis comprised of principal axes of the matrix G, then, residual gradients are given by

$$\Delta g_{11} = -\lambda_1\left(\frac{\Delta g}{g}\right) - 1/2\left(\frac{7\lambda_1+6\lambda_3}{2\lambda_1+\lambda_3}\right) \Big/\lambda_1\lambda_3\Big/^{1/2} \Delta\chi \tag{35a}$$

$$\Delta g_{22} = (\lambda_1+\lambda_3)\ \frac{\Delta g}{g} + \Big/\lambda_1\lambda_3\Big/^{1/2} \Delta\chi \tag{35b}$$

$$\Delta g_{33} = -\lambda_3\left(\frac{\Delta g}{g}\right) + 1/2\left(\frac{3\lambda_1+4\lambda_3}{2\lambda_1+\lambda_3}\right) \Big/\lambda_1\lambda_3\Big/^{1/2} \Delta\chi \tag{35c}$$

$$\Delta g_{12} = -(2\lambda_1+\lambda_3)\Delta\phi_3 \tag{35d}$$

$$\Delta g_{13} = (\lambda_1-\lambda_3)\Delta\phi_2 \tag{35e}$$

and

$$\Delta g_{23} = (\lambda_1+2\lambda_3)\Delta\phi_1 \quad , \tag{35f}$$

where

$$\Delta\phi_1 = \Delta\phi \sin\theta_o \cos\phi_o \tag{35g}$$

$$\Delta\phi_2 = \Delta\phi \sin\theta_o \sin\phi_o \tag{35h}$$

$$\Delta\phi_3 = \Delta\phi \cos\theta_o \tag{35i}$$

and λ_1, λ_2, and λ_3 are eigenvalues of G.

TABLE OF ROTATIONS
ROTATION ABOUT AN $\hat{x}_3$ AXIS

The matrix

$$Z(\phi) = \begin{bmatrix} \cos\phi & -\sin\phi & 0 \\ \sin\phi & \cos\phi & 0 \\ 0 & 0 & 1 \end{bmatrix}$$

represents a positive rotation through an angle ϕ about the $\hat{x}_3$ axis of a basis. The relation

$$\Gamma = \tilde{Z}(\phi)GZ(\phi)$$

gives gradients, γ_{ij}, in the rotated basis in terms of gradients, g_{ij}, in the initial basis, and so

$$\gamma_{11} = \frac{1}{2}(g_{11} + g_{22}) + \frac{1}{2}(g_{11} - g_{22})\cos 2\phi + g_{12}\sin 2\phi$$

$$\gamma_{22} = \frac{1}{2}(g_{11} + g_{22}) - \frac{1}{2}(g_{11} - g_{22})\cos 2\phi - g_{12}\sin 2\phi$$

$$\gamma_{33} = g_{33}$$

$$\gamma_{12} = g_{12}\cos 2\phi - \frac{1}{2}(g_{11} - g_{22})\sin 2\phi$$

$$\gamma_{13} = g_{13}\cos\phi + g_{23}\sin\phi$$

$$\gamma_{23} = g_{23}\cos\phi - g_{13}\sin\phi$$

ROTATION ABOUT AN $\hat{x}_1$ AXIS

The matrix

$$X(\theta) = \begin{bmatrix} 1 & 0 & 0 \\ 0 & \cos\theta & -\sin\theta \\ 0 & \sin\theta & \cos\theta \end{bmatrix}$$

represents a positive rotation through an angle θ about the $\hat{x}_1$ axis of a basis. The relation

$$\Gamma = \tilde{X}(\theta)GX(\theta)$$

gives gradients, γ_{ij}, in the rotated basis in terms of gradients, g_{ij}, in the initial basis, and so

$$\gamma_{11} = g_{11}$$

$$\gamma_{22} = \frac{1}{2}(g_{22} + g_{33}) + \frac{1}{2}(g_{22} - g_{33})\cos 2\theta + g_{23}\sin 2\theta$$

$$\gamma_{33} = \frac{1}{2}(g_{22} + g_{33}) - \frac{1}{2}(g_{22} - g_{33})\cos 2\theta - g_{23}\sin 2\theta$$

$$\gamma_{12} = g_{12}\cos\theta + g_{13}\sin\theta$$

$$\gamma_{13} = g_{13}\cos\theta - g_{12}\sin\theta$$

$$\gamma_{23} = g_{23}\cos\theta - \frac{1}{2}(g_{22} - g_{33})\sin 2\theta$$

ROTATION ABOUT AN $\hat{x}_2$ AXIS

The matrix

$$Y(\psi) = Z(\pi/2)X(\psi)\tilde{Z}(\pi/2) = \begin{bmatrix} \cos\psi & 0 & \sin\psi \\ 0 & 1 & 0 \\ -\sin\psi & 0 & \cos\psi \end{bmatrix}$$

represents a positive rotation through an angle ψ about the $\hat{x}_2$ axis of a basis. The relation

$$\Gamma = \tilde{Y}(\psi)GY(\psi)$$

gives gradients, γ_{ij}, in the rotated basis in terms of gradients, g_{ij}, in the initial basis, and so

$$\gamma_{11} = \frac{1}{2}(g_{11} + g_{33}) + \frac{1}{2}(g_{11} - g_{33})\cos2\psi - g_{13}\sin2\psi$$

$$\gamma_{22} = g_{22}$$

$$\gamma_{33} = \frac{1}{2}(g_{11} + g_{33}) - \frac{1}{2}(g_{11} - g_{33})\cos2\psi + g_{13}\sin2\psi$$

$$\gamma_{12} = g_{12}\cos\psi - g_{23}\sin\psi$$

$$\gamma_{13} = g_{13}\cos2\psi + \frac{1}{2}(g_{11} - g_{33})\sin2\psi$$

$$\gamma_{23} = g_{23}\cos\psi + g_{12}\sin\psi$$

REFERENCES

Goldstein, H., Classical Mechanics, p. 118, Addison-Wesley Publishing Co., Inc., Reading, Mass., 1959

Indritz, J., Methods in Analysis, p. 45, The Macmillan Co., New York, 1963

Powell, J. and Crasemann, B., Quantum Mecnanics, Chap. 9, Addison-Wesley Publishing Co., Inc., Reading, Mass., 1961

FIGURE CAPTIONS

Figure A1 Three successive dependent rotations through the Eulerian angles ϕ, θ, and ψ specifying a rotation from the basis $\{\hat{x}_i\}$ to a basis $\{\hat{y}_i\}$. Rotations are made consecutively in the following order: (1) rotation through the angle Φ about the $\hat{x}_3$ axis, represented by the matrix $Z(\Phi)$; (2) rotation through the angle θ about an $\hat{x}_1$ axis in the direction $\hat{x}_3 \times \hat{y}_3$, represented by the matrix $X(\theta)$; and (3) rotation through the angle Ψ about the $\hat{y}_3$ axis, represented by the matrix $Z(\Psi)$. Positive rotations are right handed.

Figure A2 Eigenvalues λ_1, λ_2, and λ_3 of the gradient field of a magnetic dipole having a unit gradient strength, g, shown as functions of the polar angle χ between the axis of the dipole and a position vector emanating from the dipole. Eigenvalues are indexed so that $\lambda_1 > \lambda_2 > \lambda_3$. The determinant, det G, of a matrix representing gradients at a position in a dipole field is positive for $\chi > \pi/2$ and negative for $\chi < \pi/2$. Its trace vanishes and so $\lambda_1 + \lambda_2 + \lambda_3 = 0$.

Figure A3 Basis comprised of principal axes defined by the set of eigenvectors ($\hat{e}_1$, $\hat{e}_2$, $\hat{e}_3$) at a position $\vec{r}$ in the field of a magnetic dipole $\vec{m}$. Eigenvectors $\hat{e}_1$ and $\hat{e}_3$ are in the meridian plane normal to the $\hat{x}_2$ axis, and eigenvector $\hat{e}_2$ points along the negative $\hat{x}_2$ axis. The angle α between eigenvector $\hat{e}_3$ and the position vector $\vec{r}$ ranges from 0 to $\pi/2$ as the polar angle χ ranges from 0 to π, and the angle β between the magnetic field vector $\vec{b}$ and the position vector ranges from 0 to π.

Figure A4 Orientation of principal axes, marked by eigenvectors $\hat{e}_1$ and $\hat{e}_3$, depicted for several headings in a meridian plane of the field of a magnetic dipole $\vec{m}$.

Figure A5 Definition of the position-vector basis $\{\hat{y}_i\}$. The $\hat{y}_3$ axis points along the position vector $\vec{r}$, and polar angles Ω and χ specify orientation of the dipole $\vec{m}$ in the basis $\{\hat{y}_i\}$.

Figure A6 Polar angles $(\phi_m, \theta_m; \phi_r, \theta_r)$ specifying direction of the dipole axis and position vector in a basis $\{\hat{z}_i\}$. Polar angles ϕ_m and θ_m give direction of the dipole $\vec{m}$, and polar angles ϕ_r and θ_r give direction of the position vector $\vec{r}$.

Figure A7 Location and orientation of the magnetic dipole $\vec{m}_1$ that produces a gradient field having principal axes coincident with the set of eigenvectors $(\hat{e}_1, \hat{e}_2, \hat{e}_3)$. The dipole axis and position vector are in the plane normal to the eigenvector $\hat{e}_2$. Dashed lines mark location and orientation of image dipoles that produce the same gradient field. They form the two pairs $(\vec{m}_1, \vec{r}_1; -\vec{m}_1, -\vec{r}_1)$ and $(\vec{m}_2, \vec{r}_2; -\vec{m}_2, -\vec{r}_2)$ with the first pair associated with the eigenvector $\hat{e}_2$ and the second, with the eigenvector $-\hat{e}_2$.

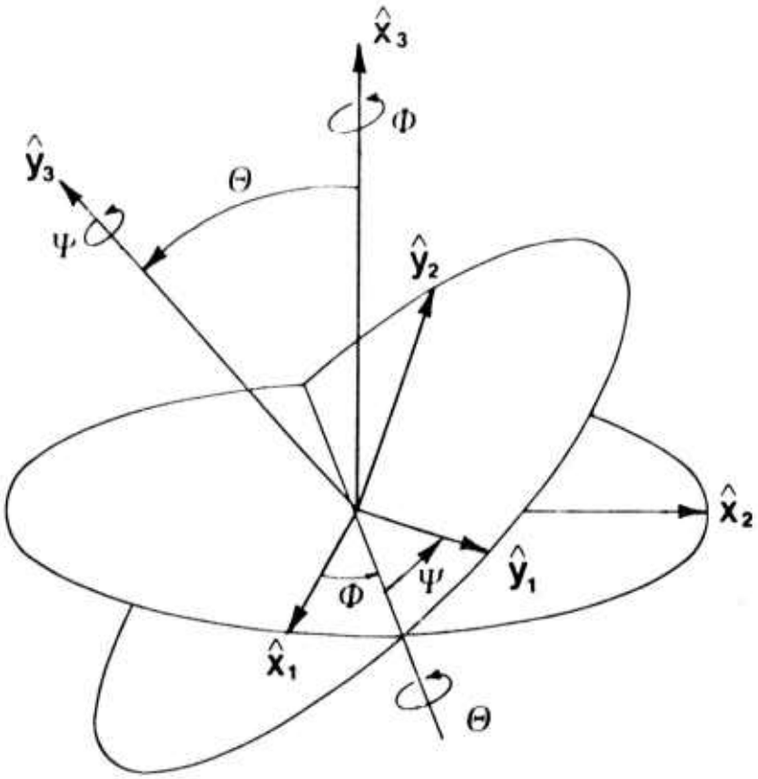
$\hat{x}_3$
Φ
$\hat{y}_3$
Θ
Ψ
$\hat{y}_2$
$\hat{x}_2$
$\hat{y}_1$
Ψ
Φ
$\hat{x}_1$
Θ

FIGURE A1

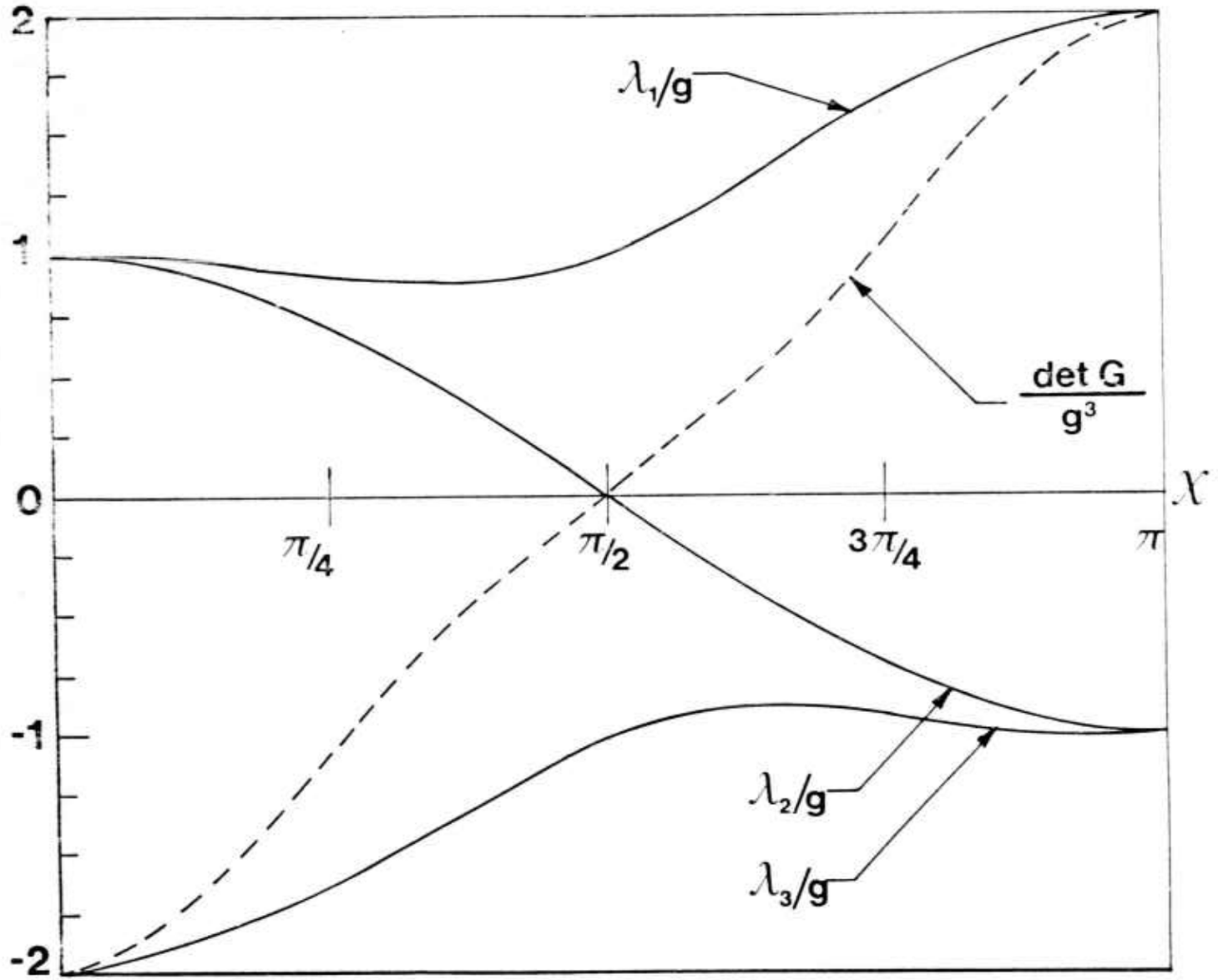
2
1
0
-1
-2
λ_1/g
$\frac{\det G}{g^3}$
χ
$\pi/4$
$\pi/2$
$3\pi/4$
π
λ_2/g
λ_3/g

FIGURE A2

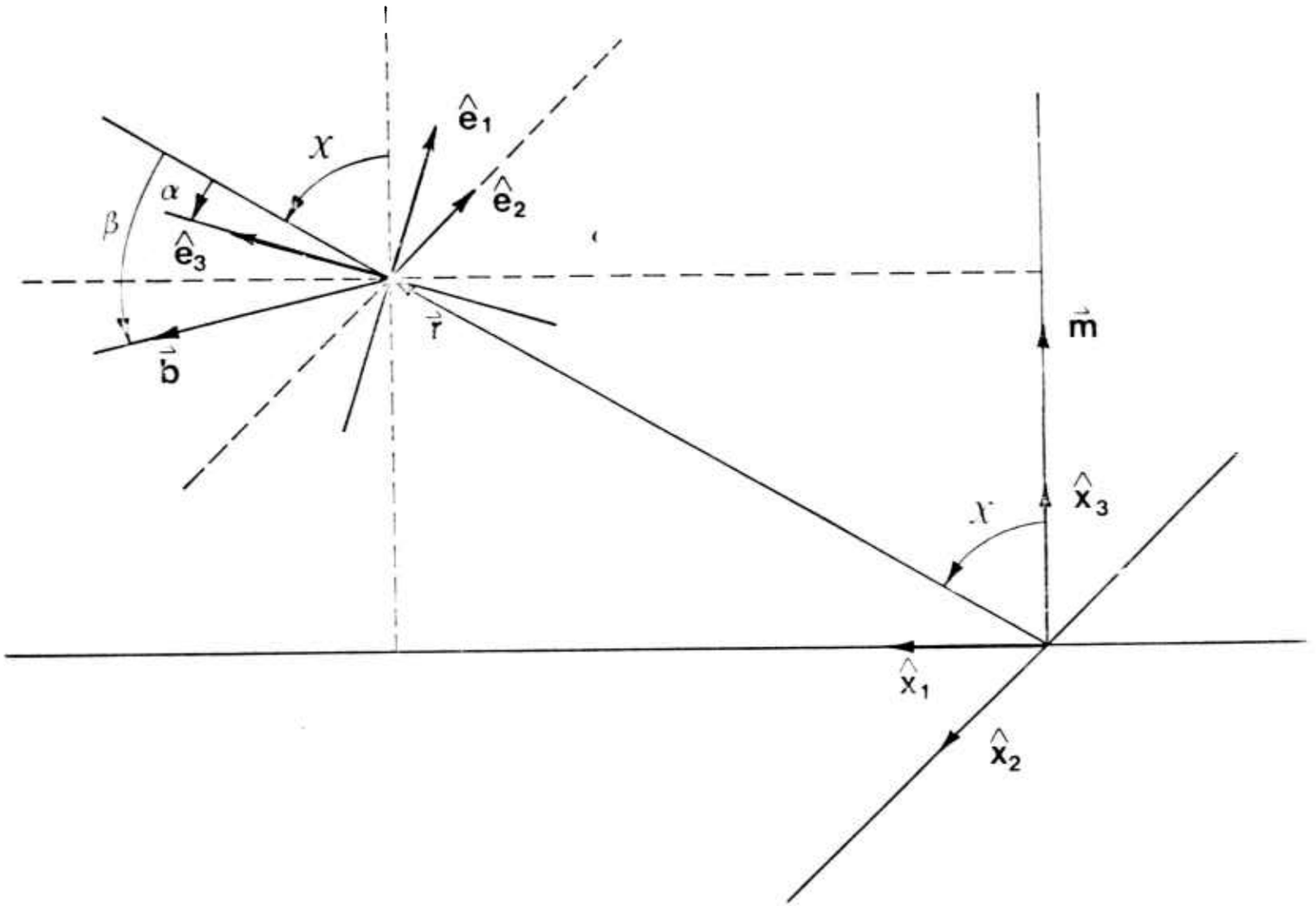
$\hat{e}_1$
χ
α
β
$\hat{e}_2$
$\hat{e}_3$
$\vec{r}$
$\vec{b}$
$\vec{m}$
γ
$\hat{x}_3$
$\hat{x}_1$
$\hat{x}_2$

FIGURE A3

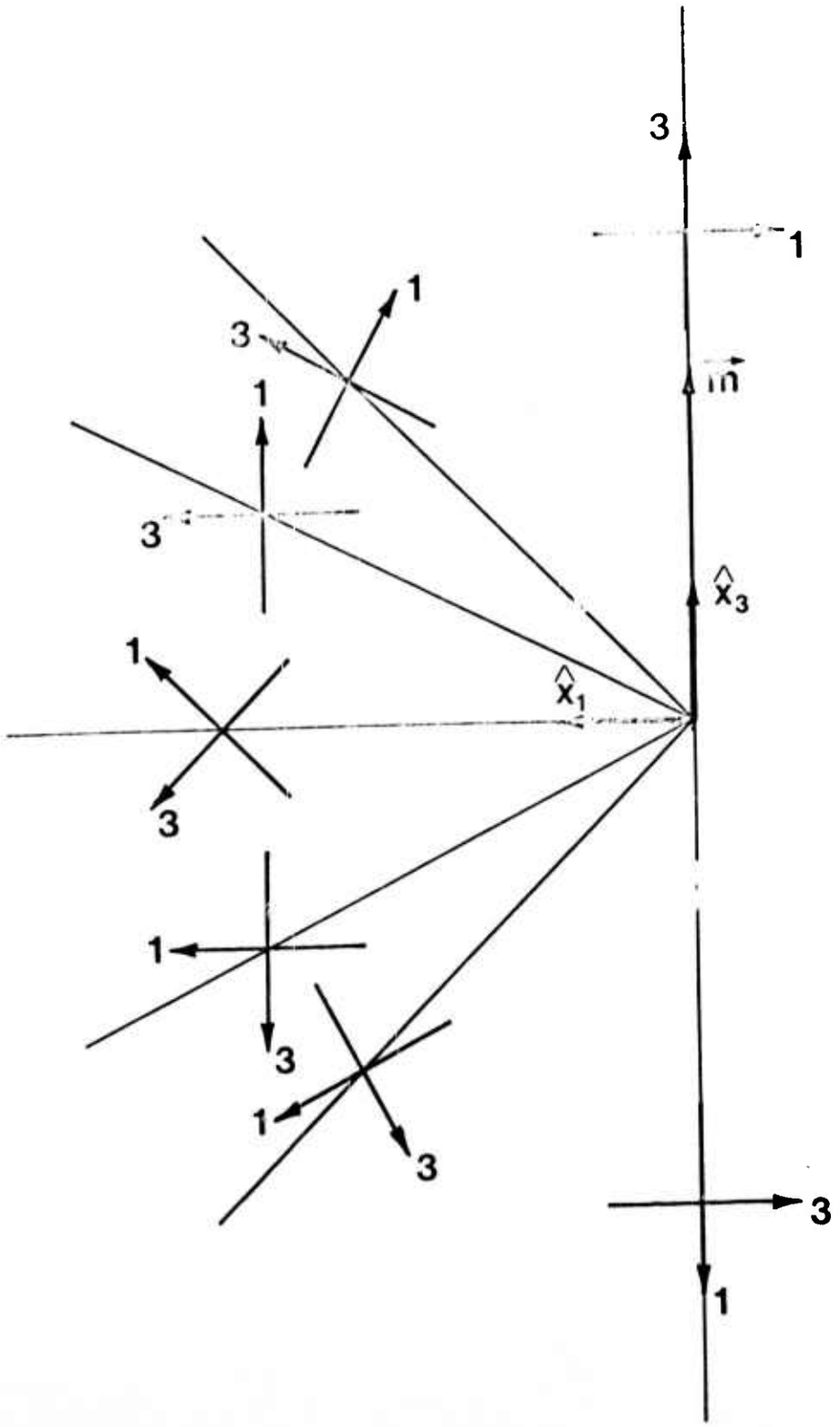

FIGURE A4

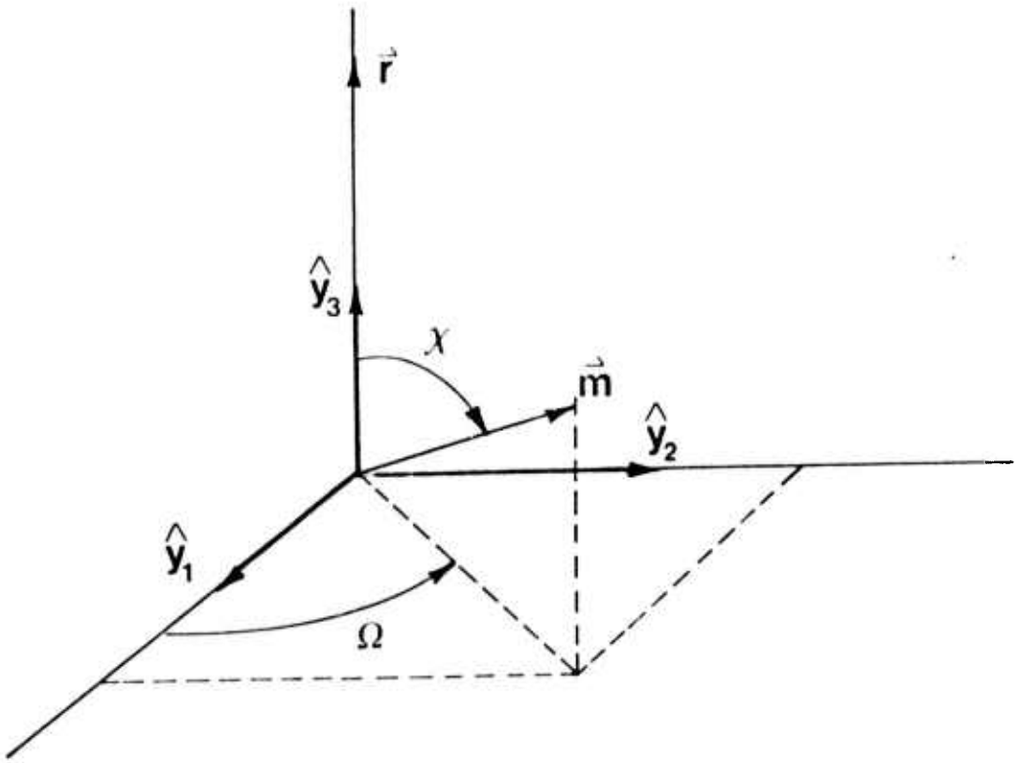

FIGURE A5

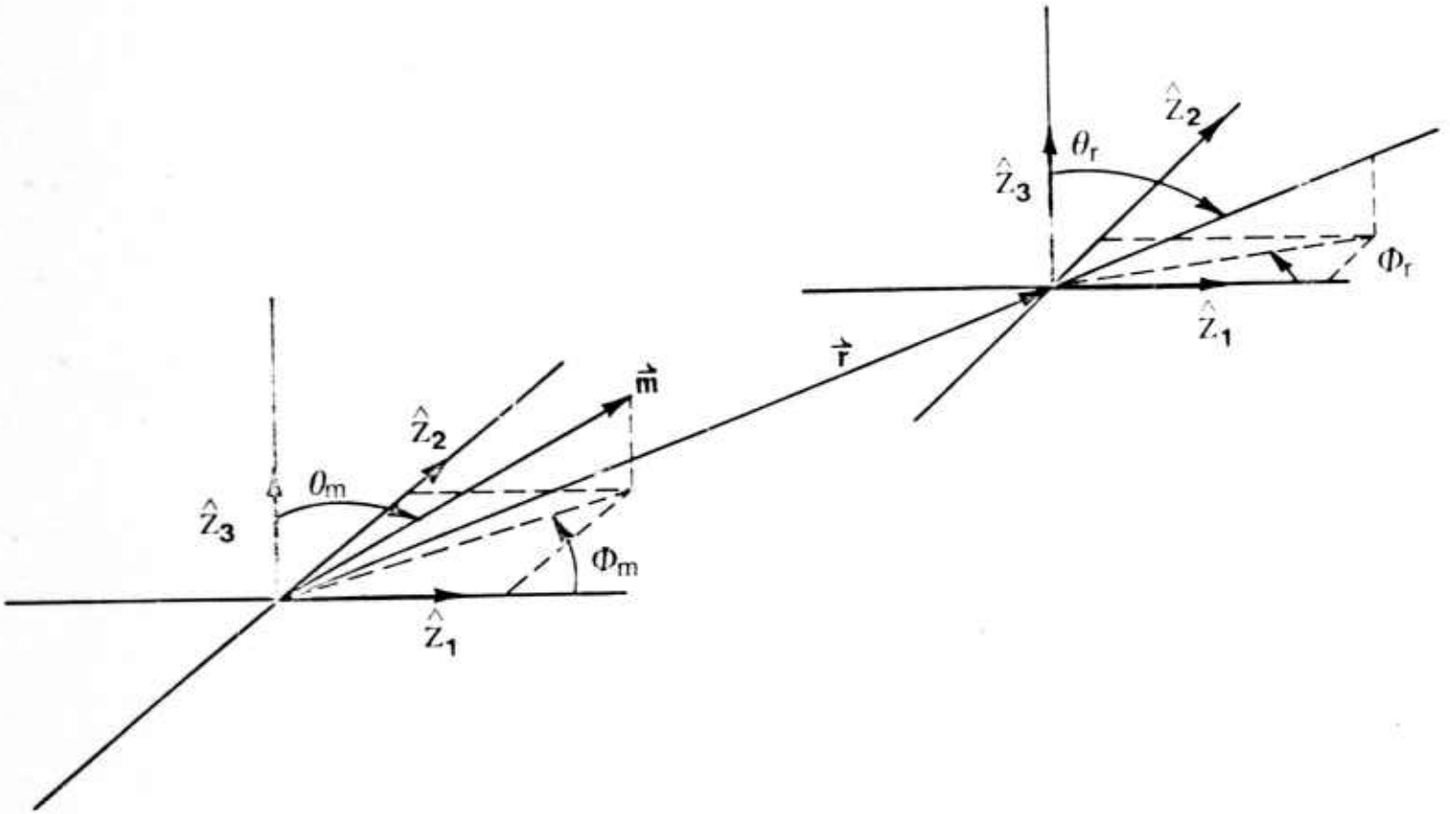
$\hat{Z}_3$
θ_m
$\hat{Z}_2$
$\vec{m}$
Φ_m
$\hat{Z}_1$
$\vec{r}$
$\hat{Z}_3$
θ_r
$\hat{Z}_2$
Φ_r
$\hat{Z}_1$

FIGURE A6

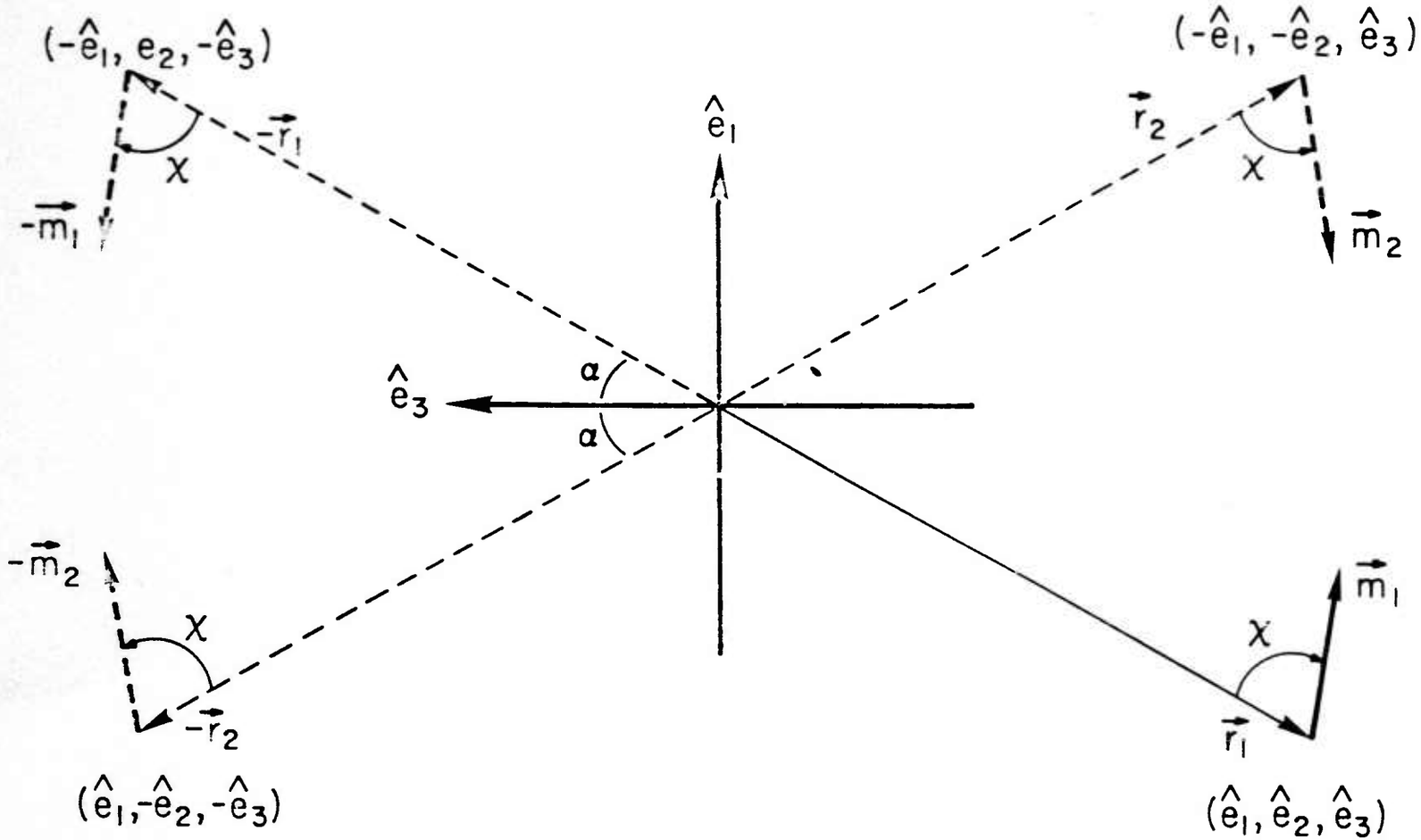
$(-\hat{e}_1, e_2, -\hat{e}_3)$
$-\vec{r}_1$
χ
$-\vec{m}_1$
$\hat{e}_1$
$(-\hat{e}_1, -\hat{e}_2, \hat{e}_3)$
$\vec{r}_2$
χ
$\vec{m}_2$
$\hat{e}_3$
α
α
$-\vec{m}_2$
χ
$-\vec{r}_2$
$(\hat{e}_1, -\hat{e}_2, -\hat{e}_3)$
$\vec{m}_1$
χ
$\vec{r}_1$
$(\hat{e}_1, \hat{e}_2, \hat{e}_3)$

FIGURE A7

METRIC SYSTEM

BASE UNITS:

Quantity	Unit	SI Symbol	Formula
length	metre	m	...
mass	kilogram	kg	...
time	second	s	...
electric current	ampere	A	...
thermodynamic temperature	kelvin	K	...
amount of substance	mole	mol	...
luminous intensity	candela	cd	...

SUPPLEMENTARY UNITS:

plane angle	radian	rad	...
solid angle	steradian	sr	...

DERIVED UNITS:

Acceleration	metre per second squared	...	m/s
activity (of a radioactive source)	disintegration per second	...	(disintegration)/s
angular acceleration	radian per second squared	...	rad/s
angular velocity	radian per second	...	rad/s
area	square metre	...	m
density	kilogram per cubic metre	...	kg/m
electric capacitance	farad	F	A·s/V
electrical conductance	siemens	S	A/V
electric field strength	volt per metre	...	V/m
electric inductance	henry	H	V·s/A
electric potential difference	volt	V	W/A
electric resistance	ohm		V/A
electromotive force	volt	V	W/A
energy	joule	J	N·m
entropy	joule per kelvin	...	J/K
force	newton	N	kg·m/s
frequency	hertz	Hz	(cycle)/s
illuminance	lux	lx	lm/m
luminance	candela per square metre	...	cd/m
luminous flux	lumen	lm	cd·sr
magnetic field strength	ampere per metre	...	A/m
magnetic flux	weber	Wb	V·s
magnetic flux density	tesla	T	Wb/m
magnetomotive force	ampere	A	...
power	watt	W	J/s
pressure	pascal	Pa	N/m
quantity of electricity	coulomb	C	A·s
quantity of heat	joule	J	N·m
radiant intensity	watt per steradian	...	W/sr
specific heat	joule per kilogram-kelvin	...	J/kg·K
stress	pascal	Pa	N/m
thermal conductivity	watt per metre-kelvin	...	W/m·K
velocity	metre per second	...	m/s
viscosity, dynamic	pascal-second	...	Pa·s
viscosity, kinematic	square metre per second	...	m/s
voltage	volt	V	W/A
volume	cubic metre	...	m
wavenumber	reciprocal metre	...	(wave)/m
work	joule	J	N·m

SI PREFIXES:

Multiplication Factors	Prefix	SI Symbol
1 000 000 000 000 = 10^{12}	tera	T
1 000 000 000 = 10^{9}	giga	G
1 000 000 = 10^{6}	mega	M
1 000 = 10^{3}	kilo	k
100 = 10^{2}	hecto*	h
10 = 10^{1}	deka*	da
0.1 = 10^{-1}	deci*	d
0.01 = 10^{-2}	centi*	c
0.001 = 10^{-3}	milli	m
0.000 001 = 10^{-6}	micro	μ
0.000 000 001 = 10^{-9}	nano	n
0.000 000 000 001 = 10^{-12}	pico	p
0.000 000 000 000 001 = 10^{-15}	femto	f
0.000 000 000 000 000 001 = 10^{-18}	atto	a

* To be avoided where possible.